

**Structural Studies on Kinesin-1 Motor Domain
and Light Chain from *Rattus norvegicus* and
*Neurospora crassa***

Thesis Submitted to the University of Hamburg in Partial Fulfilment
of the Requirements for the Degree of Ph.D.

Presented by Spyridon Mylonas
from Greece

Hamburg, 2005

1.	Introduction	1
1.1	Microtubule-associated motor: the kinesin superfamily	1
1.2	Conventional kinesin (kinesin-1)	4
1.2.1	Biological function of kinesin-1	6
1.2.2	Structure of the motor domain of kinesin-1	7
1.3	Kinesin light chains	11
1.3.1	The tetratricopeptide repeat region of KLC	13
1.4	Aim of this study	16
2	Materials and methods	17
2.1	Materials	17
2.1.1	Chemicals	17
2.1.2	Enzymes	17
2.1.3	Bacterial strains	18
2.1.4	Cloning Vectors	19
2.1.5	Expression Vectors	19
2.1.6	Media	20
2.1.7	Crystallization	20
2.1.8	Equipment and accessories	21
2.2	Molecular biology and microbiological methods	22
2.2.1	Culture and storage of <i>E.coli</i>	22
2.2.2	Transformation of <i>E.coli</i> strains	22
	Transformation by heat-shock	22
	Transformation by electroporation	23
2.2.3	Isolation of plasmid DNA	23
2.2.4	Determination of DNA concentration and purity	23
2.2.5	Ligation reaction	24
2.2.6	Restriction analysis of DNA	24
2.2.7	DNA sequencing	25
2.2.8	Mutagenesis of DNA	26
2.2.9	Gene cloning using the Invitrogen Gateway TM Technology	27
	Generation of the recombinant baculovirus vector bacmid.GST.TPR1-6t	32
2.3	Protein methods	33
2.3.1	SDS-Polyacrylamide gel electrophoresis (SDS-PAGE)	33
2.3.2	Western blotting	34
2.3.3	Protein production	34
2.3.4	Cell lysis and solubility test	35
2.3.5	Sf9-Cell culture	35
	2.3.5.1 Baculovirus expression system	36
	2.3.5.2 Expression of GST.TPR1-6t in <i>SF9</i> insect cells	36
2.3.6	Chromatography	36
	2.3.6.1 Ni-NTA affinity chromatography	36
	2.3.6.2 GST affinity chromatography	37
	2.3.6.3 Anion and cation exchange chromatography	37
	2.3.6.4 Gel filtration	38

2.3.6.5	Purification of <i>N.crassa</i> and <i>R.norvegicus</i> kinesin motor domain mutants	38
2.3.7	Determination of concentration of proteins	39
2.3.8	Concentration of protein	40
2.3.9	Solubility studies	40
2.3.10	Dynamic Light Scattering	41
2.3.11	Crystallization techniques	41
2.3.12	Testing of Nk355 ^{R207A} and Rk354 ^{R204A} crystals and data collection.	43
2.3.13	Molecular replacement	44
2.3.14	Limited proteolysis	44
3.	Results	45
3.1	Structural studies on <i>Neurospora crassa</i> and <i>Rattus norvegicus</i> kinesin-1 motor domain point mutants	45
3.1.1	Generation of the Nk355 ^{R207A} , Nk355 ^{R207K} , Rk354 ^{R204A} and Rk354 ^{R204K} mutant constructs	45
3.1.2	Expression and purification of motor domain mutants	46
	Expression and purification of <i>N. crassa</i> constructs	47
	Expression and purification of <i>R. norvegicus</i> constructs	48
3.1.3	Crystallization of Nk355 ^{R207A} , Nk355 ^{R207K} , Rk354 ^{R204A} and Rk354 ^{R204K}	50
3.1.4	Data collection and processing from a Nk355 ^{R207A} plate-like crystal	54
3.1.5	Molecular replacement	56
3.1.6	Data collection and processing from Rk354 ^{R204A} needle-like crystal	59
3.1.7	Generation of a Loop 11 deletion mutant RK354Dloop11	61
3.1.7.1	Expression and Purification of RK354Dloop11	62
3.1.7.2	Crystallization trials with the RK354Dloop11 protein	62
3.2	Generation of <i>Rattus norvegicus</i> kinesin light chain (KLC) constructs	63
3.2.1	Cloning of KLC constructs	63
3.2.2	Expression and purification of KLC constructs	65
3.2.2.1	Expression and purification of His.KLC-C and GST.TPR1-6 proteins	66
3.2.2.2	Crystallization trials with GST.TPR1-6 protein	67
3.2.2.3	Expression of His.TPR1-6 and C-his.TPR1-6 constructs	68
3.2.2.4	Crystallization trials with His.TPR1-6 protein	69
3.2.2.5	Expression of GST.TPR1-2, His.TPR1-2 and His.TPR3-4 constructs	70
3.2.2.6	Crystallization trials with GST.TPR1-2 protein	72
3.2.2.7	Expression of His.TPR1-6t protein	72
3.2.2.8	Expression of the GST.TPR1-6t protein in SF9 insect cells	73
3.2.2.9	Removal of the GST-tag from the GST.TPR1-6t protein	74
3.2.2.10	Expression of the GST.TPR1-6t protein in E.coli	75
3.2.2.11	Initial proteolytic analysis of the GST.TPR1-6 construct	76

4	Discussion	77
4.1	Structural investigation of a conserved arginine in the switch-1 region of kinesin-1	77
4.1.1	Cloning, expression and purification of point mutants	77
4.1.2	Crystallization and preliminary X-ray analysis of the Nk355 ^{R207A} and Rk354 ^{R204A} constructs	78
4.2	Investigation of a rat kinesin-1 loop11 deletion mutant	86
4.3	Crystallization studies on the TPR region of the kinesin light chains	87
4.3.1	Initial crystallization studies with GST.TPR1-6, GST.TPR1-2 and His.TPR1-6 proteins	88
4.3.2	Initial crystallization studies with GST.TPR1-6, GST.TPR1-2 and His.TPR1-6 proteins	88
5	Summary	91
6	References	93
7	Appendix	104
7.1	List of Abbreviations	104
7.2	List of Figures	105
7.3	List of Tables	107
7.4	Oligonucleotides	107
7.5	Purification buffers	110
7.6	Acknowledgements	115
7.7	Declaration	116

1. Introduction

Molecular motors comprise groups of proteins that have the ability to generate force along a cytoskeletal track through the hydrolysis of ATP. Three classes can be distinguished: the dyneins, the kinesins and the myosins. Dyneins and kinesins move along microtubules towards the minus and plus end of them respectively; while myosins move along actin filaments. The participation of motor proteins to the cellular life involves cargo transport and organization of the cytoskeleton (review: Vale, 2003).

In a molecular motor two functional parts can be distinguished: a motor domain that interacts with the cytoskeleton, hydrolyzes ATP and generates movement and a tail domain that interacts with the cargo directly or through accessory light chains (review: Gunawardena and Goldstein, 2004).

1.1 Microtubule-associated motor: the kinesin superfamily

Kinesin motor proteins move along microtubules, utilizing the energy that derives from the hydrolysis of ATP molecules, to transport vesicles and organelles (Hirokawa, 1998). They are also involved in a variety of cellular functions such as spindle assembly and function, chromosome motility and regulation of microtubule dynamics (Inoue and Salmon, 1995; Endow, 1999; Sharp et al., 2000).

In mammals, 45 genes encoding for kinesin sequences have so far been identified. Kinesins can be classified on the basis of sequence similarity as in the phylogenetic tree shown in fig. 1, which contains 155 proteins from 11 species that have been characterized until today. Another classification criterion is the directionality of movement; members of the kinesin-1 and kinesin-2 families move towards the plus end of the microtubules, while members of the kinesin-14 family as Ncd and Kar3 move towards the minus end. The position of the motor domain within the molecule can be different, either N-terminal, in the middle or C-terminal. This led to classification into N-, M- and C-type motors (Vale and Fletterick, 1997). The composition of their polypeptide chains is also often used to describe kinesins as homodimers (e.g. *Neurospora crassa* kinesin-1), heterotrimers (e.g. kinesin-2)

or homotetramers (e.g. kinesin-5). The confusion caused by using different names and classifications was ended by introducing a simplifying nomenclature (Lawrence et al., 2004) according to which all kinesins were classified in 14 families using Arabic numbers (kinesin-1 to kinesin-14).

The large number of kinesins implies that different motors transport specific cargoes. Adaptor or receptor proteins that connect kinesin to its cargo have been identified. For example, kinesin-1 transports vesicles containing the amyloid precursor protein (Kamal et al., 2000). In dendrites, vesicles containing N-methyl-D-aspartate (NMDA)-type glutamate receptors are transported by the dendrite-specific motor KIF17 (kinesin-2) (Setou et al., 2000). Kinesins can bind to their cargo receptors via scaffolding proteins. Kinesin-1 binds to cargo vesicles via the c-jun NH2-terminal kinase (JNK)-interacting proteins (JIPs), namely JIP-1, JIP-2, and JIP-3 (Verhey et al., 2001; Bowman et al., 2000). A direct connection between APP and kinesin-1 light chain has been suggested (Kamal et al., 2001). However this data still remains controversial (Lazarov et al., 2005). Kinesin-2 binds to its cargo via the mLin-10 protein, which is known to be part of a bigger complex containing mLin-2 and mLin-7 and the NRB2 subunit of the NMDA receptor (Guillaud et al., 2003; Setou et al., 2000).

Additionally to vesicle and organelle transport, a large number of kinesin proteins are involved in chromosome distribution (Inoue and Salmon, 1995; Endow, 1999). Kinesins bind to and crosslink spindle fibers and by moving along the microtubules, they play an essential role in spindle assembly and maintenance, centrosome duplication, and attachment of centrosomes to poles (Sharp et al., 2000).

Surprisingly members of the M-type family (kinesin-13) of motors as MCAK/Kif2, a chromosome-related kinesin that is required for the mitosis, has been found to destabilize microtubules (Walczak et al., 1996; Maney et al., 1998); as does the C-type motor Kar3 (kinesin-14) in vitro (Hunter et al., 2000; Endow et al., 1994).

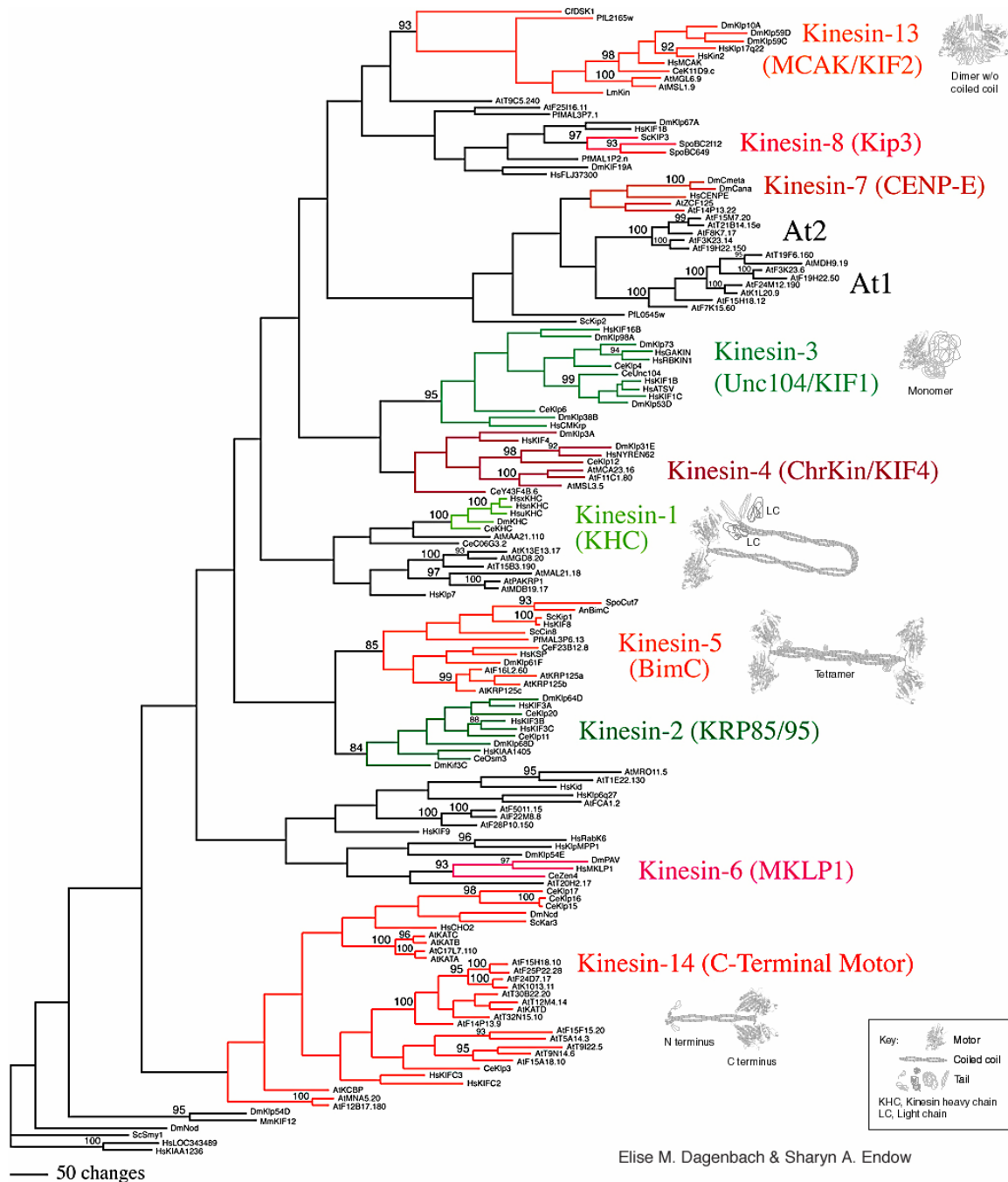


Fig. 1: Phylogenetic tree of the kinesin superfamily. The tree is built from a kinesin motor domain sequence alignment of 155 proteins from 11 species (Dagenbach and Endow, 2004).

1.2 Conventional kinesin (kinesin-1)

The conventional kinesin (kinesin-1) was the first cytoplasmic microtubule-associated motor to be identified in squid nervous tissue (Vale et al., 1985). It is a heterotetramer of two heavy chains (KHC, ~120 kD) and two light chains (KLC, ~65 kD). While single copy genes in invertebrates encode KHC and KLC, three genes encode KHCs in mammals: KIF5A (neuron-specific), KIF5B (ubiquitously expressed) and KIF5C (neuron-specific) (Xia et al., 1998). KLCs are also encoded by three genes: *klc1*, *klc2* and *klc3* (Rahman et al., 1998).

Each heavy chain consists of an N-terminal catalytic motor domain, the neck-linker and neck helix, the stalk and a globular tail domain. The catalytic motor domain contains the sequences necessary for ATP hydrolysis and microtubule binding (Kull et al., 1996). The neck linker and neck domains coordinate the movement of the two heads and specify the direction of movement along the microtubule (Cross, 2001). The stalk domain (coils 1 and 2) promotes the dimerization of the KHCs and is responsible for the association with the KLCs (Diefenbach et al., 1998; Verhey et al., 1998). The tail domain plays a role in regulation of the motor activity (Cross and Scholey, 1999). Each light chain consists of two domains: an α -helical heptad repeat region (Cyr et al., 1991) that binds to the heavy chain and a series of six tetratricopeptide repeats that mediate protein-protein interactions (Fig.2).

The chemical kinetic cycle of kinesin can be described as an ATP turnover cycle that modulates the affinity of the motor to MTs and its processive motion along MTs (reviewed by Cross, 2004; Mandelkow and Johnson, 1998). This general scheme displays similarities with that of myosin and actin filaments (Geeves, 1991). In the absence of microtubules, the dominant species is a kinesin-ADP state that is defined by its slow release of ADP (off rate, $k_{\text{off}} = 0.002 \text{ s}^{-1}$) and its weak microtubule binding (dissociation constant, $K_d = 10\text{--}20 \text{ mM}$).

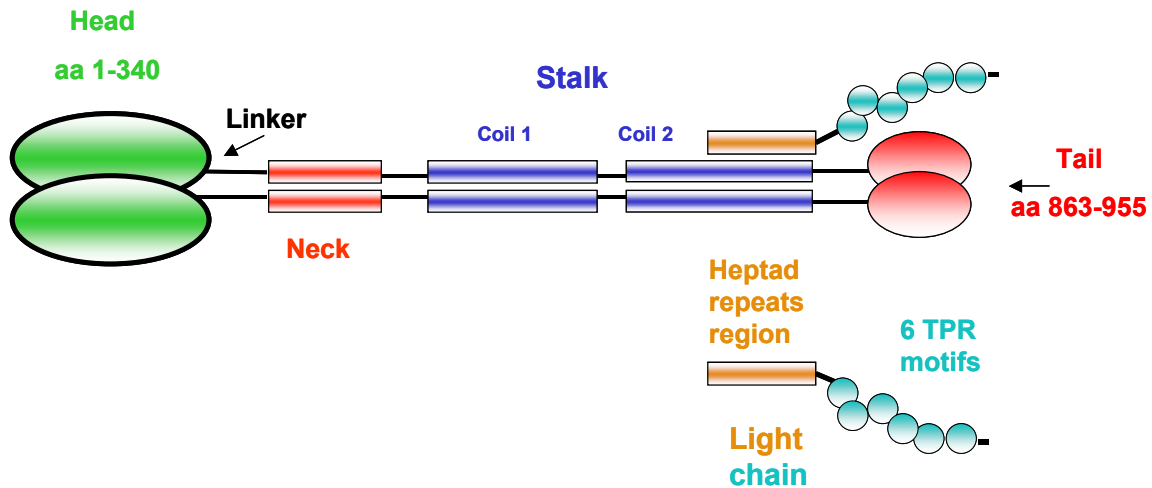


Fig. 2: Domain structure of rat kinesin-1. The numbering corresponds to the *Rattus norvegicus* sequence.

Once the motor binds to microtubules, a transition to a strong binding state occurs and ADP is rapidly released ($k_{\text{off}} = 300 \text{ s}^{-1}$). After the ADP is released, MgATP binds (on rate, $k_{\text{on}} = 2 \text{ mM}^{-1} \text{ s}^{-1}$). In this state of strong binding to microtubules, both ATP hydrolysis ($k_{\text{hyd}} = 100\text{--}300 \text{ s}^{-1}$) and phosphate release ($k_{\text{off}} > 100 \text{ s}^{-1}$) occur. Once the phosphate is released, the cycle is completed. The motor returns to the trapped ADP state and detaches from the microtubules (review: Cross, 2004).

The conventional kinesin is a processive motor or a 'porter' (Leibler and Huse, 1993) as it binds to the microtubules and takes several steps along them before detaching. It can complete more than 100 kinetic cycles while attached to the microtubules. Kinesin takes steps of 8 nm, equivalent to the axial spacing of tubulin heterodimers (Svoboda et al., 1993; Schnitzer and Block, 1997). Many models of how kinesin moves along the microtubules have been proposed including the 'walking' and the 'tighrope' models (Cross, 1995; Howard, 1996; Yildiz and Selvin, 2005). This aspect of kinesin motility is still under investigation.

The motor activity is inhibited when the tail folds back and interact with the catalytic motor domain (Hackney et al., 1992). Within the globular tail there is a region that is highly conserved in all conventional kinesins from fungi to humans. This region contains the IAK-motif (QIAKPIR in humans). Mutations in this motif

prevented the tail from folding and inhibiting the ATPase activity of the motor (Seiler et al., 2000). Furthermore, coexpression of the light chains can suppress the motor activity (Verhey et al., 1998).

1.2.1 Biological function of kinesin-1

In neuronal cells kinesin-1 mediates the fast anterograde axonal transport. Most proteins are synthesized in the cell body of the neuron and they then have to be transported distally to the axon and synapse. The kinesin-1 mediated fast axonal transport component moves vesicular proteins as well as mitochondria. The slow axonal transport component is thought to move cytoskeletal proteins. Kinesin-1 moves its cargo towards the plus-end of the microtubules, to the nerve terminal (review: Goldstein and Yang, 2000; Gunawardena and Goldstein, 2004).

Kinesin-1 is implicated in the transport of mitochondria and lysosomes (Tanaka et al., 1998), oligomeric tubulin (Terada et al., 2000), neurofilaments (Xia et al., 2003), mRNA (Tekotte and Davis, 2002), synaptic vesicles components (Ferreira et al., 1992) and viruses (Rietdorf et al., 2001; Diefenbach et al., 2002).

Mutations lacking KHC in *C. elegans* show dramatic movement defects (Patel et al., 1993). Mutations lacking KHC or KLC in *D. melanogaster* exhibit characteristic larval neuromuscular phenotypes, including posterior paralysis and flipping of the tail, and show organelle accumulations within their segmental nerves (Hurd and Saxton, 1996; Gindhart et al., 1998). Moreover, mutations in the human homologue of KIF5A (mouse KHC) lead to degeneration of neurons (Reid et al., 2002). Targeted disruption of the mouse kinesin-1 heavy chain, KIF5B, results in abnormal perinuclear clustering of mitochondria (Tanaka et al., 1998).

The structure of kinesin-1 implies that it can bind its cargo via the globular tail or the light chains. It has been demonstrated that the tail domain of the heavy chains directly binds to membranous cargo (Skoufias et al., 1994). Moreover, several proteins have been showed to bind directly to the tail domain of the heavy chain including kinectin, a mainly dendritic protein (Ong et al., 2000); Ran-binding protein 2 binds to KIF5B and KIF5C (Cai et al., 2001); the herpes simplex viral

protein US11 (Diefenbach et al., 2002); the synaptosome-associated proteins of 25 and 23 kDa (SNAP25 and SNAP23) (Diefenbach et al., 2002); the glutamate receptor-interacting protein GRIP1 (Setou et al., 2002) and the ribosome receptor p180 (Diefenbach et al., 2004).

Our knowledge about the attachment of cargoes to kinesin or the regulation of kinesin-cargo complexes during their movement on the microtubules is limited. The glycogen synthase kinase 3 (GSK3 β) was shown to inhibit the fast anterograde transport and released kinesin from its cargo by phosphorylating the KLCs (Morfini et al., 2002). Moreover, cdc2-like kinases have been shown to inhibit the fast anterograde transport (Ratner et al., 1998). Inhibition of CDK5 activity in axons was shown to lead to the activation of GSK3 by the protein phosphatase 1. This led to the phosphorylation of KLC (Morfini et al., 2004). The 14-3-3 proteins comprise a family of proteins that have been shown to regulate the JNK pathway (Nagata et al., 1998; Zhang et al., 2000) and to be involved in stress activation (Xing et al., 2000). It was demonstrated that the 14-3-3 protein bind directly to KLC2 in a phosphorylation-dependent manner (Ichimura et al., 2002), thus creating a possible link between these signaling pathways and kinesin in response to specific signal inputs (Ichimura et al., 2002). In vivo phosphorylation sites exist on both kinesin heavy and light chains.

1.2.2 Structure of the motor domain of kinesin-1

The first three-dimensional structure of a motor domain to be published was that of human kinesin-1 (Kull et al., 1996). This was followed by a number of others (Table 5) including rat kinesin (Sack et al., 1997) and *Neurospora crassa* kinesin-1 (Song et al., 2001). The general fold of all published kinesin motor domain structures is almost the same (Fig.3). A central β -sheet, consisting of eight β strands (β 1- β 8), supports the other structural elements of the motor. In the rat kinesin structure (Sack et al., 1997) the neck linker (strands β 9 and β 10) and the α -helical neck domain (helix α 7) are visible. The central β -sheet is covered with helices and loops on both sides: α 1, α 2a-L5- α 2b, α 3-L9- α 3a on one face, α 4-L12- α 5 and α 6 on the opposite face. The overall shape of the core domain (residues 2-325) is cone-like. In addition there are two lobes: the N-terminal lobe is formed

by helix α_0 and a three-stranded, antiparallel β -sheet ($\beta 1a, b, c$); the second lobe is formed by loop L8, $\beta 5a$ and $\beta 5b$.

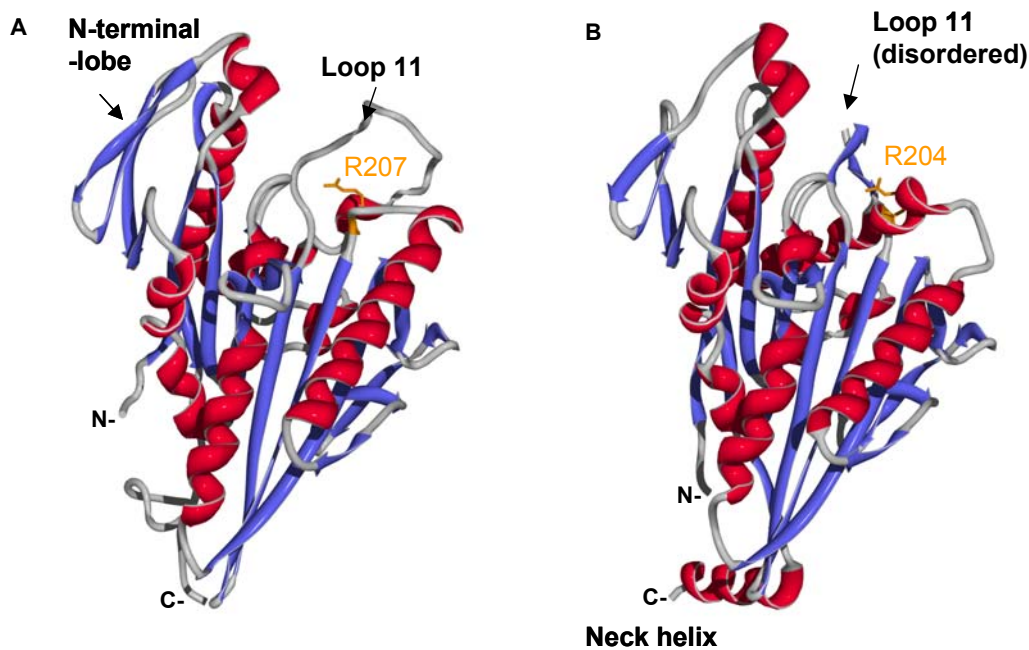


Fig. 3: Motor domain structures of *N. crassa* and *R. norvegicus* kinesin-1: (A), the motor domain of *Neurospora crassa* kinesin (Song et al., 2001); (B), the motor domain of rat kinesin (Sack et al., 1997). In orange the arginine that was mutated for this study is highlighted. The positions of loop 11 and the N-terminal lobe are also indicated. The structural models were produced by the programs: PDB viewer (Guex and Peitsch, 1997) and POV-Ray (<http://www.povray.org/>).

The nucleotide-binding site is formed by four structural elements N1-N4 (Sack et al., 1997): N1 is the so-called ‘P-loop’ ($^{86}\text{GQTSSGKT}^{93}$, rat kinesin-1 sequence) that binds oxygen atoms of the β - and γ -phosphates (Fig. 4 and 5); N2 and N3 ($^{199}\text{NEHSSR}^{204}$, and $^{232}\text{DLAGSE}^{237}$ respectively) are known as switch-1 and switch-2 in analogy to G-proteins and myosins. They function as γ -phosphate sensors. Their role is essential because their conformational changes and slight translocations result in movements of adjacent elements that transduce and amplify the motion. N4 at the C-terminus of $\beta 1$ ($^{14}\text{RFRP}^{17}$) is involved in nucleotide binding by interaction with the adenine moiety. Histidine H94 at the end of the P-loop also interacts with the base. In this study, point mutations of a critical arginine residue of the kinesin switch-1 region were generated. The purpose of this was to elucidate the mechanism of operation of kinesin on a structural basis.

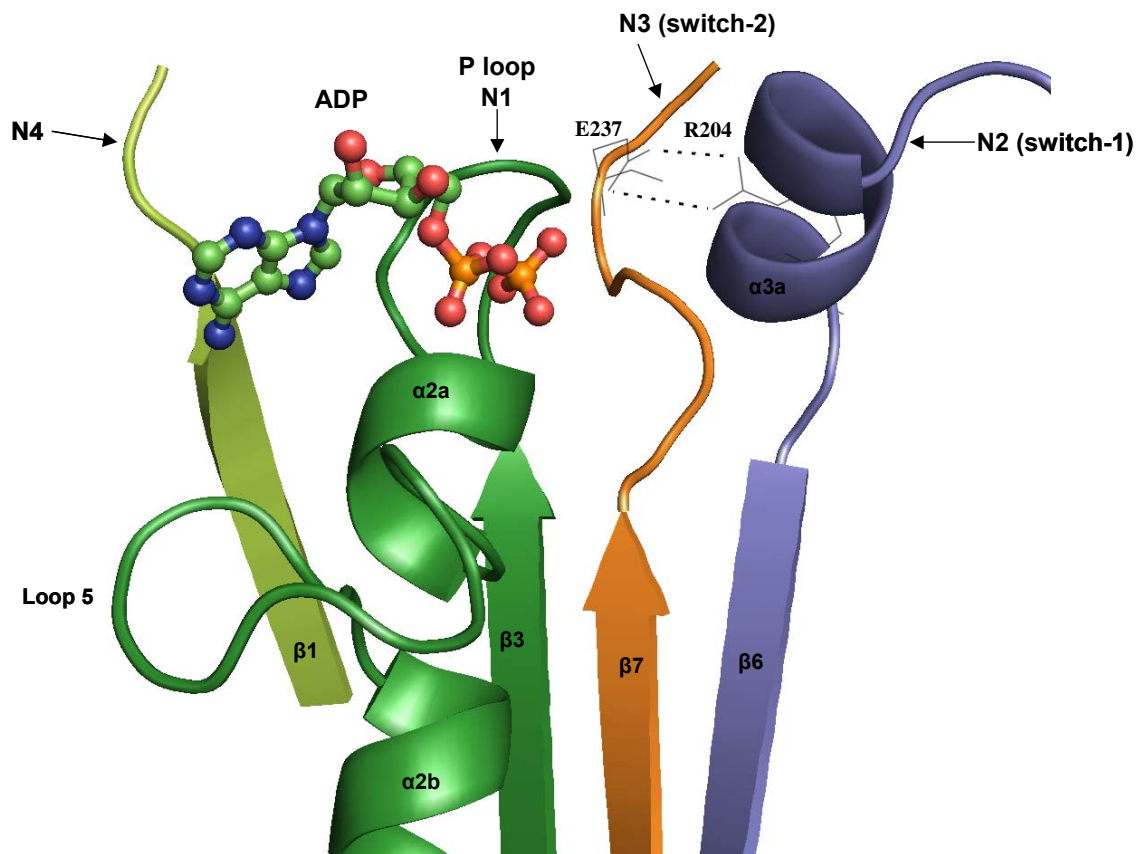


Fig. 4: The nucleotide-binding site of rat kinesin motor domain; it is defined by the four structural elements N1-N4 that are shown. The figure was created by the program PyMOL (Delano, 2002).

Point mutation analysis (Woehlke et al., 1997) and fitting crystal structures of kinesin motor domains into low-resolution electron density maps obtained by cryo-electron microscopy of microtubules saturated with kinesin (Hoenger et al., 1998; Hoenger et al., 2000; Kikkawa et al., 2000; Song et al., 2001) revealed which structural elements interact mostly with the microtubules: i) the $\beta 5a/b$ -Loop8 lobe, ii) the cluster that is formed by the helix $\alpha 4$, the loop 12 and the helix $\alpha 5$ ($\alpha 4$ -L12- $\alpha 5$) and iii) the loop L11 which is disordered in most structures with a few exceptions like the *Neurospora crassa* kinesin-1 structure (Song et al., 2001). It is suggested to be disordered in free kinesin and adopt a more rigid conformation when the motor interacts with the microtubules, linking the γ -phosphate sensor switch-2 with the microtubule-binding cluster $\alpha 4$ -L12- $\alpha 5$. Last, the neck helix $\alpha 7$ may participate in the microtubule interaction. In this study, a deletion mutant was

generated in rat kinesin-1 lacking loop L11. The purpose of this was to trigger a different packing of molecules within the crystal and/or to capture a different conformation of kinesin.

N4		
KINH_DROME	MSAEREIPAEDSIKVVVC FRPL NDSEEKAGSKFVVKFPNNVEENCISIAG----KVYLFD	56
KINH_CAEEL	-MEPRTDGAECGVQVFC IRPL NKTEKNADRFLPKFPS---EDSISLGG---KVYVFD	52
KF5C_RAT	-----ADPAECISKVMC FRPL NEAEILRGDKFIPKFKG---EETVVIGQG---KPYVFD	49
KINH_HUMAN	----MADLAECNIKVMC FRPL NESEVNRGDKYIAKFQG---EDTVVIAS----KPYAFD	49
KINH_NEUCR	-----MSSANSIKVVAR FRPQ N RV EIESGGQPI VT FQG---PD CT VDSKEAQ GS F T FD	52
	β1 α0 β1a β1b β1c	
P Loop (N1)		
KINH_DROME	KVFKPNASQEKVYNEAAKSIVTDVLAGYNGTIFAY GQTSSGK THTMEG-VIGDSVKQGII	115
KINH_CAEEL	KVFKPNTTQEQVYKGAAYHIVQDVLSGYNGTVFAY GQTSSGK THTMEG-VIGDNLGSGII	111
KF5C_RAT	RVLPPNTTQEQVYNACAKQIVKDVLEGYNGTIFAY GQTSSGK THTMEG-KLHDPQLMGII	108
KINH_HUMAN	RVFQSSTSQEQVYNDCAKKIVKDVLEGYNGTIFAY GQTSSGK THTMEG-KLHDEPEGMGII	108
KINH_NEUCR	RV F DM SC KQ SD I F DF SI K P T V DD ILNGYNG T V F AY GQT GAG K S Y T M MG T S I DDPDGR G V I	112
	β2 α1a α1b β3 α2a	
KINH_DROME	PRIVNDIFNHIYAMEVNLEFHIKVSYYEYIYMDKIRDLLDVSKVNLSVHEDKNRVPYVKGA	175
KINH_CAEEL	PRIVADIFNHIYSMDENLQFHIKVSYYEYIYNEKIRDLLDPEKVNLSIHEDKNRVPYVKGA	171
KF5C_RAT	PRIAHDFDHIYSMDENLEFHIKVSYYEYIYLDKIRDLLDVSKTNLAVHEDKNRVPYVKGC	168
KINH_HUMAN	PRIVQDIFNYIYSMDENLEFHIKVSYYEYIYLDKIRDLLDVSKTNLSVHEDKNRVPYVKGC	168
KINH_NEUCR	PR I V E Q I F T S I L SSAAN I E Y T V R V S Y M E I Y M E R I R D LLAPQNDNL P V H E E K N R G V V Y K G L	172
	α2b β4 β5 β5α β5β	
Switch-1 (N2)		
KINH_DROME	TERFVSSPEDVFEVIEEGKSNRHIAVTNM NEHSSRSH SVFLINVKQENLENQKKLSGKLY	235
KINH_CAEEL	TERFVGGPDEVLQAIEDGKSNRMVAVTNM NEHSSRSH SVFLITVKQEHQTTKKQLTGKLY	231
KF5C_RAT	TERFVSSPEEVMVDVIDEGKANRHVAVTNM NEHSSRSH SIFLINIKQENVETEKKLSGKLY	228
KINH_HUMAN	TERFVCSPEVMDTIDEGKSNRHVAVTNM NEHSSRSH SIFLINVKQENTQTEQKLSGKLY	228
KINH_NEUCR	LE I YVSS VQ EV Y EV M RRGGN R AR A VA T NM NQ E SS R SH S I F V I T I T Q K N V E T G S A K S G Q L F	232
	β5 α3 α3a β6 β7	
Switch-2 (N3)		
KINH_DROME	L V D L A G S E KVSKTGAEGTVLDEAKNINKSLSALGNVISALADGNKTHIPYRDSKLTRILQ	295
KINH_CAEEL	L V D L A G S E KVSKTGAQGTVLEAKNINKSLTALGIVISALAEGTKSHVPYRDSKLTRILQ	291
KF5C_RAT	L V D L A G S E KV-----NKSLSALGNVISALAEGTKTHVPYRDSKMTRILQ	238
KINH_HUMAN	L V D L A G S E KVSKTGAEGAVLDEAKNINKSLSALGNVISALAEBS-TYVPYRDSKMTRILQ	287
KINH_NEUCR	L V D L A G S E K V G K T G A S Q T L E A A K K I N K S L S A L G M V I N A L T D G K S S H V P Y R D S K L T R I L Q	292
	Loop11 α4α α4 α5 α5	
KINH_DROME	ESLGGNARTTIVICCSPASFNESETKSTLDFGRRAKTVKNVVCVNEELTAEWKR-----	350
KINH_CAEEL	ESLGGNSRTTIVICASPSPHFNEAETKSTLLFGARAKTIKNVVQINEELT-----	340
KF5C_RAT	DSLGGNCRTTIVICCSPSVFNEAETKSTLMFGQRAKTIKNTVSVNLELTAEWKKKYEKE	330
KINH_HUMAN	DSLGGNCRTTIVICCSPPSYNESETKSTLLFGQRAKTI-----	325
KINH_NEUCR	E S L G G N S R T T I I N C S P S S Y N D A E T L S T L R F G M R A K S I K N K A K V N A E L S P A E L K Q M L A K A	352
	α5 β8 α6	

Fig. 5: Alignment of primary sequences of kinesin-1 motor domains from various species: *D. melanogaster* (KINH_DROME), *C. elegans* (KINH_CAEEL), *R. norvegicus* (KF5C_RAT), *H. sapiens* (KINH_HUMAN), *N. crassa* (KINH_NEUCR). According to the structure of *Neurospora crassa* kinesin-1 (Song et al., 2001) the residues that comprise the β strands are colored blue; the residues that form α-helices are colored red. The P-loop, switch-1, switch-2 and N4 elements are shown in green. The Arg²⁰⁷ (*N.crassa* numbering) in α3a that was mutated for this study is indicated too. The alignment was performed using the CLUSTALW program version 1.8.

1.3 Kinesin light chains

Besides the conserved tail region that binds to cargo, the light chains (KLCs) of kinesin-1 mediate kinesin-cargo interactions via their tetratricopeptide repeat region. KLCs cloned from a variety of organisms show that they are highly conserved for most of their sequence (Fig.6).

Each KLC contains two distinct domains: a heptad repeat region and a series of six tetratricopeptide repeats (Fig.2). Heptad repeats promote coiled-coil interactions of proteins. There are 15 heptad repeats at the N-terminus of KLC that interact with the C-terminal region of the stalk domain of the kinesin heavy chain (Diefenbach et al., 1998). The tetratricopeptide repeats (TPRs) were identified as a α -helical structural motif in cell division cycle proteins in yeast (Sikorski et al., 1990).

Many different isoforms of KLCs are present in cDNA libraries (Beushausen et al., 1993; Cyr et al., 1991). Alternative splicing generates different carboxy-terminal 'tails', which can specifically associate kinesin to certain cargoes (Beushausen et al., 1993). A KLC isoform (KLC2) was found to associate specifically with mitochondria (Khodjakov et al., 1998), while two other isoforms (KLC-D and KLC-E) were shown to associate preferentially with the Golgi complex (Gyoeva et al., 2000). Moreover, an anti-KLC antibody inhibited binding of kinesin to brain vesicles in vitro (Yu et al., 1992).

An antibody against the TPR domain of KLC displaced the motor from its cargo (Stenoien and Brady, 1997). Mutants lacking KLC in *Drosophila melanogaster* die at the third larval instar stage and display accumulations of motors and vesicles in the axons (Gindhart et al., 1998).

KLC1_HUMAN	MSTMVYIKEDK----	LEK LTQDEIIISKTKQVIQGLEALKNEHNSILQSL	LETLKCLKKDD	56	
KLC1_RAT	MSTMVYMKEEK----	LEKLTQDEIIISKTKQVIQGLEALKNEHNSILQSL	LETLKCLKKDD	56	
KLC_STRPU	MSGSKLSTPNNSGGGQGNLSQE	QIITGTREVIKGLEQLKNEHNDILNSL	YQSLKMLKKDT	60	
KLC_DROME	-----	MTQMSQDEIIITNTKTVLQGLEALRVEHVSIMN----	GIAEVQKDN	41	
KLC_CAEL	-----	MSNMSQDDVTTGLRTVQQGLEALREEHSTISNTL	ETSVKGVKED	45	
KLC1_HUMAN	--	ESNLVEEKSNMIRKSLEMLELGLSEAQVMMALSNHLNAVESEKQKLRQVRRRLCQENQ		114	
KLC1_RAT	--	ESNLVEEKSSMIRKSLEMLELGLSEAQVMMALSNHLNAVESEKQKLRQVRRRLCQENQ		114	
KLC_STRPU	PGDSNLVEEKT	DIIEKSLESLELGLGEAKVMMALGHHLNMVEAEKQKLRQVRRRLVQENT		120	
KLC_DROME	-----	EKSMDLRKNIENIELGLSEAQVMMALTSHLQNI	EAEKHKLKTQVRRRLHQENA	93	
KLC_CAEL	---	APLPKQKLSQINDNLDKLVCGVDETSMLMVFQLTQGMDAQHQKYQAQRRRLCQENA		102	
KLC1_HUMAN	WL	REDELANTQQKLQKSEQSVAQLEEEKKHLEFMNQLKKYDDDISPSEDKD	TSTKEPLDD	174	
KLC1_RAT	WL	REDELANTQQKLQKSEQSVAQLEEEKKHLEFMNQLKKYDDDISPSEDKD	SSTKEPLDD	174	
KLC_STRPU	WL	RELAATQQKLQTSQENLADLEVYKHLEYMNSI	KKYDEDRTPDEE---	ASSDPLDL	177
KLC_DROME	WL	REDELANTQQKFQASEQLVAQLEEEKKHLEFMASVKKYDENQE	QDDACD-KSRTDPVVE	152	
KLC_CAEL	WL	RELSSTQIKLQQSEQMVAQLEEEENKHLKYMASI	KQFDDGTQSDTKTSVDVGPQPV	162	
TPR1					
KLC1_HUMAN	LFPNDE----	DDPGQG----	IQQQHSSAAAAAQGGYEIPAR	LRTLHNLVIQYASQGRY	225
KLC1_RAT	LFPNDE----	DDPGQG----	IQQQHSSAAAAAQGGYEIPAR	LRTLHNLVIQYASQGRY	225
KLC_STRPU	GFPED----	DDGGQADESYPPQPTGSGSVSAAAGGYEIPAR	LRTLHNLVIQYASQSR	231	
KLC_DROME	LFPDEE----	NEDRHN----	MSPTPPSQFANQTSGYEIPAR	LRTLHNLVIQYASQGRY	202
KLC_CAEL	ETLQELGFGPEDEEDMNASQFNQPTPANQMAASANVGYEIPAR	LRTLHNLVIQYASQGRY		222	
TPR2					
KLC1_HUMAN	EVAVPLCKQALEDLEKT	SGHDHPDVATMLNIALVYRDQNKYKDAANLLNDALAI	IREKTL	285	
KLC1_RAT	EVAVPLCKQALEDLEKT	SGHDHPDVATMLNIALVYRDQNKYKDAANLLNDALAI	IREKTL	285	
KLC_STRPU	EVAVPLCKQALEDLEKT	SGHDHPDVATMLNIALVYRDQNKYKEAGNLLHDALAI	IREKTL	291	
KLC_DROME	EVAVPLCKQALEDLERT	SGHDHPDVATMLNIALVYRDQNKYKEAANLLNDALSIR	KGTL	262	
KLC_CAEL	EVAVPLCKQALEDLEKT	SGHDHPDVATMLNIALVYRDQNKYKEAANLLNEALSIR	EKCL	282	
TPR3					
TPR4					
KLC1_HUMAN	GKDHPAV	AATLNNLAVLYGKRGKYKEAEPLCKRALEIREKV	LGKDHPDV	AKQLNNLALLC	345
KLC1_RAT	GRDHPAV	AATLNNLAVLYGKRGKYKEAEPLCKRALEIREKV	LGKDHPDV	AKQLNNLALLC	345
KLC_STRPU	GPDHPAV	AATLNNLAVLYGKRGKYKEAEPLCKRALEIREKV	LGKDHPDV	AKQLNNLALLC	351
KLC_DROME	GENHPAV	AATLNNLAVLYGKRGKYKDAEPLCKRALEIREKV	LGKDHPDV	AKQLNNLALLC	322
KLC_CAEL	GESHPAV	AATLNNLAVLFGKRGKFKDAEPLCKRALEIREKV	LGDDHPDV	AKQLNNLALLC	342
TPR5					
KLC1_HUMAN	QNQKGYYEEVEYYYQRALEI	YQTKLGPDDPNVAKTKNNLASCYLKQGGFKQAEATLYKEILT		405	
KLC1_RAT	QNQKGYYEEVEYYYQRALEI	YQTKLGPDDPNVAKTKNNLASCYLKQGGFKQAEATLYKEILT		405	
KLC_STRPU	QNQKGYYEEVEYYYQRALEI	YQTKLGPDDPNVAKTKNNLAAAYLKQGGKYKAEATLYKQVLT		411	
KLC_DROME	QNQKGYYDEVEKYYQRALDI	YESKLGPD	PNVAKTKNNLAGCYLKQGRYTEAEILYKQVLT	382	
KLC_CAEL	QNQKGYYEEVEKYYKRALEI	YESKLGPD	PNVAKTKNNLSSAYLKQGGKYKEAEELYKQILT	402	
KLC1_HUMAN	RAHER	EFG-SVDD-ENKPIWMHAEERECKGKQKDGTSFGYEGGWYKACKVDS----	PT	458	
KLC1_RAT	RAHER	EFG-SVDD-ENKPIWMHAEERECKGKQKDGSSFGYEGGWYKACKVDS----	PT	458	
KLC_STRPU	RAHER	EFGLSADDKDNKPIWMQAEEREE-KGKFKDNAPYGDYGGWHKAAKVDSSRSRSP		470	
KLC_DROME	RAHER	EFG-AIDS-KNKPIWQVAEEREKFDNRENTPYGEYGGWHKAAKVDSS----	PT	435	
KLC_CAEL	RAHER	EFG-QISG-ENKPIWQIAEEREENKHKG-EGATANEQAGWAKAAKVDSS----	PT	454	
TPR6					
KLC1_HUMAN	V	TTTLKNLALYRRQGGKFAEAETLEEAAMRSRKQGLDNVHKQR--	VAEVLNDPENMEKRR	516	
KLC1_RAT	V	TTTLKNLALYRRQGGKFAEAETLEEAALRSRKQGLDNVHKQR--	VAEVLNDPENVEKRR	516	
KLC_STRPU	V	TTTLKNLALYRRQGGKYDAEETLEECAMKSRRNALDMVRETK--	VRELLGQDLSTDVPR	528	
KLC_DROME	V	TTTLKNLALYRRQGMFEEAETLEDCAAMRSKKEAYDLAKQTK--	LSQLLTSN--	EKRR 490	
KLC_CAEL	V	TTTLKNLALYRRQGGKYEAETLEDVALRAKKQHEPLRSGAMGGIDEMSQSMMASTIGG		514	
KLC1_HUMAN	SRESLNVDVVKYESGP-----	DGGEVSVMSVEWNGGVSGRASFC-----		555	
KLC1_RAT	SRESLNVDVVKYESGP-----	DGGEVSVMSVEWNG-----		546	
KLC_STRPU	SEAMAKERHHRSSGTPRHGSTESVSYEKTDGSEEVSIGVAWKAKRKAKDRSRSIPAGYV			588	
KLC_DROME	SKAIK-----	EDLDFSEEKNAKP-----		508	
KLC_CAEL	SRNSMTTSTSTQTLKN-----	KLMNALGFNS-----		540	
KLC1_HUMAN	-----	GKRQQQQWPGRRHR-----		569	
KLC1_RAT	-----	MRKMKLGLVK-----		556	
KLC_STRPU	EIPRSPPHVLVENGDGKLRRSGSLSKLRASVRRSSTKLLNKLKGRESDDDGGMKRASSMS			648	
KLC_DROME	-----				
KLC_CAEL	-----				

Fig. 6: Alignment of KLCs from human, rat, *S. purpuratus*, *D. melanogaster* and *C. elegans*, respectively. The heptad repeat region is marked blue and the six TPR repeats with red. The alignment was generated by CLUSTALW version 1.8.

1.3.1 The tetratricopeptide repeat region of KLC

The tetratricopeptide repeats (TPRs) of KLCs have been shown to interact with a variety of proteins and link kinesin to its cargo. One of the goals in this study was the crystallization of the TPR domain of the rat kinesin light chain.

The TPR motif was first identified as a protein interaction module in cell division cycle proteins in yeast (Hirano et al., 1990; Sikorski et al., 1990). Its name denotes the number of the 34 residues that comprise the basic repeat (34 = tetratriaco in Greek). Since then, TPRs have been proved to be ubiquitous. The TPR motif is a degenerate 34 amino acid repeat. There is no strict consensus of its primary sequence. A preference for certain amino acids on the basis of their size, hydrophobicity and spacing exist. Particularly eight residues show a higher frequency of conservation: residues at positions 4, 7, 8, 11, 20, 24, 27 and 32 (Fig.7B).

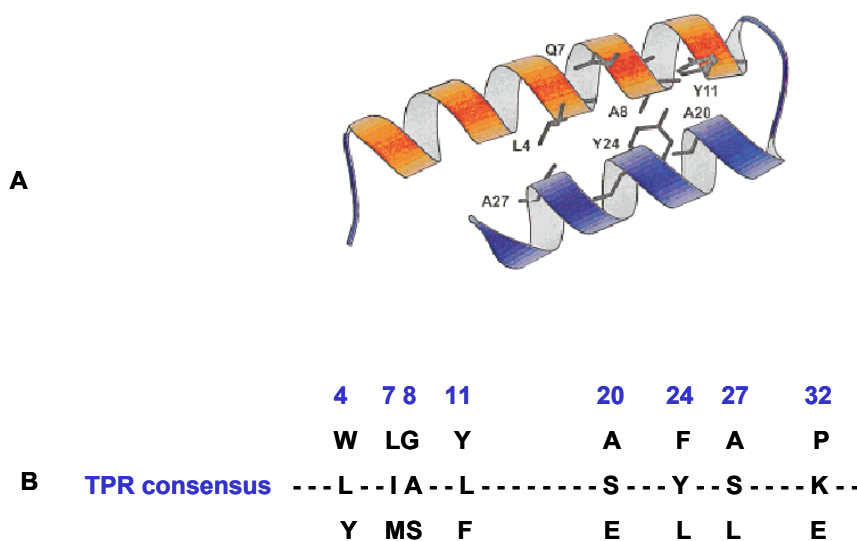


Fig. 7: The TPR motif: (A) the helix-turn-helix conformation of a single TPR motif. Consensus residues that are essential for the packing are visible. (Blatch and Lassle, 1999); (B) the consensus sequence of a TPR.

TPR- containing proteins participate in a broad range of functions and are often arranged in tandem repeats (review: Blatch and Lassle, 1999; D' Andrea and Regan, 2003). The first structure of a TPR to be solved was the three-TPR domain of protein phosphatase 5 (Das et al., 1998). It showed that the motif adopts a helix-turn-helix arrangement, with adjacent motifs packed in a parallel fashion, resulting in a spiral of repeating anti-parallel α -helices (Fig.7A and 8). The two helices are named A and B and span consensus residues 4, 7, 8, 10 and 11, as well as 20, 24 and 27, respectively. This packing generates an amphipathic channel (Fig.8). The surface of the channel is formed by the side-chains of the residues of helix A, while residues of both helices form the opposite side. A number of other structures showed that although the general fold is maintained, some variety is also observed: short amino acid insertions, modified loop regions or length-changing helices.

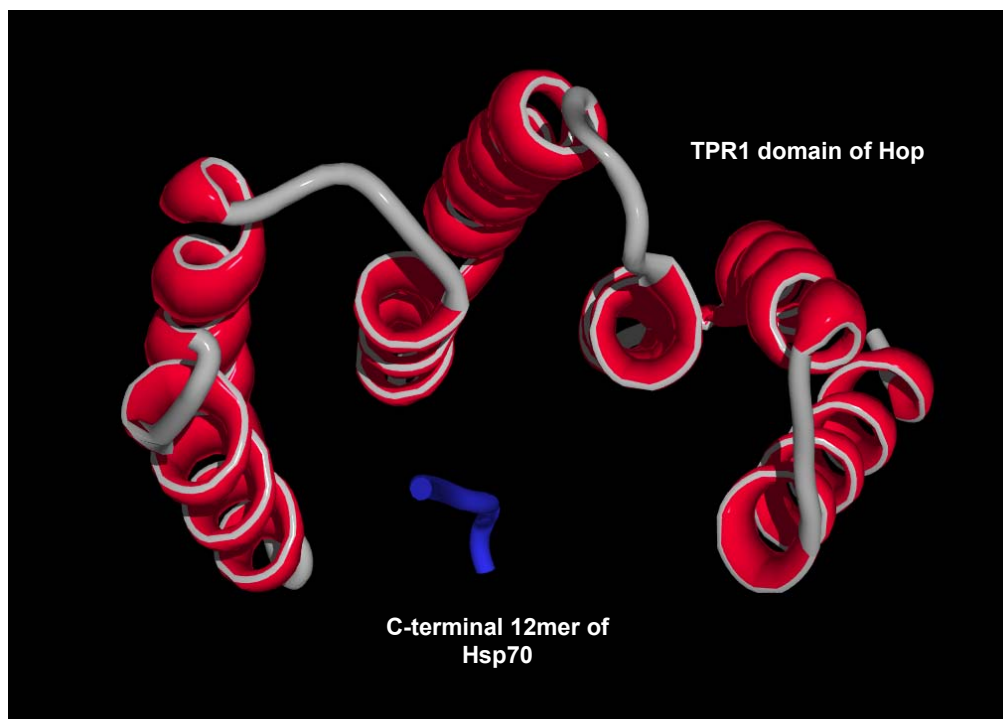


Fig. 8: A TPR - ligand interaction paradigm. Three adjacent TPRs in the Hop protein (in red) form an amphipathic channel; within this groove the Hsp70 c-terminal 12mer (in blue) is accommodated in an extended conformation (Scheufler et al., 2000).

A number of proteins were shown to bind directly to the TPR domain of KLCs, including the heat shock cognate protein 70 (Hsc70). The binding of Hsc70 to the TPR domain of KLCs results in the release of kinesin from its cargo (Tsai et al., 2000). A breakthrough in the kinesin field was achieved when the c-Jun NH2-terminal kinase interacting proteins (JIPs) were identified as binding partners for KLCs (Verhey et al., 2001; Bowman et al., 2000). The JIPs are scaffolding proteins for the c-Jun NH2-terminal kinase-signaling pathway. JIP3 was found to bind directly to the TPRs of KLCs and its mutation caused organelles to accumulate in axons (Bowman et al., 2000). JIP-1 and JIP-2 bind to the TPRs via their carboxyl-terminus. JIP-3 interacts via internal sequences (Verhey et al., 2001). Mutations of JIP-1, that inhibit binding to the TPRs, influence the localization of JIP-1 at the nerve terminal, thus JIPs are considered as cargo for kinesin.

The JIPs are also suggested to serve as adaptors between kinesin and its cargoes. As scaffolding proteins in the JNK signaling pathway they can bind to the mitogen activated protein kinase kinase kinase (MAPKKK), MAPKK and MAPK components of the pathway. In addition, JIP-1 binds to the nucleotide exchange factor of the G protein Rho (RhoGEF), and JIP-1 and -2 bind to the cytoplasmic domains of transmembrane receptors such as ApoER2, the receptor for the Reelin ligand that controls neuronal migration (Kamal et al., 2000; Verhey et al., 2001).

The amyloid precursor protein (APP), a transmembrane protein that plays an important role in development of the Alzheimer's disease, is thought to be transported by kinesin-1 in axons by binding directly to the TPR region via its cytoplasmic c-terminal domain (Kamal et al., 2001). Additional genetic data from mice and *Drosophila* suggest that APP is required for kinesin-1 mediated transport in axons (Gunawardena and Goldstein, 2001). It is thought to act as a receptor for kinesin-1 (Gunawardena and Goldstein, 2001) and mediate the transport of a subclass of vesicles that contained BACE, presenilin- 1, synapsin-1, GAP43, and TrkA (Kamal et al., 2001).

1.4 Aim of this study

Aim of this study was to contribute structural information about different domains of the motor protein kinesin-1, using the X-ray crystallography technique. The motor domain structure of kinesin-1 from various organisms has been determined, while biochemical studies have tried to elucidate the mechanism by which the energy from the hydrolysis of ATP is translated to movement. Based on kinetic data that demonstrated the importance of an arginine (Arg²⁰⁴ in rat) within the region switch-1 of the kinesin-1 for the motor ATPase activity, the microtubule attachment and the coordination of the two motor domains within the dimer, this residue has been substituted in a series of mutants. Crystallization of these could provide insight into the conformational changes in the active site of the motor. This could in turn increase the understanding of how the motor operates.

One more construct was generated where loop L11 was deleted. This loop is known to be critical for the microtubule binding and is disordered in most of the kinesin motor domain structures. Crystallization of this mutant could lead to different packing of molecules or 'force' the motor to adopt a different conformation maybe of biological importance, since the loop is suggested to be disordered in free kinesin.

The crystallization of the light chain and in particular its TPR was also attempted in this study. The purpose of this was to reveal how kinesin interacts with its cargo. To this end, a number of constructs were generated and crystallization trials were carried out.

The TPR motif is known to play a critical role in protein-protein interactions and in the assembly of multiprotein complexes. Crystallization of the KLC TPR domain has not yet been achieved. In light of the link between the KLC TPR domain and APP or JIPs, it would be interesting to determine the structural basis of these interactions. The successful crystallization of the TPR domain of KLC with one of its binding partners is an aim that has not yet been accomplished.

2 Materials and methods

2.1 Materials

2.1.1 Chemicals

All used chemicals were of the highest purity available (ACS grade) and were purchased from the following companies:

Amersham Pharmacia Biotech

AppliChem

Fluka

Kodak

Merck

New England Biolabs

Qiagen

Sigma

In addition, chemicals for crystallization were purchased from the following companies as reformulated screens or separate reagents:

Molecular Dimensions

Hampton Research

Jena Biosciences

2.1.2 Enzymes

All restriction enzymes used for DNA engineering and the T4 ligases were purchased from the companies New England Biolabs, United States Biochemical and Stratagene. The BP-clonase and LR-clonase enzyme mixtures were purchased from Invitrogen.

2.1.3 Bacterial strains

Strain	Genotype	Features
XL2-Blue	recA1 endA1 gyrA96 thi-1 hsdR17 supE44 RelA1 lac[F' proAB lacI ^q ZΔM15 Tn10 (Tet ^r) Amy Cam ^r] ^a	Host for cloning and plasmid propagation. From Stratagene
DH5α Library Efficiency	F'φ80lacZ ΔM15 Δ(lacZYA-argF)U169 recA1endA1 hsdR17 (r _k m _k ⁺)phoA supE44 thi-1gyr A96 relA1 λ	Host for cloning and propagation of Gateway vectors. From Invitrogen
BL21(DE3)	E.coli B F ⁻ dcm ompT hsdS(r _B ⁻ , m _B ⁻) gal λ(DE3)	Host for high level expression of T7 promoter containing plasmids. Methionine auxotrophe. From Novagen
BL21-Codon-Plus(DE3)-RIL	E.coli B F ⁻ ompT	High yield expression in T7 promotor-containing plasmids. T7 RNA polymerase is carried on bacteriophage λ(DE3), which is integrated in the genome of BL21. It provides the tRNA for the following rare codons: AGA and AGG (R), AUA (I) and CUA (L) (Stratagene).
BL21-AI	F ⁻ ompT hsdS(r _B ⁻ , m _B ⁻) dcm araB:T7RNAP-tetA	The T7 RNA polymerase gene is contained in the araB locus of the araBAD operon, allowing the regulation of the expression of the T7 RNA polymerase by the sugars L-arabinose and glucose. Glucose represses basal expression. The strain is suitable for high yield expression from T7 based expression vector (Invitrogen).
AD494	Δara-leu7967 ΔlacX74 ΔphoAPvull phoR ΔmalF3 F'(lac ⁺ pro) trxB:kan	A thioredoxin reductase mutation trxB enables disulfide bond formation, providing the potential to produce properly folded, active proteins (Novagen).
DH10Bac™	Not available	Generation of recombinant bacmids for baculovirus expression system. Contains a baculovirus shuttle vector with a mini-attTn7 target site and a helper plasmid. From Invitrogen.

Table 1: Cell strains and feature list. The first column lists the names of the E.coli strains used for cloning, vector propagation and protein expression; the second column contains the genotype and the third some remarks about the purpose and their features.

Table 1 shows the bacterial strains used in this study: XL2-Blue (Bullock, 1987) and library efficiency DH5 α (Hanahan, 1983), were used as cloning hosts, BL21 (DE3) (Studier et al., 1990), BL21- Codon Plus (DE3) RIL, AD494 (Derman et al., 1993) and BL21 AI (Studier, 1986, Lee et al., 1987) were used for protein expression.

2.1.4 Cloning Vectors

Most inserts used in this study were amplified by PCR and cloned into the pDONR201 vector of the recombination-based GatewayTM cloning system (2.2.9). A table for all vectors used in this study follows (Table 2).

2.1.5 Expression Vectors

The expression vectors used in this study for the high-yield expression of recombinant proteins carry cloned inserts under control of the T7 promoter. Thus, only *E.coli* strains engineered to express the T7 RNA polymerase upon IPTG induction can be used for expression, eg BL21 (DE3). The GatewayTM vectors used in this study are of 2 types: the donor vector pDONR201 and the destination vectors pDEST15/17/20 (Table 2). The BL21 AI strain that was used for expression of Gateway expression vectors is arabinose inducible (*araBAD* promoter).

Vector	Expression System	Features
pDONR201	Used for generation of entry clone	Kan ^R
pDEST15	<i>E.coli</i>	Amp ^R , N-terminal GST tag
pDEST17	<i>E.coli</i>	Amp ^R , N-terminal His ₆ - tag
pDEST20	SF9 insect cells	Polyhedrin promoter, N-Terminal GST tag, Tn7 element, Amp ^R , Cm ^R , Gen ^R
pET16b	<i>E.coli</i>	Amp ^R , N-terminal His ₁₀ -tag
pNG2 (pET derived)	<i>E.coli</i>	Amp ^R , No tag

Table 2: A summary of the vectors used in this study.

2.1.6 Media

Antibiotics: Ampicillin (15 mg/ml stock solution) in ddH₂O, 50 µg/ml working concentration, Kanamycin (25 mg/ml stock solution) in ddH₂O, 25 µg/ml working concentration and Carbenicillin (15 mg/ml stock solution) in ddH₂O, 50 µg/ml working concentration.

Luria-Bertani (LB) medium: 1% (w/v) bacto-tryptone, 0.5% (w/v) bacto-yeast extract, 1% (w/v) NaCl; sterilized by autoclaving. Purchased from Life Technologies as dried powder.

LB agar plates: LB medium and 1.5 % (w/v) bacteriological agar. Sterilized by autoclaving. Plates were poured when temperature reaches 50°C.

SOB medium: 2% (w/v) bacto-tryptone, 0.5% (w/v) bacto-yeast extract, 0.5 % (w/v) NaCl. A solution of KCl was added to a final concentration of 25 mM. The pH was adjusted to 7 with 5N NaOH and the solution sterilized by autoclaving. Before use a sterile solution of MgCl₂ was added to a final concentration of 0.1 M.

SOC medium: SOB medium supplemented with 1.8 % (v/v) glucose. Sterilized by filtration through a 0.22 µm filter.

2.1.7 Crystallization

Crystallization supplies and tools:

Supplies and tools including crystallization plates, siliconised cover slides (round and square slides of different thickness), sealing tape, forceps and tools for crystal manipulation were purchased from Hampton Research.

Crystallization solutions:

Crystallization screens were purchased from Hampton Research:

Crystal Screen 1	Additive screen 1
Crystal Screen 2	Additive screen 2
PEG/Ion Screen	Additive screen 3
Grid Screen NaMalonate	Index Screen
Grid Screen PEG6000	Grid Screen Ammonium sulfate

Crystallization screens that were purchased from Jena Biosciences:

JB Screen

2.1.8 Equipment and accessories

Centrifuges:

Cold centrifuge J2-21 M/E	Beckman
Ultracentrifuge	Beckman
Table centrifuge 5402	Eppendorf
Table centrifuge 5415C	Eppendorf

Rotors:

JA-10, JA-20	Beckman
45Ti	Beckman

Äkta purification system and corresponding accessories:

Mono-S column HR10/10	Pharmacia
HiLoad™ 16/60 Superdex™ 200	Pharmacia
Mono-Q column HR10/10	Pharmacia
Ni-NTA Superflow	QIAGEN
GST-sepharose beads	Amersham Biosciences
Super loop 2ml, 50ml	Pharmacia

Other equipments and accessories:

French Press	Aminco
Gel dryer model 583	Bio-Rad
Incubator shaker innova 4300	New Brunswick Scientific
UV/Visible Spectrophotometer Ultraspec1000	Pharmacia
Dynamic Light Scattering	Firma Dierks and Partner

2.2 Molecular biology and microbiological methods

2.2.1 Culture and storage of *E.coli*

Bacteria were grown on LB agar plates or in liquid LB medium at 37°C unless stated otherwise. For positive selection, media and plates were supplemented with appropriate antibiotics in the following concentrations: 50 µg/ml ampicillin, 50 µg/ml carbenicillin, 25 µg/ml kanamycin. All media and manipulation tools were sterilized by autoclaving, or if heat-labile, by filtration through a 0.22 µm filter. For permanent storage at –80°C, cell strains were flash-frozen in liquid nitrogen after mixing with glycerol for cryoprotection. BL21 and XL2blue strains were preserved in 30% (v/v) glycerol in LB; DH5α strain in 50% (v/v) glycerol in LB.

2.2.2 Transformation of *E.coli* strains

Transformation by heat-shock

E.coli cells competent for transformation were either purchased from the companies as stated in table 1 or prepared in the laboratory.

XL2-Blue, DH5α library efficiency and BL21 AI cells were transformed by the heat-shock method: 20-100 ng of DNA was added to an aliquot of competent cells (~20-50 µl) previously thawed on ice for approximately 10 minutes. The mixture of DNA and competent cells was incubated on ice for 30 minutes. After the heat-shock at 42°C for 30 seconds, 200-400 µl of SOC medium were added and the cells were incubated at 37°C for 1 hour with shaking. Finally,

100-200 μ l cells were plated on a selective medium plate and incubated overnight at 37°C.

Transformation by electroporation

Electrocompetent *E.coli* cells BL21 (DE3), BL21- Codon Plus (DE3) RIL and AD494 were prepared within the laboratory according to the procedure of Dower et al., 1988.

Transformation: 10-20 ng of DNA was added to an aliquot of cells (20 μ l), previously thawed on ice for approximately 10 minutes. It was then placed at the bottom of a 0.2 cm electroporation cuvette. The cuvette was placed inside an electroporator (BTX electro cell manipulator 600, Invitrogen) and the electro-shock was performed at 2500 volts and 129 Ohm resistance. The time constant of discharge under these conditions was 3-4 ms. After the discharge, the cells were quickly placed on ice and 200 μ l of SOC medium was added. Then the cells were incubated for 1 hour at 37°C with shaking.

The electroporation method is a highly efficient method. Therefore, the cells were further diluted in a ration 1:100-1:500 with SOC medium before plating. Furthermore, the salt concentration in the transformation solution was maintained at less than 1mM in order not to affect the transformation efficiency.

2.2.3 Isolation of plasmid DNA

All plasmid mini-preparations were carried out with the Invisorb Spin Plasmid Mini Kit (Invitex) following the user manual. All midi-preparations were carried out with the Nucleobond AX Kit (Macherey-Nagel) according to the manual.

2.2.4 Determination of DNA concentration and purity

The concentration and the degree of purity of double stranded plasmid DNA was determined based on the Beer-Lambert Law by measuring the absorbance at 260 nm and 280 nm:

$$A_{260} = \epsilon_{260} c l \text{ and } A_{260} \times 50 = \mu\text{g/ml (when } l = 1 \text{ cm)}$$

The molar absorptivity coefficient is calculated from the sequence of the oligonucleotide. A_{260} is the absorbance at 260 nm, ϵ_{260} is the molar absorptivity coefficient, c is the molar concentration and l is the optical path. For a protein-free and RNA-free solution of DNA the ratio of A_{260}/A_{280} should be close to 2. Protein contaminants would decrease this ratio, whereas RNA contamination would increase it.

To further estimate the concentration and purity of DNA preparations agarose gel electrophoresis was carried out.

2.2.5 Ligation reaction

The components below were mixed in a 500 μ l Eppendorf tube. The mix was incubated at 16°C overnight. The molar ratio between the digested vector and the digested insert was around 1:5.

10x Buffer	1 μ l
Ligase (5U/ μ l)	1 μ l
Digested vector	200ng
Digested insert	200ng
H ₂ O	x μ l
Total volume	10 μ l

2.2.6 Restriction analysis of DNA

DNA samples were analyzed with the use of restriction enzymes. In each case the sample was mixed with the desired restriction enzyme/s and the proper reaction buffer in a final volume of 20 μ l. The mixture was incubated for 45 min at 37°C. The cut DNA was loaded immediately onto an agarose gel to check the result of the restriction analysis.

2.2.7 DNA sequencing

DNA sequencing reactions were performed to confirm the sequence of a construct and the existence of mutations, especially after PCR amplification steps. The reactions were performed using fluorescent dye labeling and the Sanger Method (Sanger et al., 1977) in a Robocycler Gradient 96 (Stratagene) PCR machine. The protocol for the temperature cycle reaction was:

Terminator ready reaction mix	8	μl
dsDNA	500	ng
Primer (10pmol/ μl)	1	μl
ddH ₂ O to a final volume of	20	μl

The PCR program for sequencing was:

1. Denaturation	96 ⁰ C	10	sec	} x25
2. Annealing	45 ⁰ C	5	sec	
3. Elongation	60 ⁰ C	4	min	

After the reaction, the DNA was precipitated by using the Pellet Paint NF Co-Precipitant (Novagen). To 20 μl reaction volume, 2 μl Pellet Paint NF Co-Precipitant and 2 μl of 3M NaAcetate (pH 5.2) were added. Then, 40 μl ethanol was added and the mixture was incubated at room temperature for 2 min. The sample was centrifuged at 13 krpm for 5 min. The dark blue visible pellet was washed two times with 70% and 100% ethanol and centrifuged at 13 Krpm for 5 min. Last, the pellet was air dried and resuspended in 30 μl of HPLC-grade dd H₂O.

The ABI PRISM 310 Genetic Analyser (PE Applied Biosystems) was used to sequence the DNA. The sequencing results were analyzed with the NTI vector software (Informax).

2.2.8 Mutagenesis of DNA

All mutations described in this thesis were created by site-directed mutagenesis, which was performed using the Quick Change Site-Directed Mutagenesis Kit (Stratagene). The method utilizes the Pfu Ultra High Fidelity polymerase to replicate the parental plasmid by using two synthetic oligonucleotide primers containing the desired mutation.

The primers, each complementary to opposite strands of the vector, are extended during temperature cycling by the DNA polymerase. Temperature cycling generates copies of the plasmid by linear amplification, incorporating the mutation of interest. The temperature cycling reaction was performed as follows:

10x Pfu Ultra High Fidelity buffer	2 μ l
ds DNA template (25ng/ μ l)	5 μ l
dNTPs (2.5 mM)	2 μ l
Primer 1 (0.5 pmoles/ μ l)	1 μ l
Primer 2 (0.5 pmoles/ μ l)	1 μ l
Pfu polymerase (2.5 U/ μ l)	0,5 μ l
ddH ₂ O to a final volume of	20 μ l

As a control reaction, cells transformed with the pWhitescript plasmid will appear as white colonies on an LB-ampicillin plate, because the β -galactosidase activity has been eliminated. The two mutagenic primers restore the β -galactosidase activity; therefore cells containing the mutated plasmid will appear blue on the plates.

The temperature cycling program used was:

Step	Cycles	Temperature	Time
1	1x	95°C	30 seconds
2	16x	95°C	30 seconds
3		55-58°C	1 minute
4		68°C	12 minutes

Step 2, which is the primer annealing temperature, was calculated each time according to the melting temperature (T_m) of the primers, while the step 4 extension time was calculated accordingly to the length of the plasmid. Next, a treatment with DpnI endonuclease was carried out to digest the parental methylated DNA template, allowing the selection of the newly synthesized DNA containing the mutation. A portion of 2-4 μ l was used to transform XL2-Blue cells.

2.2.9 Gene cloning using the Invitrogen Gateway™ Technology

The Gateway™ cloning technology is a method that enables rapid cloning of a gene in various expression systems. Gateway™ uses a well-characterized lambda phage site-specific recombination system, thus restriction enzymes and ligases are not required in any step. Two reactions, 'BP-reaction' and 'LR-reaction', constitute the Gateway™ Technology.

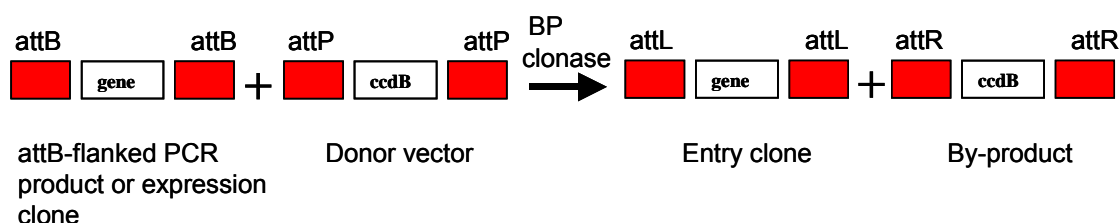
Reaction	Reaction sites	Product	Product Structure
BP reaction	attB x attP	Entry clone	attL1-gene-attL2
LR reaction	attLx attR	Expression clone	attB1-gene-attB2

Table 3: Summary of reactions and nomenclature in Gateway™

First, an entry clone is generated from a PCR product that spans the attB recombination sequences (BP reaction, see Fig.9). Once a positive clone is verified and sequenced the second step is to transfer the gene of interest to a variety of expression vectors (LR reaction, see Fig.9), featuring different tags and/or different expression systems (e.g. *E.coli*, insect cells). The ccdB gene

interferes with the E.coli DNA gyrase, thus, every cell that takes up an unreacted vector that still carries the *ccdB* gene or a by-product, will fail to grow.

BP reaction to generate an entry clone



LR reaction to generate an expression clone

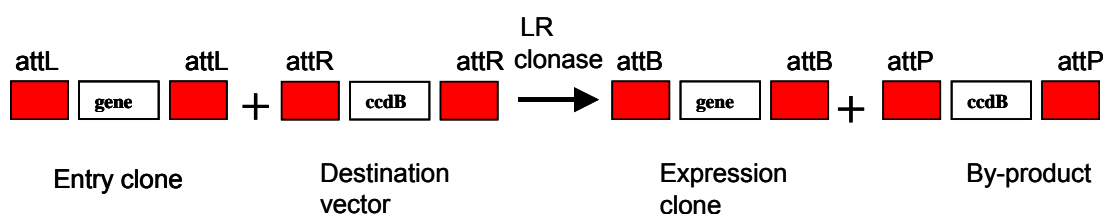


Fig. 9: Overview of the Gateway™ technology.

Generation of kinesin light chain constructs with the Gateway™ technology

The first step to enter the system was to obtain the proper PCR product with the required attB recombination sequences. In this study, this was achieved in two steps, with a set of primers specific for each construct and a set of primers for the completion of the attB sites. The resulting DNA sequence would be **attB –TEV cleavage site – fragment of interest – attB**. The encoding sequence of the TEV cleavage site is incorporated in order to be able to remove the tag after expression and purification of the relevant protein, if necessary. The primers were designed as follows:

Primers to amplify the ORF:**attB1-Tev-f (forward primer)**

5'-**AAAAAGCAGGCT**TC **GAAACCTGTATTTTCAGGGC**- coding sequence-3'

AttB1 (12 bases) - 2 bases for frame - **TEV cleavage site**

12attB1-stop-r (reverse primer)

5'-**AGAAAGCTGGGTC** **TTA** – coding sequence-3'

AttB1 (13 bases) - **stop codon**

Adapter primers to generate complete attB sites :**AttB1-f (forward primer)**

5'-GGGGACAACCTTTGTACA**AAAAAGCAGGCT**-3'

AttB1-r (reverse primer)

5'-GGGGACCACTTTGTACA**AGAAAGCTGGGT**-3'

(The bold sequences show the part that hybridize with the first set of primers)

PCR reactions

The first PCR step is done with primers that do not have too long non-specific overhangs in order to obtain a high success rate in amplification. The attB sites that are needed, were generated with a second PCR step using the adapter primers.

1st PCR

200 ng template DNA

5 µl 10x reaction buffer

10 pmoles forward primer

10 pmoles reverse primer

2 µl of 12.5 mM dNTPs

ddH₂O up to 50 µl

The PCR program used was as follows:

Step	Time	Temperature	Cycles
Initial denaturation	1 minute	95°C	1x
Denaturation	15 seconds	95°C	10x
Annealing	30 seconds	Depends on each primer	
Extension	30 seconds	68 °C	

2nd PCR

10 µl of the first reaction are transferred to a new tube containing:

5 µl 10x reaction buffer

40 pmoles of attB1-f adapter primer

40 pmoles of attB1-r adapter primer

2 µl of 12,5 mM dNTPs

ddH₂O up to 50 µl

The cycling parameters for the second PCR were:

Step	Time	Temperature	Cycles
Initial denaturation	1 minute	95°C	1x
Denaturation	15 seconds	95°C	5x
Annealing	30 seconds	45°C	
Extension	30 seconds	68°C	
Denaturation	15 seconds	95°C	20x
Annealing	30 seconds	55°C	
Extension	30 seconds	68°C	

The PCR products were treated with DpnI in order to digest the template plasmid.

50 µl PCR product

5 µl 10x DpnI buffer

10 units DpnI

30 minutes at 37°C (digestion reaction)

15 minutes 65 °C (DpnI heat inactivation)

The PCR products were then checked with agarose gel electrophoresis and purified with the pellet paint protocol (refer to section 2.2.9).

BP reaction:

purified PCR product 200 ng

pDONR201 (150 ng/µl) 2.5 µl

5x BP reaction buffer 5 µl

BP-clonase enzyme mix 2 µl

ddH₂O up to 25 µl

The mixture was incubated at 25 °C overnight and the next morning 2 µl of proteinase K were added to stop the reaction. Next, 1 to 3 µl were used to transform DH5α library efficiency *E. coli* cells with a chemical protocol (refer to section 2.2.2). The clones were screened by setting up a PCR reaction with the attL1-f and attL2-r primers and by restriction analysis. Positive clones were then sequenced (section 2.2.7) using the primers attL1-f (proximal to attL1) and attL2-r (proximal to attL2) (see Appendix for primers' sequence). When a positive clone was identified, it was used for setting up an LR reaction in order to generate an expression clone.

LR reaction:

LR buffer 5x	4 µl
Destination vector (150 ng/ µl)	3 µl
Entry clone (150 ng/ µl)	1 µl
Topoisomerase I	0.5 µl
LR clonase mix	2 µl
ddH ₂ O up to	20 µl

The topoisomerase was added to relax the entry clone plasmid because a supercoiled state of entry vectors was often observed in agarose gel electrophoresis. The supercoiled state of DNA inhibits the LR reaction.

The mixture was incubated at 25°C overnight and the next day 2 µl of proteinase K were added to stop the reaction before using 1-2 µl to transform either DH5α library efficiency competent cells for plasmid propagation, or BL21 AI cells for expression of recombinant protein.

2.2.9.1 Generation of the recombinant baculovirus vector bacmid.GST.TPR1-6t

Following the procedure described in section 2.2.9 the plasmid pDEST15.TPR1-6t was generated, encoding the entire TPR domain and the tail of KLC-C. The pDEST20 vector contains the polyhedrin gene promoter

from the *Autographa californica* multi nuclear polyhedrosis virus and the mini-Tn7 elements for site-specific transposition into the bacmid DNA (Table 2). The plasmid was transformed into DH10BacTM cells (Invitrogen) with a chemical transformation protocol (section 2.2.2). This *E.coli* strain contains a baculovirus shuttle vector (bacmid) and a helper plasmid. Transposition occurred between the mini-Tn7 element of the pDEST20.TPR1-6t vector and the mini-att Tn7 target site on the bacmid, to generate bacmid-TPR1-6t. The reaction occurred in the presence of transposition proteins encoded by the helper plasmid. Clones that contain the recombinant bacmid were selected. The bacmid.GST.TPR1-6t was isolated and the presence of the KLC insert was verified by PCR analysis with M13 primers (Appendix). The recombinant bacmid was then used to transfect SF9 insect cells.

2.3 Protein methods

2.3.1 SDS-Polyacrylamide gel electrophoresis (SDS-PAGE)

SDS-PAGE was performed in the lab following a modified protocol (Matsudaira and Burgess, 1978; Laemmli, 1970). The stacking gel was 4% acrylamide and the separating gel was 10% or 17% (Table 4). Protein samples were diluted 1:1 in 2xSDS-PAGE loading buffer, and heated for 2 min at 95°C. Electrophoresis was carried out at 150V and maximal 35mA in SDS-PAGE running buffer (25mM Tris-HCl, 190mM Glycin, 0.1% (w/v) SDS). The gels were then stained in a 0.1% (w/v) solution of Coomassie brilliant blue R-250, 45% (v/v) methanol and 9% (v/v) acetic acid for 20 min on a shaking platform. Next, the gels were destained in an intensive destaining solution (50 % (v/v) methanol, 10% (v/v) acetic acid) for 20 min and for a minimum of 1 hour in a normal destaining solution (5% (v/v) methanol, 7.5% (v/v) acetic acid).

Molecular weight marker proteins were:

β-Galactosidase (116 kD), bovine serum albumin (66.2 kD), ovalbumin (45 kD), lactate-dehydrogenase (35 kD), restriction endonuclease Bsp98I (25 kD), lactoglobulin (18 kD) and lysozyme (14.4 kD).

	Stacking gel (4%)		10%		17%	
40% acrylamide/ bis-acrylamide (38/1)	5.4	ml	15	ml	25.6	ml
1M Tris-HCl pH 8.8	-		22	ml	22	ml
0.25 M Tris-HCl pH 6.8	27	ml	-		-	
H₂O	20.9	ml	22	ml	11.4	
10% SDS	0.54	ml	0.6	ml	0.6	ml
TEMED	0.108	ml	0.12	ml	0.12	ml
10% APS	0.15	ml	0.065	ml	0.065	ml

Table 4: Solutions for preparing SDS-PAGE gels

2.3.2 Western blotting

Western blotting was performed following a modified method within the lab (Towbin et al., 1979):

1. The SDS polyacrylamide gel was washed with blotting buffer for 10 minutes.
2. The protein was electro-transferred from the gel to the PVDF membranes (Millipore) with a current of 1mA/cm² for 30-60 minutes.
3. The membrane was blocked for 1 hour at 37°C with 5% milk powder/PBST.
4. The primary antibody was diluted into 5% milk powder/PBST and incubated with the PVDF membrane for 1 hour at 37°C. Then the membrane was washed three times with PBST.
5. The secondary antibody was diluted into 5% milk powder/PBST and incubated with the PVDF membrane for 1 hour at 37°C. Then the membrane was washed 3 times with PBST.
6. The substrate reaction was carried out with ECL Western blotting detection reagents. This generates the chemiluminescence that is detected by a light sensitive film (Hyperfilm).

2.3.3 Protein production

The following strategy was applied with every new expression construct: First, 5 ml LB supplemented with the appropriate antibiotics was inoculated with the desired expression strain and grown at 37°C overnight. The next morning this

culture was used to inoculate a new 100 ml LB culture, which was left to grow at 37°C, shaking at 280 rpm until OD₆₀₀=0.6. A sample of 1 ml was centrifuged and kept as a non-induced control and the rest was induced by adding 0.5 mM IPTG or 2% arabinose where necessary. The cultures were left to grow either for 3 hours at 37°C or at lower temperature 25-30°C overnight. Cells were then harvested by centrifugation at 8 Krpm for 5 min (Eppendorf 5810R).

2.3.4 Cell lysis and solubility test

Cells were lysed using a French press. First, they were thoroughly resuspended in lysis buffer (2-3 ml of buffer/100ml culture) and then they were transferred to a French press cell. Application of 20 000 PSI in two rounds ensured the lysis. Lysates were kept on ice and centrifuged at 14 krpm for 20 min at 4°C. A sample of the supernatant in which all soluble proteins were present and one of the pellet resuspended in lysis buffer and were mixed 1:1 with 2x SDS-PAGE sample buffer loaded onto an SDS gel together with samples before and after induction. In this way expression and solubility of the desired protein was tested in a first approach. For large-scale production of proteins, cultures of 2-6 Litres were grown as described above.

2.3.5 Sf9-Cell culture

Spodoptera frugiperda (Sf9) cells double normally every 18-24 hours, when they grow in medium with 10% FCS (refer to Appendix). The Sf9 cell cultures were grown in spinning culture bottles (suspension culture) or in cell culture flasks (adherent cells) at 27°C and in darkness. The cells were counted three times a week to monitor that their density reaches 0.5×10^6 cells/ml.

2.3.5.1 Baculovirus expression system

For the expression of the GST.TPR1-6t construct in Sf9 cells, the baculovirus system “BaculoGold” was used (PharMingen). As transfer plasmid, a modified form of pVL1392 was employed. Viral particles were produced by coprecipitation of 1 µg transferplasmid and 0.25 µg linearized “BV BaculoCold DNA” to 2×10^6 Sf9 cells, followed by incubation at 27°C in TNM-FH Medium (Pharmingen). The Virus supernatant was filtrated through a membrane (0.22-0.45 µm) and the working solution was stored at 4°C.

2.3.5.2 Expression of GST.TPR1-6t in SF9 insect cells

Cultures of SF9 cells with a density of 1.8×10^6 cells/ml were transfected with 1 ml of virus carrying the gene of interest and cells were harvested after 60 hours with centrifugation at 12 krpm for 15 minutes. The cells were suspended in PBS and were frozen instantly in liquid nitrogen and thawed immediately in a water bath at 50°C. This freeze and thaw procedure was repeated 3 times. The solution was then centrifuged at 4°C at 14 Krpm for 15 minutes. The supernatant was loaded onto GST spin columns to purify the GST- tagged protein.

2.3.6 Chromatography

Purification of proteins was performed by fast performance liquid chromatography (FPLC) using Äkta purifier and Äkta primer machines (Pharmacia).

2.3.6.1 Ni-NTA affinity chromatography

Immobilised metal affinity chromatography (IMAC) makes use of the binding properties of metals towards proteins for purification purposes; nickel-nitriloacetic (Ni-NTA) resin (QIAGEN) contains chelated nickel, which is able to specifically bind to stretches of polyhistidine in proteins. Many expression systems include a tag of six histidines either at the N- or at the C-terminus or

on both. One ml of resin needs to be used per every 20 mg of tagged protein, since the maximum capacity of 50 mg protein/ml resin is highly dependent on individual cases.

The resin was cast on a Pharmacia self-packed XK26 column or a batch protocol was performed with the use of a frit. The material was rinsed with ddH₂O to remove the 20% (v/v) ethanol preservative and equilibrated with the appropriate loading buffer. The buffers should not contain DTT or other reducing agents in high concentrations, or be too dense with cell debris and DNA, as this might strip the nickel off the column. Once the column is equilibrated, the sample was loaded two times. After loading, the column was washed with loading buffer equating to 10 column volumes and finally, the protein was eluted with 3 volumes of elution buffer. All buffers are listed in the Appendix.

2.3.6.2 GST affinity chromatography

The glutathione-S-transferase affinity (GST) resin (Pharmacia) is an agarose material derivatised with glutathione.

Glutathione-S-transferase resin was self-packed in a column (Pharmacia) or prepacked 5 ml GSTTrap (Pharmacia) columns were used. The column was rinsed with 10 volumes of ddH₂O and 10 volumes of loading buffer. The sample was loaded onto the column with a low flowrate of 0.2 ml/min and passed twice over the column. Next, the column was washed with 7-10 volumes of loading buffer. Elution was achieved with 4 volumes of GST elution buffer. Eluate fractions were pooled together and kept at 4°C for further processing.

2.3.6.3 Anion and cation exchange chromatography

Protein separation by ion exchange chromatography depends on the reversible adsorption of charged molecules to an immobilised ion exchange group of opposite charge. Varying conditions such as ionic strength and pH can control

these interactions. To ensure electrostatic binding, the total ionic strength needs to be low.

Generally, 100mM NaCl was included into the anion exchange buffers. The columns for anion exchange chromatography (AEX) and cation exchange chromatography (CEX) were MonoQ HR 10/10 and MonoS HR 10/10 (Pharmacia). After equilibration with 5 column volumes of the AEX/CEX buffer A, the sample was loaded and the washing step followed with 5-7 more volumes of AEX/CEX buffer A. The elution was performed with a linear gradient of AEX/CEX buffer B in two steps: first from 0 to 60% in 5-8 column volumes and then to 100% in 1-2 column volumes. Eluted fractions containing the protein of interest were pooled together. Additionally, a cation exchanger that was used, was the phosphocellulose P11 (Whatman) material in a self-packed column.

2.3.6.4 Gel filtration

On a gel filtration (or size exclusion) column the molecules are separated according to differences in their sizes. The protein is injected into a 1 ml loop with a syringe. Prior to this, the protein must be concentrated down to a volume of 1-2 ml. Small molecules, which can diffuse into the pores of the gel beads are delayed in their passage through the column in contrast to the larger molecules, which cannot diffuse into the gel. The larger molecules thus leave the column first, followed by the smaller ones in order of their sizes. Gel filtration was performed with a Superdex 200 HR 26/60 column (Pharmacia).

2.3.6.5 Purification of *N.crassa* and *R.norvegicus* kinesin motor domain mutants

As the first purification step for the *N.crassa* and *R.norvegicus* kinesin motor domain mutants, the cation-exchanger phosphocellulose P11 (Whatman) was used in a self packed column, following a batch protocol. After this step, the protein was dialysed overnight against a buffer with low salt concentration. The second step for the *N.crassa* mutants Nk355^{R207A} and Nk355^{R207K} was a cation exchange column MonoS HR 10/10. The second purification step for rat

mutants Rk^{R204A} and Rk^{R204K} was an anion exchange column MonoQ HR 10/10. The final step for all mutants was a gel filtration step over a Superdex 200 HR 26/60 column (for all buffer compositions see the appendix section). The rat deletion mutant of loop 11 was purified as the other rat kinesin mutants with a slight difference in the pH of the buffers (see appendix).

2.3.7 Determination of concentration of proteins

The concentrations of the prepared proteins were determined by the use of the extinction coefficients (ϵ) of the proteins. The extinction coefficient of each protein can be determined by using its amino acid sequence and data coming from the absorbance spectra of proteins and compounds measured in native and denaturing conditions (Gill and von Hippel, 1989).

The maximum of absorbance is normally measured at 280 nm and comes from tryptophan, tyrosine and cysteine residues.

$$\epsilon = a \epsilon_{\text{Tyr}} + b \epsilon_{\text{Trp}} + c \epsilon_{\text{Cys}}$$

where ϵ_{Tyr} , ϵ_{Trp} , ϵ_{Cys} are the extinction coefficients of tyrosine, tryptophan and cysteine respectively and a, b and c are the number of each amino acid in the protein sequence. The extinction coefficients used were the ones determined for the following standard compounds (Gill and von Hippel, 1989):

N- acetyl-tryptophanamide	$A_{280}=5690$
Gly-L-Tyr-Gly	$A_{280}=1280$
Cysteine	$A_{280}=120$

From the absorbance at 280 nm the concentration can be determined, using the Beer - Lambert equation: $c = A_{280} / \epsilon_{280} l$ (where l =length of the cuvette in cm; c = molar concentration and ϵ = extinction coefficient).

2.3.8 Concentration of protein

The protein solutions were concentrated using the Amicon (Millipore) device. In this device, a membrane with a molecular weight cut-off smaller than the protein of interest is placed at the bottom of a cell, which is filled with the protein solution. The cell is then placed in a 50 ml Falcon tube and centrifuged at 3000g. In this way, the flow through contains only lower molecular weight components, while the protein is concentrated in the chamber.

2.3.9 Solubility studies

The solubility of a protein depends strongly on the composition of the lysis buffer. Using the procedure described below, the solubility of a specific protein was tested under many different conditions.

pH solubility screens:

A number of lysis buffers differing in pH and salt concentration were used routinely to determine the optimal pH for the solubility of the desired protein:

Buffer	pH
50 mM Na Acetate	5
50 mM MES	6
50 mM Tris	7
50 mM Tris	8
50 mM AMPPO	9

Salt solubility screen:

Keeping an optimal pH in the lysis buffer, different concentrations of salt were tested as follows:

Salt	Concentration
NaCl	0.1 M, 0.5 M, 1.0 M
KCl	0.1 M, 1.0 M

Detergent solubility screen:

Keeping the parameters of pH and salt concentration stable, different detergents were added in the lysis buffer, to examine whether they optimised further the solubility of the protein, as follows:

Detergent	Concentration
NP 40	0.2%
Triton X-100	0.2%
Tween-20	0.2%
CHAPS	0.2%

2.3.10 Dynamic Light Scattering

Dynamic Light Scattering (DLS) was used routinely to assess the heterogeneity of the protein solutions prior to crystallization trials. DLS experiments were conducted in a Dimingon-A machine (Firma Dierks and Partner, Hamburg) thermostated at 20°C and data were processed with software provided by the manufacturer. Samples were centrifuged in an Eppendorf tabletop centrifuge at maximum speed (13 krpm), in order to remove dust without removing high molecular weight aggregates. In each measurement 20 µl of protein solution of desired concentration (~ 10-20 mg/ml) were measured in a 0.1 mm quartz cuvette.

2.3.11 Crystallization techniques

A variety of methods exist to crystallize biological macromolecules. All of them have the aim to bring the protein solution into a supersaturated state. Among them, vapour diffusion is the most widely used method that has also been used in this study. The vapour diffusion method utilises small volumes (down to 2 µl or less with the use of robots). A droplet containing the protein solution to be crystallized, buffer, crystallizing agent and additives is equilibrated against a reservoir containing a solution of crystallizing agent at a higher concentration than in the droplet. Equilibration proceeds by diffusion of the volatile species (water or organic solvent) until the vapour pressure in the droplet is equal to

the one in the reservoir. If equilibration occurs by water exchange (from the drop to the reservoir), it leads to a decreasing volume of the droplet. This method was used in this study in two variations, either as hanging or as sitting drops (figure 9).

Crystallization solutions and supplies are described in the material section 2.1.7. Prior to each crystallization experiment, the highly concentrated protein solution (10-15 mg/ml) was centrifuged in an Eppendorf tabletop centrifuge at 13 Krpm for 5 minutes at 4°C in order to eliminate precipitates or dust. First screens were set up in sitting drop Cryschem plates but also in hanging drop plates. During optimization trials, the hanging drop method was preferred. For each trial 1 µl of protein solution was mixed with 1 µl of reservoir. The plates were sealed with tape in the case of sitting drop and with a siliconized cover slip in the case of hanging drop trials and kept at 19°C and/or at 4°C. The plates were examined each day during the first week and 2 times a week during the first 2 months. The initial screens were performed by the use of the commercial screens described in section 2.1.7.

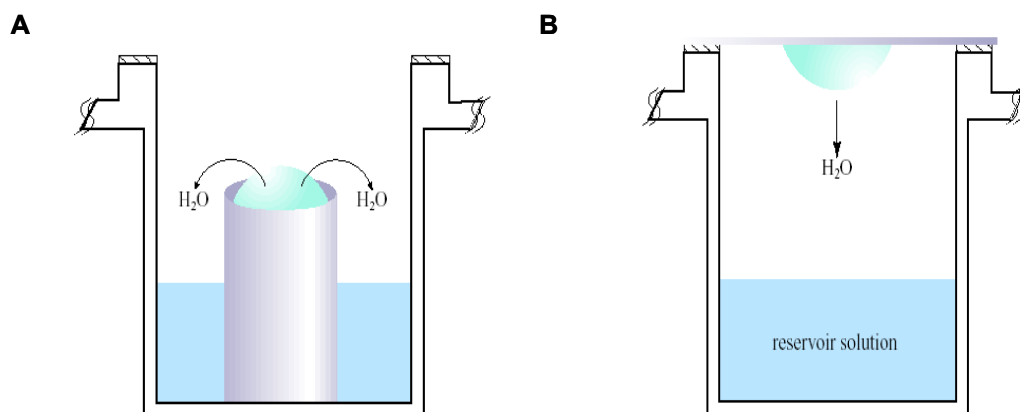


Fig. 10: Set up of crystallization trials using: A) the sitting or B) the hanging drop vapour diffusion technique,

Additionally, the batch crystallization method was tried: the protein sample was mixed with the precipitant and the appropriate additives, creating a homogeneous solution, requiring no equilibration with a reservoir. The experiment was performed in a capillary. After the set up, the ends of the capillary were sealed with wax.

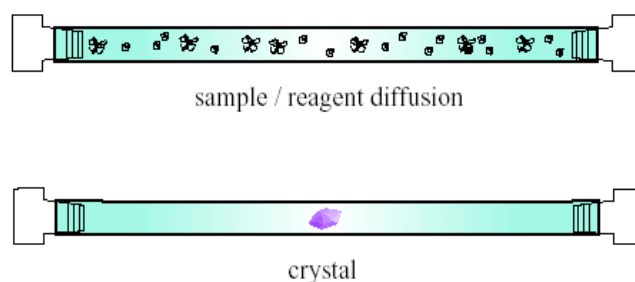


Fig. 11: A batch crystallization experiment setup.

Occasionally, the technique of seeding crystals was performed in an attempt to improve the size and quality of microcrystals, bad-shaped crystals or to avoid excessive nucleation. First, a drop with existing microcrystals was transferred to an Eppendorf tube, diluted with the proper buffer and a small plastic ball was added. Vortexing this solution resulted in breaking the nuclei/crystals and made it possible to transfer a small portion of them by a cat whisker to new drops of lower concentration of protein and/or precipitant agent. This technique can lead to a slower growth thus yielding bigger crystals.

2.3.12 Testing of Nk355^{R207A} and Rk354^{R204A} crystals and data collection.

The Nk355^{R207A} plate-like crystals were tested for diffraction at the BW7A and X13 beamlines of the Hamburg Outstation of EMBL at DESY, using the synchrotron radiation of the DORIS storage ring (Hamburger Synchrotronstrahlungslabor, HASYLAB).

Diffraction images were recorded with a CCD detector (marcCCD165, Mar Research GmbH, Norderstedt, Germany) at a wavelength $\lambda=0.8034$ Å. The distance between detector and sample was 280 mm. Glycerol 20% was added to the protein solution as cryoprotectant. The crystals were flash-cooled to 100K by a stream of cold nitrogen. The data set was autoindexed, reduced and scaled with the programs DENZO and SCALEPACK (Otwinowski and Minor, 1997). Data collection details and data processing statistics are shown in table

6 (section 3.1.5). The crystals of Rk354^{R204A} were tested for diffraction at the X13 beamline and diffractions images were recorded at a wavelength $\lambda=0.8034$ Å. The distance of detector and sample was 280 mm. As the crystals were grown in a PEG3350 solution, no high concentrated cryoprotectant was necessary. The crystals were flash-cooled to 100K by a stream of cold nitrogen. The data set was autoindexed, reduced and scaled with the programs DENZO and SCALEPACK (Otwinowski and Minor, 1997). Data collection details and data processing statistics are shown in table 7 (section 3.1.6).

2.3.13 Molecular replacement

The phase problem was approached and solved using the molecular replacement (MR) method, which is used routinely in the determination of kinesin motor domain structures. The principle on of the method is simple: if the structure that one is trying to solve is very similar to one that has already been determined, then the elements of the known structure that are common to both can be used to 'phase the data'.

In this study, the method was performed using the CCP4 suite of programs (The CCP4 suite, 1994) and the program PHASER (Storoni et al., 2004). As a search model for MR the wild type crystal structures of *N. crassa* (Song et al., 2001; PDB code 1GOJ) and rat kinesin-1 (Sack et al., 1997; PDB code 2KIN) were used.

2.3.14 Limited proteolysis

The GST.TPR1-6 construct was treated with trypsin in a ratio 100 to 1. The sample was mixed 1 to 1 with protease reaction buffer (Appendix) and divided into 7 aliquots. Two were used as controls (untreated, heat control for 1h) and the others for different time points of the reaction (5,10,15,30 and 60 min). In each reaction 5x SDS-buffer was added and the sample was heated to 90°C for 10 min. Freezing in liquid nitrogen was used to stop any remaining protease activity. The result was assessed with SDS-PAGE analysis.

3. Results

3.1 Structural studies on *Neurospora crassa* and *Rattus norvegicus* kinesin-1 motor domain point mutants

3.1.1 Generation of the Nk355^{R207A}, Nk355^{R207K}, Rk354^{R204A} and Rk354^{R204K} mutant constructs

Biochemical studies (Klumpp et al., 2003) with *Drosophila* kinesin-1 revealed that a mutant protein, in which the arginine 210 of switch-1 region is replaced by an alanine, shows dramatic effects. The mutation causes loss of cooperativity between the two heads within a dimer, an ATP hydrolysis defect, and a reduced affinity for microtubules. These effects can be mostly reversed if a lysine was introduced at this position. Both these mutations were introduced into the monomeric rat kinesin-1 construct Rk354 and into the monomeric *N. crassa* kinesin-1 construct Nk355 (Fig. 3).

The construct for the expression of monomeric *Neurospora crassa* kinesin-1 motor domain (Nk355) was previously donated by M. Schliwa and G. Woehlke (University of Munich) (Song et al., 2001) and it was used as a template to generate two point mutants for the present study. The wild type construct of Rk354 was previously cloned in the lab (Kozielski et al., 1997).

The mutants were generated by site directed mutagenesis. The oligomers used to introduce the mutations into the wild type plasmids can be looked up in Appendix. Positive clones were verified by sequencing (Fig.12).

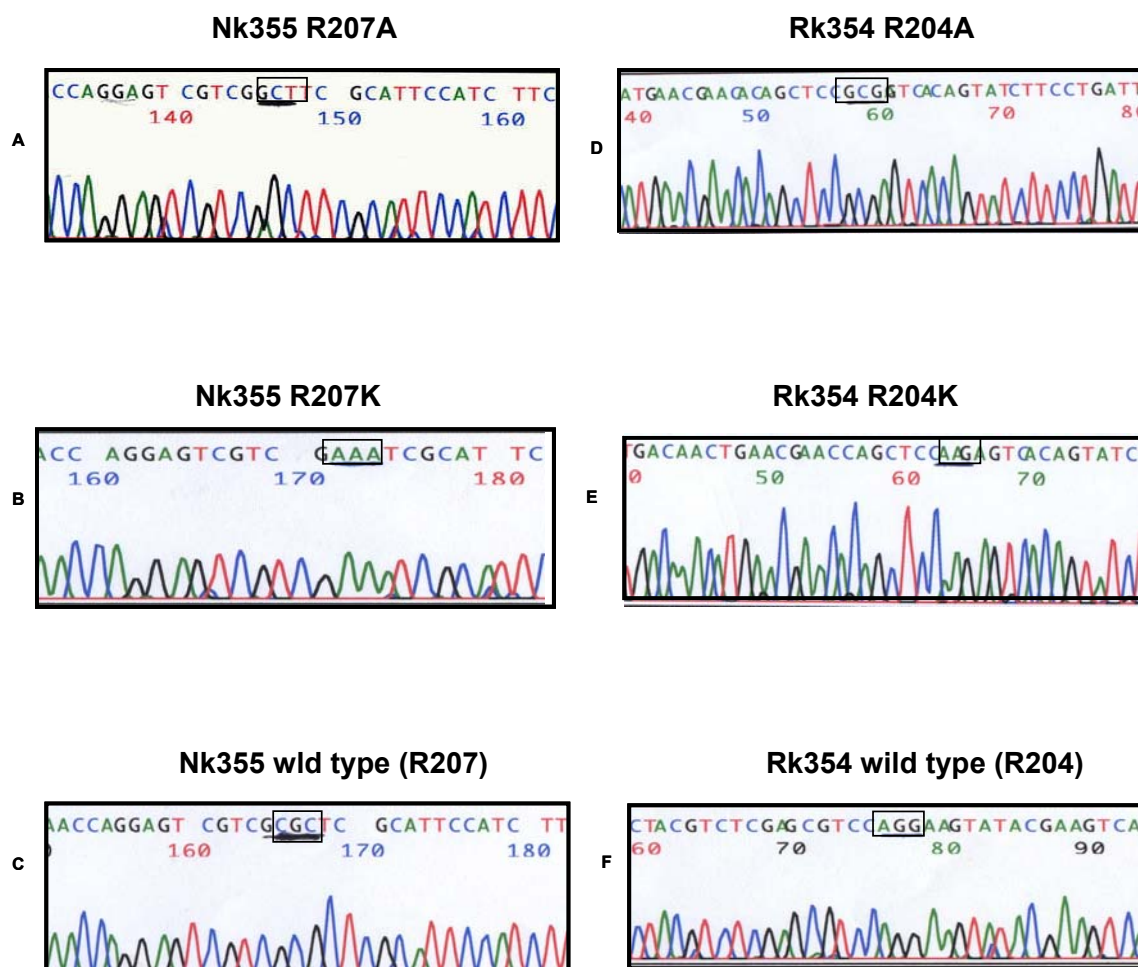


Fig. 12: The chromatograms of the sequencing analysis for the motor domain mutants: (A-C) Nk355^{R207A}, Nk355^{R207K} mutants. (A) An alanine (codon GCT) was introduced. (B) A lysine (codon AAA) was introduced. (C) The arginine of the wild type (codon CGC) at position 207 of the primary sequence, (D-E) Rk354^{R204A}, Rk354^{R204K} mutants (D) An alanine mutation (codon GCG) was introduced at the position 204. (E) A lysine (codon AAG) was introduced. (F) An arginine (codon AGG) exists at position 204 in the wild type primary sequence.

3.1.2 Expression and purification of motor domain mutants

Expression and purification of *N. crassa* constructs

BL21 RIL cells (Table 1) were transformed with the plasmids Nk355^{R207A}, Nk355^{R207K} using the electroporation protocol (section 2.2.2). Expression was carried out overnight at 24°C with 0.5 mM IPTG (section 2.3.3). The proteins were purified in three steps (section 2.3.6.5): with a cation exchange phosphocellulose column, a cation exchange MonoS column and a gel filtration column as it is shown in Fig. 13 (buffer compositions can be looked up in the Appendix). The yield of purified protein was estimated approximately 6 mg per liter cell culture.

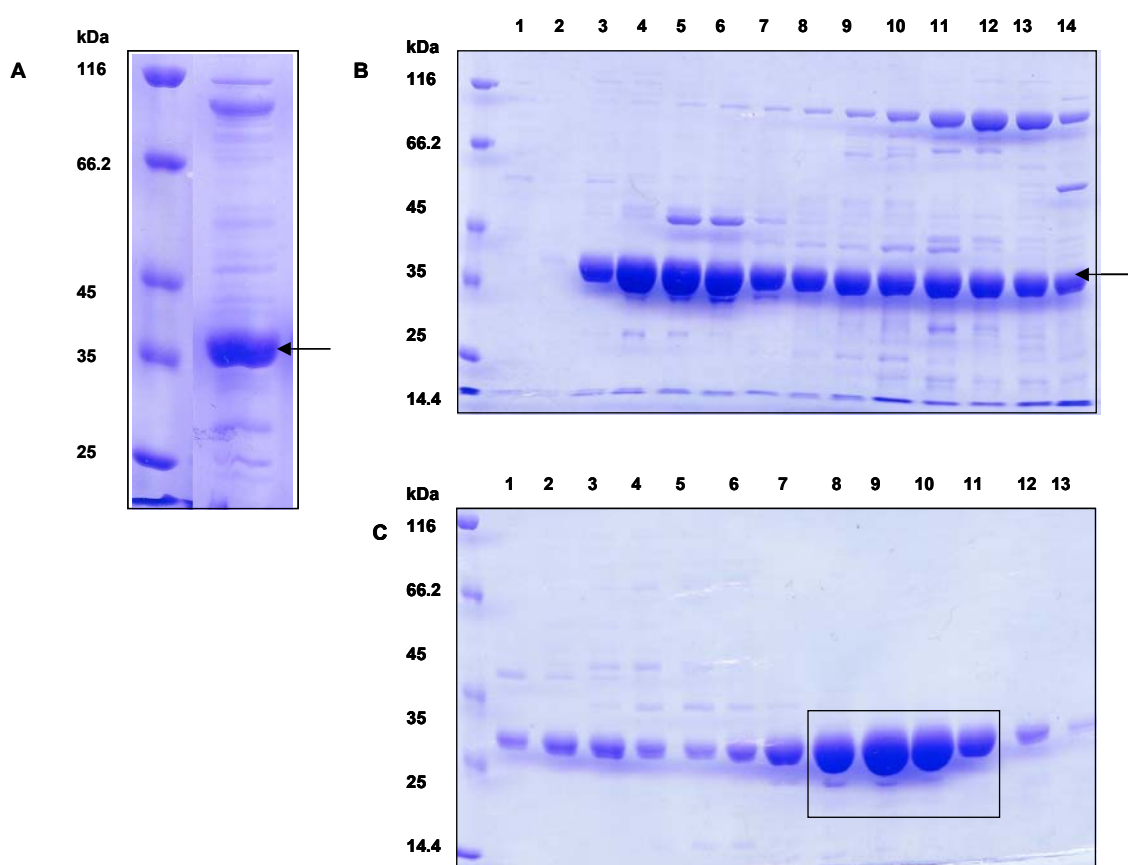


Fig 13: Purification of the Nk355^{R207A} mutant: the eluates of (A) the phosphocellulose column (PC), (B) the cation exchange column MonoS. The main protein peak corresponds to fractions 3-8. (C) the gel filtration G200; the fractions 8-11 were pooled and used for crystallization trials (boxed). The SDS-PAGE analysis was performed with 10% gels. The PC column was performed as a batch. In MonoS the protein eluted in 150-200 mM NaCl. The Nk355^{R207A} protein is indicated by arrows.

For the Nk355^{R207K} mutant construct the purification steps were identical and the resulted pure protein can be seen in fig.14.

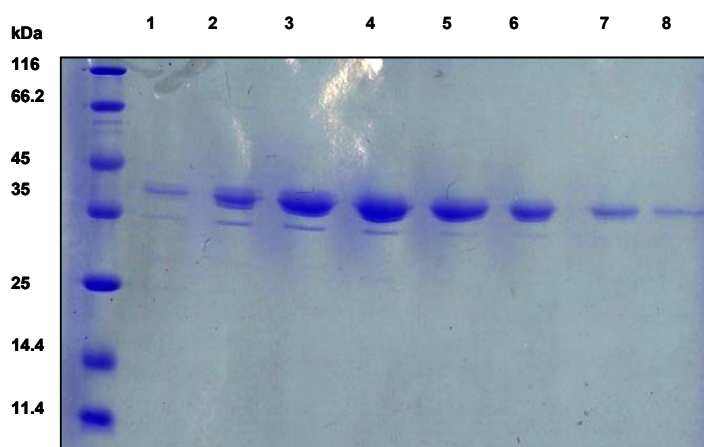


Fig. 14: Purified Nk355^{R207K} mutant: 10% SDS-PAGE gel of G200 HK 16/60 column eluted fractions of the Nk355^{R207K} mutant construct. Fractions 3-6 were pooled and used in crystallization trials.

Expression and purification of *R. norvegicus* constructs

The mutant constructs Rk354^{R204A}, Rk354^{R204K} were expressed overnight at 24⁰C. The purification strategy (section 2.3.5.5, Fig. 15) consisted of three steps: a cation exchange phosphocellulose column was followed by an anion exchange a MonoQ column and a final gel filtration column was employed. The protein expression was very high. A significant amount of protein was observed during the PC batch not to bind, possibly because the amount of material used was not enough to bind the high amounts of the expressed protein. The purified Rk354^{R204K} protein is shown in fig.16.

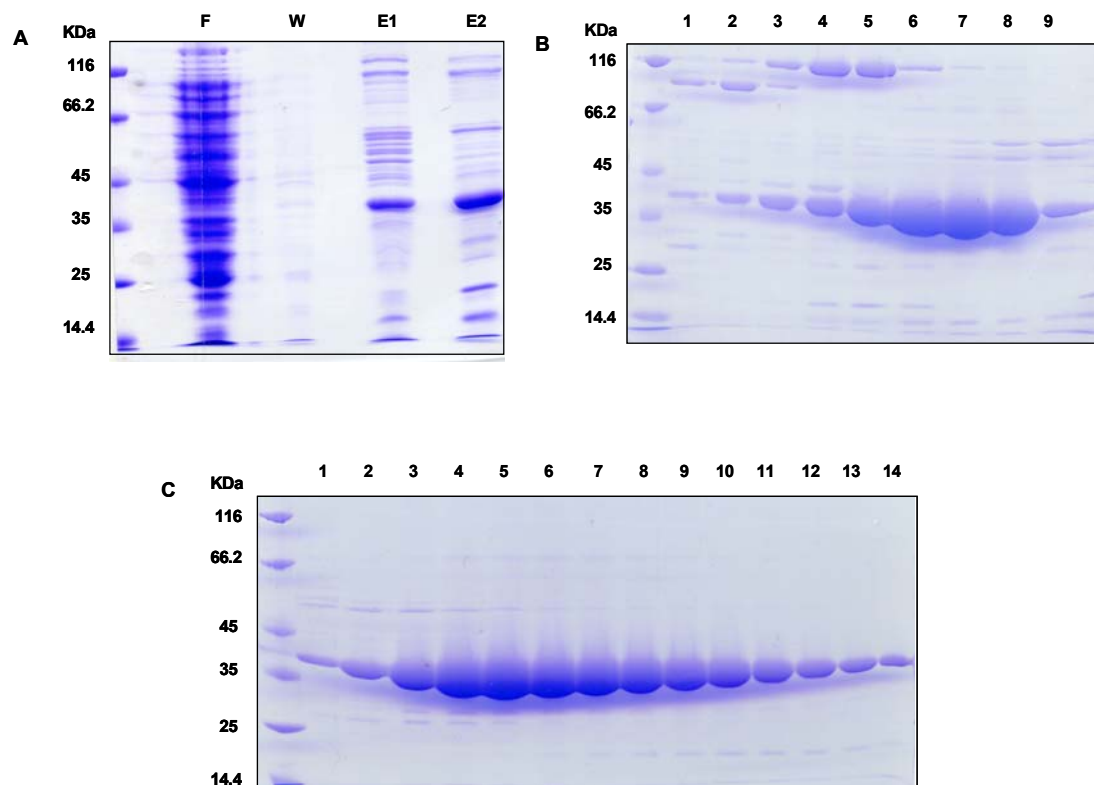


Fig.15: Purification of the Rk354^{R204A} mutant: (A) Phosphocellulose cation exchange chromatography for the Rk354^{R204A} mutant. F is for flowthrough, W for wash and E1-2 for subsequent elutions. (B) The MonoQ column fractions. Fractions 6-8 represent the main peak of the protein. (C) The G200 eluate fractions.

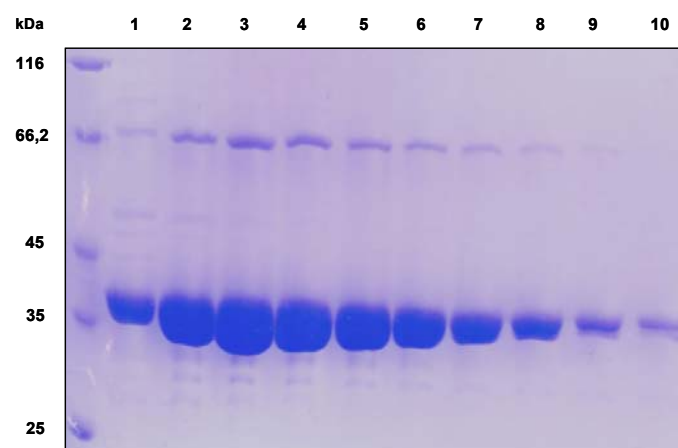


Fig.16: Purified Rk354^{R204K} mutant: 10% SDS-PAGE gel showing the fractions eluted from the gel filtration column G200/60.

3.1.3 Crystallization of Nk355^{R207A}, Nk355^{R207K}, Rk354^{R204A} and Rk354^{R204K}

The first kinesin structure to be published was the motor domain of human kinesin-1 (Kull et al., 1996). The list of kinesin x-ray structures deposited in the Protein Data Bank has expanded up to 26 entries so far. The 3D x-ray structures available today are of motor domains or mutants from 11 different kinesins from a variety of organisms.

Members of different classes of kinesin motors have been crystallized (Table 5) including the N-type motors rat kinesin-1 (Sack et al., 1997; Kozielski et al., 1997), *Neurospora* kinesin-1 (Song et al., 2001), kinesin-3 (KIF1A, Kikkawa et al., 2001; Nitta et al., 2004) and Eg5 (kinesin-5, Turner et al., 2001; Yan et al., 2004). The C-type motors Ncd (Sablin et al., 1998), Kar3 (Gulick et al., 1998; Yun et al., 2001) and KCBP (Vinogradova et al., 2004) that belong to the kinesin-14 family, as well as the M-type kinesins (kinesin-13) KinI (Shipley et al., 2004) and Kif2C (Ogawa et al., 2004) have been structurally determined.

A close look at the crystallization conditions of the published structures revealed a tendency of the different kinesins to crystallize under similar conditions. In most conditions a polyethylene glycol (PEG) or a sulfate salt is used as a main precipitant in combination with an additional salt (NaCl or KCl) in most cases in a pH region that varies from 4.6 to 9.1. In more than 60% of the cases, a PEG is used as precipitant: PEG3350, PEG4000, PEG2000MME or PEG8000. Alternatively, either ammonium or lithium sulfate is used. The PEG or lithium sulfate choice has been of critical importance to capture two different conformations of the motor domain of kinesin-1. In the lithium sulfate-grown crystals of the rat kinesin-1 motor domain, an ordered, docked neck linker and neck helix are visible (Sack et al., 1997). In the human kinesin-1 motor domain crystals that were grown with PEG4000, the neck linker and neck helix are not visible. Once the same human motor domain construct was crystallized with lithium sulfate the neck linker and neck helix become ordered and visible (Sindelar et al., 2002).

Protein	Precipitant	Additional salt	pH	Reference
Rat kinesin-1 (dimer)	Ammonium sulfate	NaCl	7.5	Kozielski et al., 1997
Rat kinesin-1 (monomer)	Lithium sulfate	KCl	7.5	Sack et al., 1997
Ncd (kinesin-14) (monomer)	PEG 4000	NaCl	7.2	Fletterick et al., 1995
Ncd (dimer)	Lithium sulfate	NaCl	7.5	Sablin et al., 1998
Ncd (dimer)	PEG 4000	NaCl	6.8	Kozielski et al., 1999
Human kinesin-1	PEG 4000	KCl	4.6	Kull et al., 1996
Human kinesin-1	Lithium sulfate	KCl	7.5	Sindelar et al., 2002
Kar3 (kinesin-14, monomer)	PEGMME 2000	NaCl	7.0	Gulick et al., 1998
Eg5 (kinesin-5, monomer)	PEG 3350	NaNO ₃	5.3	Turner et al., 2001
Eg5 (monomer) + monastrol	PEG 3350	Phosphate	8.0	Yan et al., 2004
<i>Neurospora crassa</i> kinesin-1 (monomer)	PEGMME 2000	NaCl	7.0	Song et al., 2001
KinI (kinesin-13, monomer)	Ammonium sulfate	NaNO ₃	5.0	Shipley et al., 2004
Kif2C (kinesin-13, monomer)	K-Na-tartrate	NaCl	6.0	Ogawa et al., 2004
KCBP (kinesin-14, monomer)	PEG 3350	Phosphate	9.1	Vinogradova et al., 2004
CENP-E (kinesin-7, monomer)	PEG 3350	NaNO ₃	7.0	Garcia-Saez et al., 2004
Kif1A (kinesin-3, monomer)	PEG 4000	Na-acetate	8.5	Nitta et al., 2004

Table 5: Crystallization conditions for successfully crystallized kinesin motor domains. The PEG conditions are indicated by a gray background and the salt-based conditions with no coloring.

In most cases including kinesin-1, KCl or NaCl were used as additional salts, but also phosphate and NaNO₃ were applied sometimes (Table 5).

All four purified proteins were concentrated using the Amicon devices to a concentration of 15-20 mg/ml. The crystallization conditions for the wild types proteins were initially used to carry out a screening, varying either the precipitant concentration, the salt concentration, the pH or the protein concentration. Drops of varying ratios of protein sample to crystallization solution and both sitting drop and hanging drop vapour diffusion methods were employed, too. In table 5 the crystallization conditions for the monomeric rat and the *N.crassa* wild type proteins are described. For the crystallization of *N.crassa* kinesin-1, glycerol (up to 3%) was successfully used as an additive (Song et al., 2001).

The initial screen to crystallize the *N.crassa* mutants with PEGMME 2000 as a precipitant yielded small, needle-like crystals, which could be optimized to plate-like crystals in subsequent crystallization trials for the Nk355^{R207A} (Fig. 17 A and B) but not for the Nk355^{R207K} mutant.

The crystallization trials with both the rat kinesin mutants yielded heavy precipitation in most drops. Lowering the protein and/or the precipitant concentration did not improve the result. Therefore, a wider screening was performed using the commercial kits listed in section 2.1.7. Needle-like crystals were obtained for both mutants (Fig. 17 D and E).

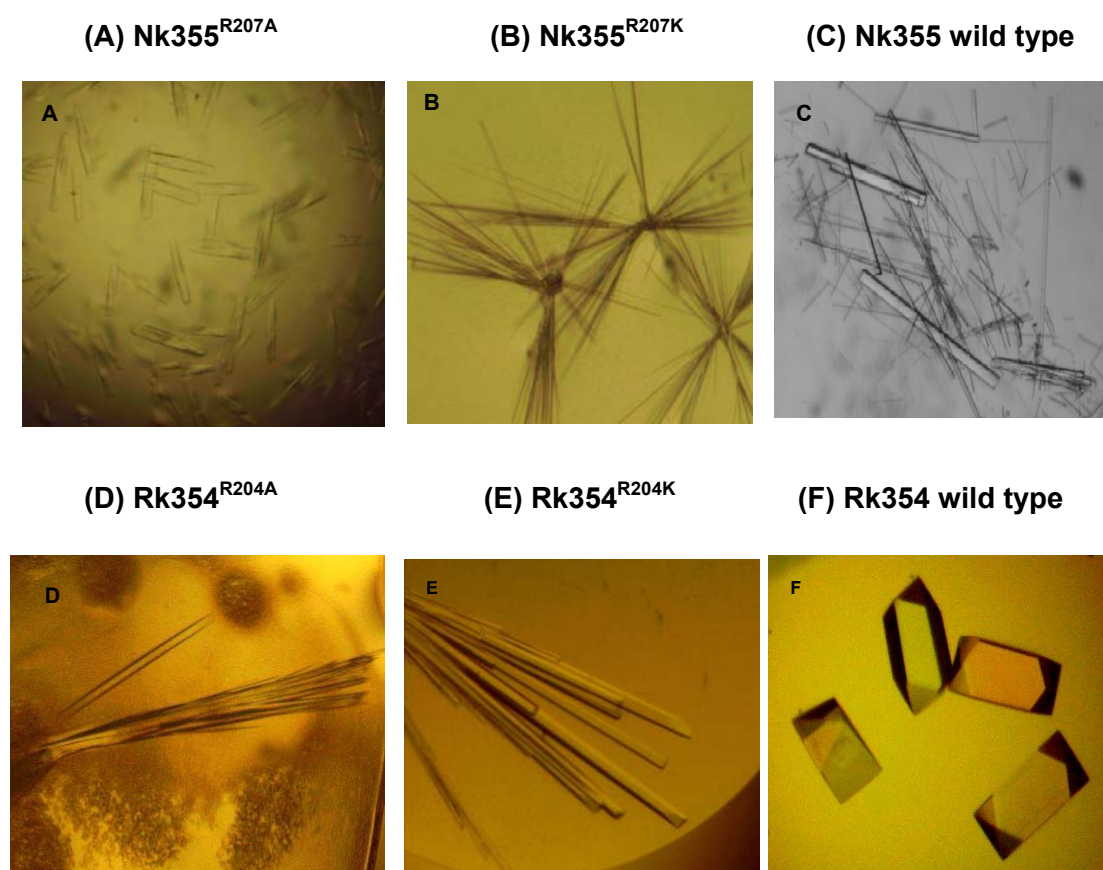


Fig. 17: Pictures of crystals of (A) Nk355^{R207A}, (B) Nk355^{R207K}, (C) Nk355 wild type (Song et al., 2001), (D) Rk354^{R204A}, (E) Rk354^{R204K} and (F) Rk354 wild type (Sack et al., 1997). All crystals but the wild types' (C, F) were produced for this study. The Rk354^{R204K} crystals were produced in collaboration with Dr. J. Mueller.

The successful optimization of Nk355^{R207A} crystals was achieved by altering the original condition significantly: 20% PEG3350, 0.2M magnesium acetate, 0.1M Tris-HCl pH 7.5 (Fig. 17A). The long, thin needles of Nk355^{R207K} were obtained in 17-20% PEG2000MME, 0.1 M HEPES pH 7-7.5 (Fig. 17B). The wild type crystals (Fig.17C) are shown for comparison (Song et al., 2001). The crystals of Rk354^{R204A} (Fig. 17D) were obtained in 0.2M ammonium sulfate, 0.1M Tris pH 8.5, 25% w/v PEG3350 (Index Screen Kit condition No69, Hampton Research). Last, the crystals of Rk354^{R204K} (Fig. 17E) were obtained using a reservoir of the same composition as for the Rk354^{R204A} crystals. Crystals of wild type Rk354 (Sack et al., 1997) are shown for comparison (Fig. 17F).

3.1.4 Data collection and processing from a Nk355^{R207A} plate-like crystal

The Nk355^{R207A} plate-like crystals were tested for diffraction at the beamline of the X13 consortium (EMBL/ University of hamburg) at DESY, using the synchrotron radiation of the DORIS storage ring (Hamburger Synchrotronstrahlungslabor, HASYLAB). Diffraction images were recorded with a CCD detector at a wavelength $\lambda=0.8034$ Å. The distance between detector and sample was 280 mm. A solution of 20% glycerol, 20% PEG3550 and 0.1M Pipes pH 7.3 was used as cryoprotectant. The crystals were flash-cooled to 100K by a stream of cold nitrogen. A diffraction image of a Nk355^{R207A} crystal can be seen in figure 18. The data collection and analysis was done in collaboration with Dr. A. Marx.

The data set was autoindexed, reduced and scaled with the programs DENZO and SCALEPACK (Otwinowski and Minor, 1997). Data collection details and data processing statistics are shown in Table 6. The Nk355^{R207A} crystals belong probably to the $P2_1$ space group. The unit cell dimensions are: $a=51.454$ Å, $b=139.469$ Å, $c=51.754$ Å, $\alpha=90^\circ$, $\beta=119.39^\circ$, $\gamma=90^\circ$.

Beamline	X13
Space group	$P2_1$
Unit cell (Å, °)	$a=51.454$ Å, $b=139.469$ Å, $c=51.754$ Å, $\alpha=90^\circ$, $\beta=119.39^\circ$, $\gamma=90^\circ$.
Mosaicity (°)	0.463
Wavelength	0.8034 Å
Resolution	3.05 Å
Completeness	98.4 %
Reflections measured	39640 (total) 11881 (unique)
{I} / σ{I}	6.12 (2.09)
R_{sym} (%)	17.9 (49.8)

Table 6: Data collection details for the measured Nk355^{R207A} crystal.

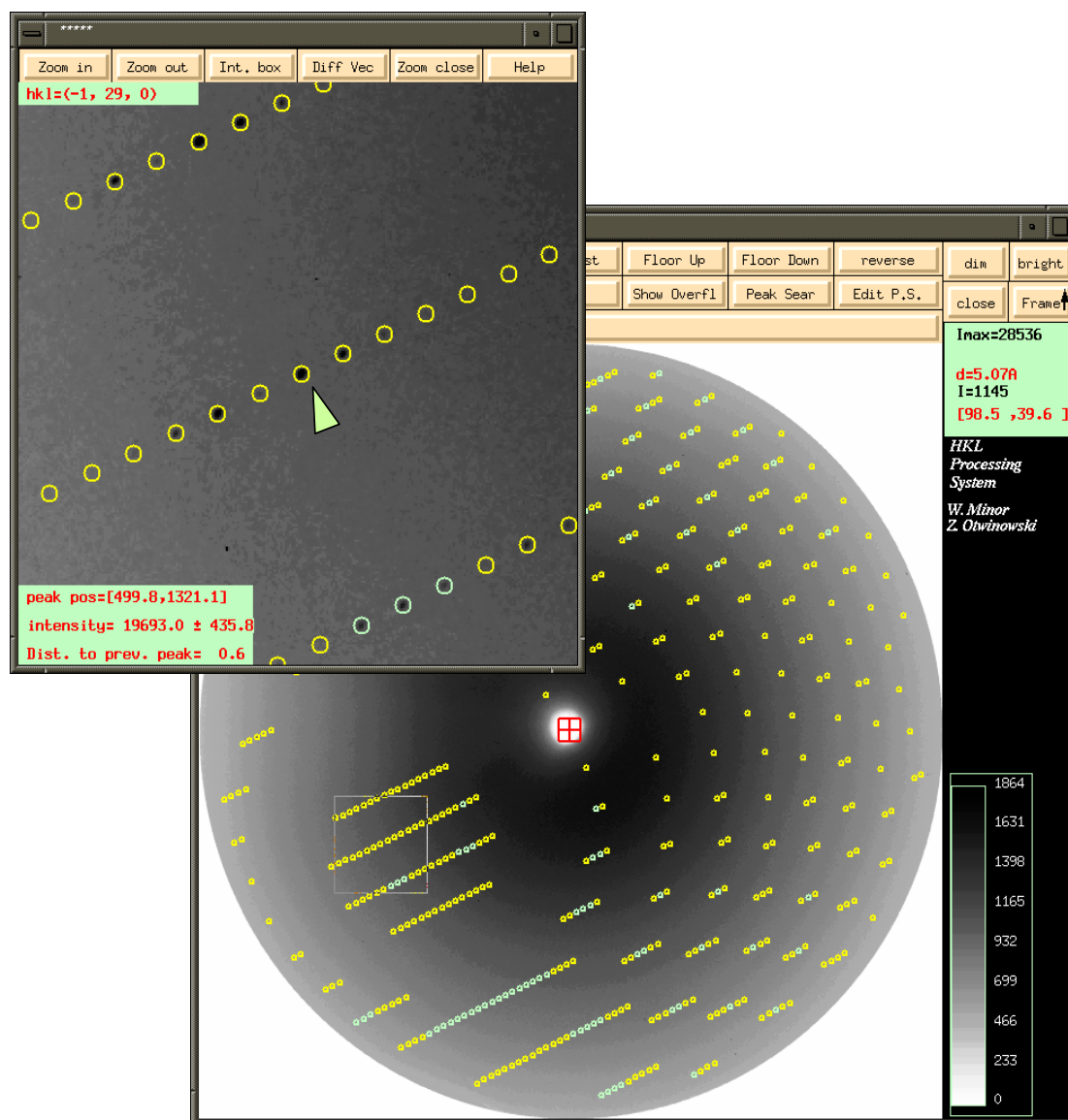


Fig.18: Sample diffraction pattern of the measured Nk355^{R207A} crystal, as displayed in DENZO/XDISP (Otwinowski and Minor, 1997).

The $P2_1$ space group is characterized by a primitive unit cell and one 2-fold screw axes. $P2_1$ is a monoclinic spacegroup ($\alpha=\gamma=90^\circ$, while the other cell parameters can have any value). The monoclinic angle β is very close to 120° and the cell constants a and c are almost the same. In fact, all reflections could also be indexed assuming a hexagonal or C-centered orthorhombic cell. The observed intensities clearly rule out the hexagonal symmetry as combination of reflection intensities with SCALEPACK result in very poor statistics. However,

scaling with the assumption of spacegroup $C222_1$ results in a dataset of high quality, comparable to that obtained with spacegroup $P2_1$. Thus, at this stage of analysis the space group appears as $P2_1$, but the final crystal analysis could reveal the existence of even higher symmetry, presumably the space group $C222_1$.

The data set reached an effective maximum resolution of 3.05 Å (mean $I / \sigma I > 2$). The data collection and processing details and statistics are shown in Table 6.

The Matthews coefficient V_M was calculated with MATTHEWS_COEF (CCP4 suite of programs for protein crystallography, 1994; Matthews, 1968) assuming four molecules (2 asymmetric units) per unit cell and had a value of 2.07 Å³ Da⁻¹ corresponding to a solvent content of 40 %. Since other numbers of molecules per asymmetric unit produce rather low or high solvent contents, it was tentatively assumed that the asymmetric unit was composed of two molecules (Fig.19).

3.1.5 Molecular replacement

The phasing problem was approached and solved with the molecular replacement method (MR) using the CCP4 suite of programs (The CCP4 suite, 1994) and the PHASER program (Storoni et al., 2004), by Dr. Alexander Marx. As a search model for MR the wild type protein crystal structure was used (Song et al., 2001; 1GOJ in PDB). MR was successful and PHASER yielded a unique solution with a high Z-score of 36 (Storoni et al., 2004). According to the MR solution the packing of the Nk355^{R207A} molecules in the crystal is two molecules per asymmetric unit ($a=51.454$ Å, $b=139.469$ Å, $c=51.754$ Å), in agreement with the previous calculations. The packing of the molecules is shown in figure 19.

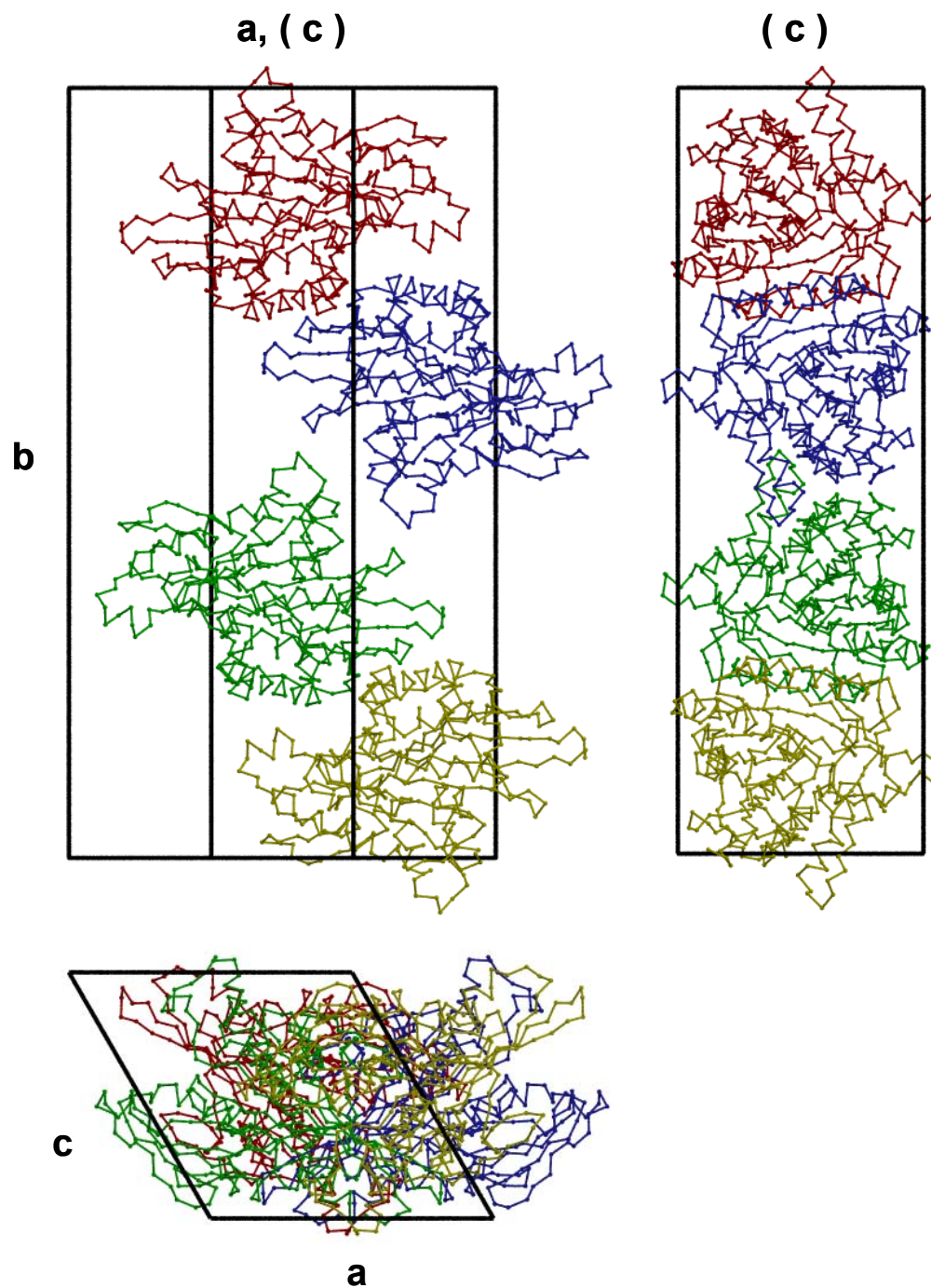


Fig.19: Packing of the protein molecules in the crystals of Nk355^{R207A} mutant according to the PHASER solution. Space group P2₁. There are two molecules per asymmetric unit and two asymmetric units per unit cell ($a=51.454$ Å, $b=139.469$ Å, $c=51.754$ Å). Cell constants in parentheses indicate that the corresponding cell edges are shown in projection. The figure was generated by Dr. A. Marx.

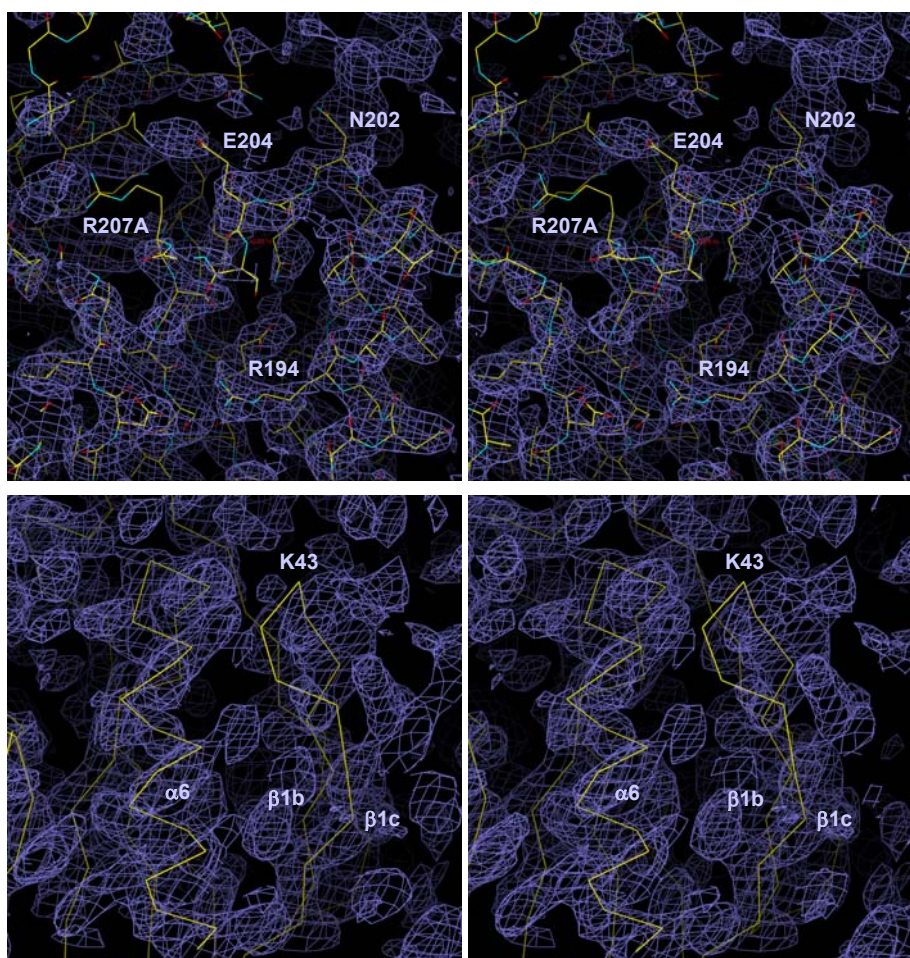


Fig. 20: Composite omit maps for Nk355^{R207A} mutant calculated with the MR solution of Phaser (1GOJ, residues 2-333) using CNS (2fo-fc omit map, contour level 1 σ). The maps are represented as stereo images. The upper two images show part of helix $\alpha 3$ (right side), loop9, $\alpha 3a$, and part of strand $\beta 6$ (left side); the position of mutated residue R207 is shown as in the wild type. The lower two images show the "L2 finger" (β hairpin between $\beta 1b$ and $\beta 1c$). In all images the electron densities of the mutant are shown in overlay with the C_{α} trace of the search model (wild type, yellow line). The figure was generated by Dr. A. Marx.

An initial look at the electron density map generated with the CNS program (Brunger et al., 1998) revealed that the structure of the Nk355^{R207A} mutant is essentially the same with the wild type protein. Differences can be observed in surface structural motifs such as loops, which could be explained by the different packing of the molecules in the crystals.

As it is shown in figure 20 the area of the mutation is well defined in the electron density map. There seems to be no electron density at the location of the side chain of arginine 207 in the wild type, as it is expected by its

substitution with an alanine. At this stage of the crystal analysis no remarks can be made about the possible changes at the active site triggered by the mutation. The model has to be refined before any residue movements can clearly be seen in the active site. After refinement the well-defined electron density map at this area of the molecule should be able to provide a detailed view of the region of the mutation and shed light into any structural changes.

There are areas where the electron densities do not agree with the Nk355 structure, as can be seen in figure 20 in the lower images where the L2 finger, a surface loop, is shown. The electron density around K43 is weak and suggests that the actual trace of the L2 finger in the mutant is shifted from the position of the wild type to the right. This is due to a crystal contact with the end of helix $\alpha 4$ of an adjacent molecule (not shown).

Loop 11, an important structural element that was visible in the wild type structure is probably disordered, as the electron density in this area appears very weak. Moreover, loop10 between $\beta 6$ and $\beta 7$ seems also to be disordered in the mutant. Refinement of the model will reveal if these loops are truly disordered or have adopted a different conformation that cannot be detected at this stage of analysis.

3.1.6 Data collection and processing from Rk354^{R204A} needle-like crystal

The Rk354^{R204A} needle-like crystals were tested for diffraction at the X13 consortium beamline (EMBL/ University of hamburg), using the synchrotron radiation of the DORIS storage ring (Hamburger Synchrotronstrahlungslabor, HASYLAB). Diffraction images were recorded with a CCD detector at a wavelength $\lambda=0.8034$ Å. The distance between detector and sample was 280 mm. As the crystallization buffer contained 25% PEG3550 no additional cryoprotectant was necessary to prevent ice formation. The crystals were flash-cooled to 100K by a stream of cold nitrogen.

The data set was autoindexed, reduced and scaled with the programs DENZO and SCALEPACK (Otwinowski and Minor, 1997). Data collection details and

data processing statistics are shown in table 7. The Rk354^{R204A} crystals belong to the P2₁ space group, the unit cell dimensions are: a=57.400 Å, b=72.604 Å, c=128.249 Å, $\alpha=90^\circ$, $\beta=86.899^\circ$, $\gamma=90^\circ$ (Fig 35 in section 4.2.2).

Beamline	X13
Space group	P2 ₁
Unit cell (Å, °)	a=57.400 Å, b=72.604 Å, c=128.249 Å, $\alpha=90^\circ$, $\beta=86.899^\circ$, $\gamma=90^\circ$.
Mosaicity (°)	0.518
Wavelength	0.8034 Å
Resolution	3.05 Å
Completeness	99.4 %
Reflections measured	88334 (total) 20533 (unique)
{I} / σ{I}	8.70 (2.63)
R_{sym} (%)	16.1 (53.4)

Table 7: Data collection details for the measured Rk354^{R204A} crystal.

The data set reached an effective maximum resolution of 3.05 Å (mean I / σ I > 2). The space group was determined to be P2₁

The Matthews coefficient V_M was calculated with MATTHEWS_COEF (CCP4 suite of programs for protein crystallography, 1994; Matthews, 1968) assuming four molecules (2 asymmetric units) per unit cell. This assumption led to a value of 3.4 Å³ Da⁻¹ corresponding to a rather high solvent content of 67 %. Nevertheless, unique molecular replacement solutions were found using either the wild type *N.crassa* (Song et al., 2001, PDB code: 1GOJ) or the *R. norvegicus* (Sack et al., 1997, PDB code: 2KIN) motor domain structure as search models (z-scores: 20 and 28 respectively). Calculations of the Matthews coefficient assuming six molecules (3 asymmetric units) per unit cell, corresponded to a value 2.2 Å³ Da⁻¹ and a solvent content of 44.7%. However, attempts to find a MR solution with this assumption were unsuccessful. Interestingly, the measured crystals of Nk355^{R207A} and Rk354^{R204A} mutants both belonged to the same space group P2₁. Both wild type crystal forms

belonged to space group $P2_12_12_1$. Data collection and analysis were performed by Dr J. Mueller.

3.1.7 Generation of a Loop 11 deletion mutant RK354 Δ loop11

Loop 11 is an important structural element of the kinesin motor domain, as it participates in the microtubule binding. Interestingly it is not ordered in most kinesin structures with a few exceptions like *N.crassa* kinesin-1. A deletion mutant was generated for the monomeric rat kinesin construct Rk354 (Fig. 21).

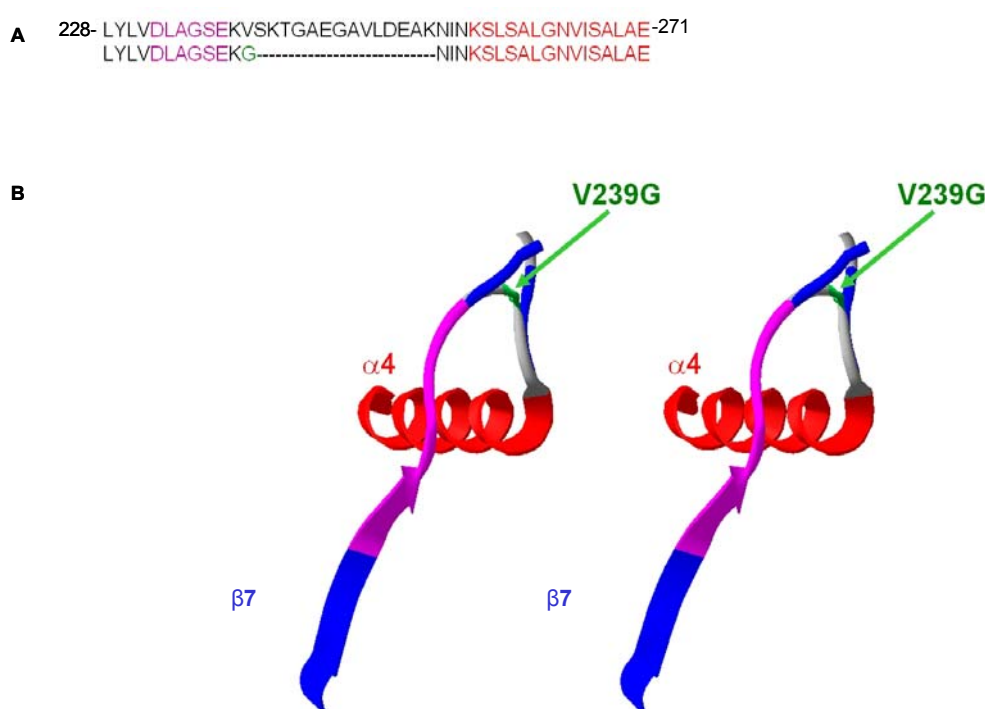


Fig. 21: Model of RK354 Δ loop11 construct. (A) Sequence detail of the wild type Rk354. Residues in purple correspond to the conserved DLAGSE motif of switch-2 region that is followed by the loop 11 (in black color) and the helix $\alpha 4$ (red). The residues deleted for this study are shown with dashes. (B) Stereoscopic image view of a detail of the wild type Rk354 structure (Sack et al., 1997) illustrating the region around $\beta 7$, $\alpha 4$ and loop 11 (deleted). Val²³⁹ has been substituted by a glycine to serve as a bridge. Colors of structural elements correspond to the residue colors in A. Figure was produced in collaboration with Dr. A. Marx.

The deletion of the 14 residues ²⁴⁰SKTGAEGAVLDEAK²⁵³ was performed in one step by the method of site-directed mutagenesis (section 2.2.10). Additionally, the Val²³⁹ was mutated to a glycine (V239G), in order to provide

the needed flexibility to the structure after the deletion of loop 11. A restriction site of BamHI was incorporated in the oligonucleotide to simplify the selection of positive clones, which were verified by sequencing (2.2.7).

3.1.7.1 Expression and Purification of RK354 Δ loop11

BL21 RIL cells (Table 1) were transformed with the plasmid RK354 Δ loop11 using the electroporation protocol. Expression was carried out overnight at 24⁰C (section 2.3.3). The protein was purified (Fig. 22) in three steps: with a phosphocellulose column following a batch protocol, with a MonoQ anion exchange column and finally, a gel filtration column (section 2.3.6.5, buffer compositions can be looked up in the Appendix). The yield of purified protein was approximately 7 mg per liter culture.

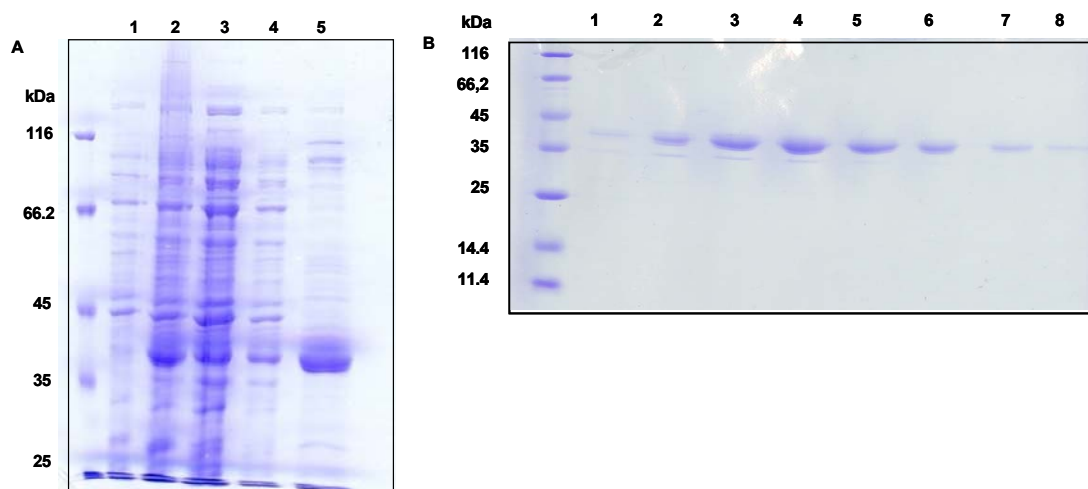


Fig. 22: Purification of RK354 Δ loop11: (A) Phosphocellulose column for RK354 Δ loop11 protein: lane 1 refers to uninduced sample, lane 2 to IPTG-induced sample, lane 3 to flowthrough, lane 4 to unbound proteins washed out and lane 5 to the PC eluate. (B) Gel filtration fractions. The main protein peak corresponds to fractions 3-5. The SDS-PAGE gel of the MonoQ chromatography step is not shown.

3.1.2.2 Crystallization trials with the RK354 Δ loop11 protein

The protein displayed excessive precipitation everytime an aliquot was thawed to be used in crystallization trials. The addition of glycerol in the working solutions did not reverse the precipitation. Therefore, the protein produced was set up in crystallization plates immediately after preparation. The working protein concentration was 15 mg/ml.

A wide screening around the wild type condition (Table 5) was carried out. The parameters of precipitant, salt, protein concentration, and pH were investigated. One parameter was altered each time. Different ratios of protein to reservoir were used in hanging drop vapor diffusion plates. Heavy precipitation and denatured protein were observed. Lowering the protein concentration to 7 mg/ml did not help to obtain any crystals.

3.2 Generation of *Rattus norvegicus* kinesin light chain (KLC) constructs

Kinesin light chains are involved in many cargo interactions via their tetratricopeptide repeat (TPR) domain (as described in sections 1.3 and 1.3.1). In this study a number of constructs of the TPR domain were cloned, expressed and used in crystallization trials.

3.2.1 Cloning of KLC constructs

The plasmids pCDNA3.HA.KLC-C encoding the kinesin light chain isoform C of *Rattus norvegicus* and pGST.HA.KLC.TPR that encodes the TPR domain of KLC-C were kindly provided by Dr. BJ Schnapp (Department of Cell and Developmental Biology, Oregon Health Sciences University, Portland). The pCDNA3.HA plasmid is a vector for mammalian expression. Therefore, the KLC-C insert was recloned into the *E.coli* expression vector pET16b, a vector that provides an N-terminal His₁₀-tag (Table 2).

The pCDNA3.HA.KLC-C and pET16b plasmids were digested with BamHI and the BamHI-KLC-C insert was ligated (section 2.2.5) in frame into the pET16b BamHI-digested vector, in order to generate the pET16b.KLC-C plasmid. Positive, right orientated clones were confirmed by restriction analysis with NdeI. A further XhoI digestion was carried out to remove 24 base pairs that belonged to the original pCDNA3.HA vector and not to the KLC ORF. The pET16b.KLC-C- XhoI treated plasmid was relegated.

Two more constructs were generated from the pHA.GST.TPR plasmid; one with a polyhistidine-tag N-terminal to the TPR ORF and one with a C-terminal His₆-tag, generating the pET16b.Nhis.TPR. and pNG2.Chis TPR constructs, respectively. The first necessary step was to remove an internal NdeI restriction site in the pHA.GST.TPR plasmid (1685-1690 bp). Site directed mutagenesis was performed to introduce a silent mutation {5'-C (mutated to an A) ATATG-3'} that would not affect the amino acid composition of the encoding region. Positive clones having the mutation were confirmed by sequencing (section 2.2.7), using oligonucleotides as stated in Appendix.

Using the oligonucleotides SMklc_1 and 2, the TPR domain was amplified by PCR and cloned with the TOPO blunt end kit (Invitrogen), following the manual of the company. The insert was sequenced and ligated into the pET16b vector. Both insert and vector were digested with BamHI and NdeI prior to ligation. The orientation of the insert in the resulting plasmid was checked by restriction analysis with NcoI and StuI. The resulting plasmid was named pET16b.Nhis.TPR.

The plasmid pNG2.Chis.TPR was generated by amplifying the TPR domain and incorporating a six histidine-tag C-terminal of the TPR-encoding region. The insert was subcloned with the TOPO blunt end kit (Invitrogen), following the manual of the company. The insert was sequenced and ligated into the pNG2 vector (generated in our lab from a pET vector) after BamHI-NdeI digestion of both of them. Positive clones were confirmed by sequencing (2.2.7). A number of constructs were prepared using the GatewayTM technology (Invitrogen) as it is described in the methods section (2.2.9).

The plasmids pHA.GST.TPR, pET16b.Nhis.TPR and pNG2.Chis.TPR code for the complete first five TPR motifs and extend up to aa 505 of the sixth repeat. Furthermore, a series of constructs that span two TPR motifs or the full TPR domain and the KLC 'tail' were generated (Table 8).








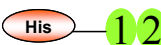

KLC Construct	Plasmid	Protein	Mw (kDa)
	pET16b.KLC-C	His.KLC-C	67
	pHA.GST.TPR	GST.TPR1-6	61
	pET16b.Nhis.TPR	His.TPR1-6	34
	pNG2.Chis.TPR	C-His.TPR1-6	33.7
	pDEST15.TPR1-6t	GST.TPR1-6t	68
	pDEST20.TPR1-6t	GST.TPR1-6t	62.4
	pDEST17.TPR1-6t	His.TPR1-6t	43
	pDEST15.TPR1-2	GST.TPR1-2	36
	pDEST17.TPR1-2	His.TPR1-2	11.3
	pDEST17.TPR3-4	His.TPR3-4	12.1

Table 8: Summary of constructs of rat KLC-C.

3.2.2 Expression and purification of KLC constructs

During expression trials of the KLC-C constructs, the solubility and/or the stability of the proteins proved to be a bottleneck. Various *E.coli* strains (Table 1) were tested to obtain higher protein yields and/or soluble proteins. Attempts of solubilization were focused onto the addition of a variety of solubilizing agents in the lysis buffer. Lower expression temperatures and/or shorter induction time were also tried. Lysis and purification buffer compositions can be looked up in Appendix. The Gateway™ constructs (pDEST vector series) were favorably expressed in BL21 AI cells (Table 1).

3.2.2.1 Expression and purification of His.KLC-C and GST.TPR1-6 proteins

The full length KLC-C displayed good expression but poor solubility. BL21 DE3 cells were transformed with the plasmid by an electroporation protocol. After cell lysis the soluble fraction of proteins and the pellet (fraction of insoluble material) were analysed by western-blot (section 2.3.2). The protein was detected in the insoluble fraction. The lysis buffer used was: 50mM Pipes pH=6.9, 100mM NaCl, 1mM β -mercaptoethanol. Usage of AD494 cells or the BL21 RIL strains (Table 1) and variation of the expression conditions (temperature, time of cell growth after induction, IPTG concentration) did not improve the solubility.

The pHA.GST.TPR plasmid was transformed into BL21 (DE3) cells by electroporation and expression was carried out. The protein was well expressed and soluble. The purification protocol used to purify the protein included three steps: 1) a GST-Sepharose affinity purification step to isolate the GST-tagged protein, 2) a cation exchange chromatography step with an SP-Sepharose column HR 10/10 (Pharmacia) to remove bulk contaminants and 3) a gel-filtration step (Fig. 23).

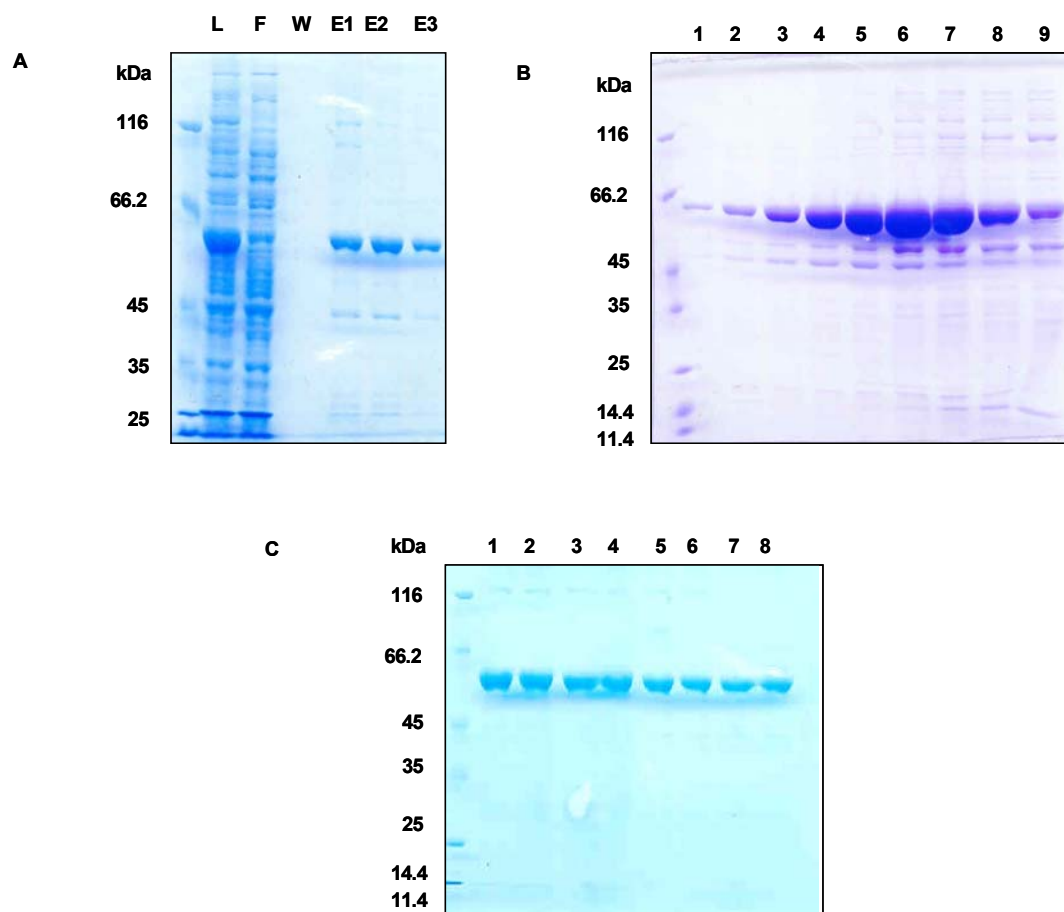


Fig. 23: Purification of GST.TPR1-6 protein; 10% Coomassie-stained SDS-PAGE gels from (A) GST-Sepharose column following a batch protocol. L: lysate; F: flow through; W: wash; E1-3: eluates, (B) SP-sepharose fractions; fractions 5-7 correspond to the protein peak, (C) gel filtration fractions.

In gel filtration, the protein was eluted in the form of dimers (~ 130 kD) due to intrinsic property of GST to form dimers. Higher molecular weight aggregates like trimers, tetramers etc were also observed. Increasing the salt concentration in the gel filtration buffer minimized these interactions.

3.2.2.2 Crystallization trials with GST.TPR1-6 protein

The protein was concentrated to 10 mg/ml (section 2.3.6) and filtered through a centrifuge filter device (Ultrafree Amicon with cutoff 0.45 μ m) prior to crystallization trials, to remove high molecular weight aggregates. The vapour diffusion sitting drop method was mainly used to set up crystallization plates

both at room temperature and 4°C. Additionally trials were carried out with the batch method. Numerous conditions were screened using commercial kits (Crystal Screen 1, Crystal Screen 2, Additive screen 1,2,3, PEG/Ion Screen, Grid Screen NaMalonate, Index Screen, Grid Screen PEG6000, JB Screen). Moreover, a number of conditions that were successful to crystallize other GST-fusion proteins were screened. Despite the high purity of the protein, no crystals were observed. The failure of the protein to crystallize could be attributed to the inter-domain flexibility introduced by the GST segment in the fusion protein.

3.2.2.3 Expression of His.TPR1-6 and C-his.TPR1-6 constructs

The failure of crystallizing the construct GST.TPR1-6 led to the cloning of the same TPR segment fused with either a His₁₀-N-terminal tag or a His₆-C-terminal tag, to overcome the possible negative effect of GST in crystallization.

His.TPR1-6 was expressed (2.3.3) in AD494 cells in significantly higher amounts than in BL21 (DE3) or BL21 RIL (Table 1). The protein was soluble and purified with a Ni-NTA affinity chromatography step to high purity. A final gel filtration step was added to remove any high or small molecular weight contaminants and exchange the Ni-NTA imidazole-containing elution buffer. All buffer compositions can be looked up in Appendix. The purified protein is shown in Fig. 24.

The pNG2.Chis.TPR construct was expressed in BL21 RIL, BL21 (DE3) as well as in AD494 cells. No expression was observed. Western-blotting analysis using an anti-GST antibody, confirmed this finding.

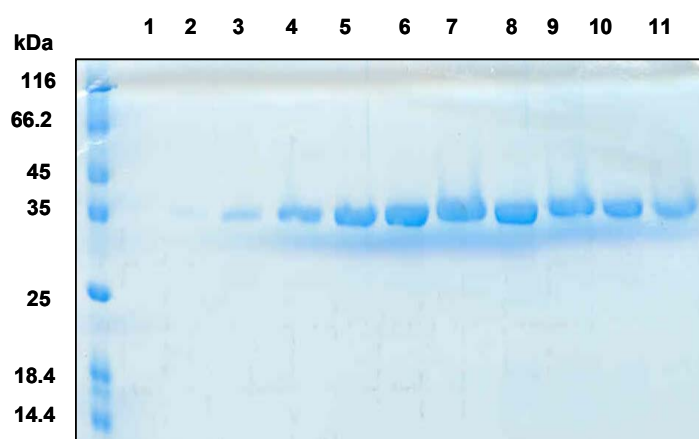


Fig. 24: Gel filtration eluate fractions of His.TPR1-6 construct: fractions 5-10 corresponded to the main protein peak.

3.2.2.4 Crystallization trials with His.TPR1-6 protein

The protein sample was concentrated to 8-10 mg/ml and filtered through a centrifuge filter device (cutoff 0.45 μ m) prior to the crystallization trials, to remove high molecular weight aggregates. The vapour diffusion sitting drop method was used both at room temperature and 4°C. Numerous conditions were screened (Crystal Screen 1, Crystal Screen 2, Additive screen 1,2,3, PEG/Ion Screen, Grid Screen NaMalonate, Index Screen, Grid Screen PEG6000, JB Screen). Nevertheless, nothing but amorphous precipitate or denatured protein could be observed in the drops. In a few cases some crystalline precipitate grew, but efforts to further optimize these conditions did not succeed. Moreover, the protein displayed precipitation problems during thawing the stored aliquots. Increasing the ionic strength of the buffers and the concentration of β -mercaptoethanol reduced the observed precipitation.

3.2.2.5 Expression of GST.TPR1-2, His.TPR1-2 and His.TPR3-4 constructs

Three shorter constructs that span two TPR motifs, either the first two or the third and the fourth were cloned in order to observe the behavior of the KLC-C TPR domain if it was truncated and crystallize them in a 'carrier protein-driven crystallization' (Donahue et al., 1994). The possibility of crystallizing small peptides and domains fused with the GST has been demonstrated (reviewed in Zhan et al., 2001). Additionally, the small size of the His.TPR1-2 (103 amino acids) and His.TPR3-4 (105 residues) proteins could make them good candidates for NMR structural analysis.

Expression tests were carried out for the His.TPR1-2 and the His.TPR3-4 constructs. Cells were lysed to assess the expression levels and the solubility. The expression in BL21 AI cells (Table 1) was high, but the solubility proved to be a bottleneck (Fig. 25). Solubility studies were carried out without success. Increasing the salt concentration, pH variations or addition of detergents had no effect on the solubility.

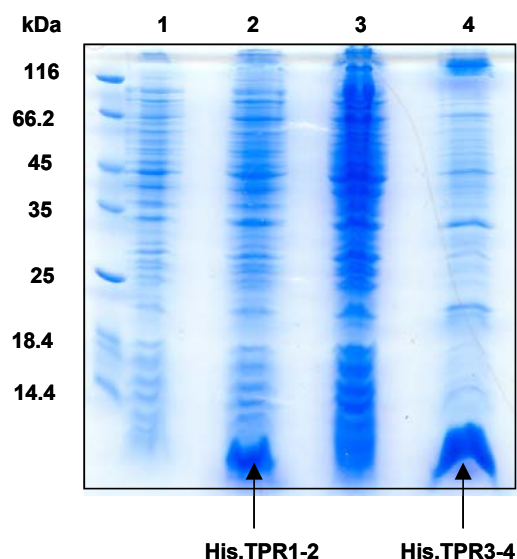


Fig. 25: Solubility study with the His.TPR1-2 and His.TPR3-4 constructs: 17% SDS –PAGE gel of the soluble (lanes 1,3) and insoluble (lanes 2,4) fractions of the lysates of His.TPR1-2 and His.TPR3-4, respectively. Both proteins (Mw=11.3 and 12.1, respectively) appear insoluble.

In the initial expression tests, the GST.TPR1-2 protein was mostly insoluble (Fig. 26A) but the addition of 0.2% of the nonionic detergent NP-40 increased its solubility. The GST.TPR1-2 protein was purified by a GST-Sepharose batch step (Fig. 26B). Despite the addition of protease inhibitors (buffer compositions in Appendix), some degradation was observed and verified by western-blotting analysis.

Further purification of the protein with an anion exchange chromatography column (MonoQ HR 10/10) yielded poor results, as it failed to separate any contaminants. The NP40 detergent caused this non-separation effect by forming high molecular weight micelles (~ 90 kD) that interfered in the purification process. Once the micelles are formed they are difficult to remove by chromatography or dialysis. Lowering the NP40 concentration down to 0.05% solved the problem. The degradation of the protein was not avoided by adding higher concentrations of inhibitors.

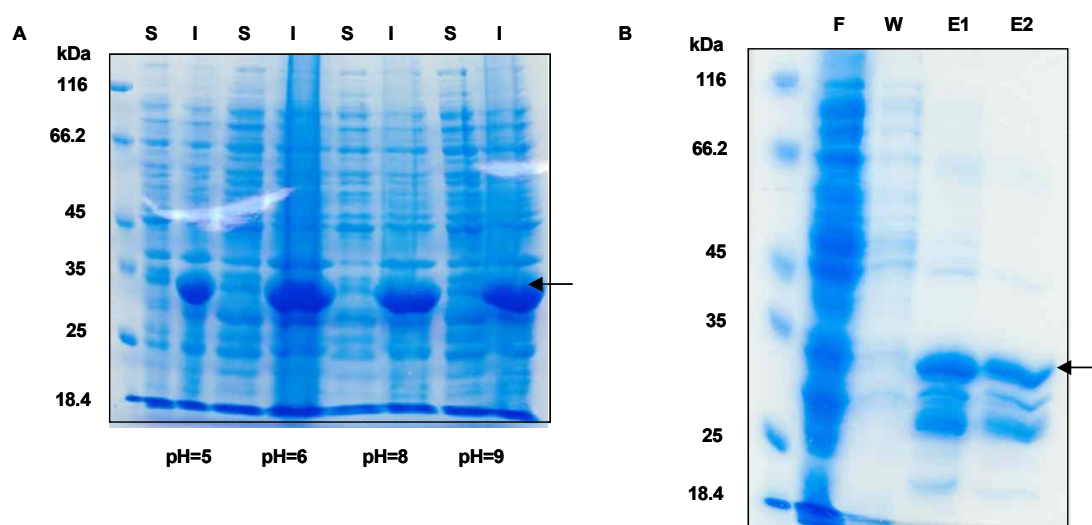


Fig. 26: Expression of GST.TPR1-2 protein: (A) 10% SDS-PAGE gel depicting soluble (S) and insoluble fractions (I) of solubility studies at different pHs. (B) GST-affinity chromatography: F: flowthrough; W: wash; E1-2: eluates. Addition of 0.2% NP40 in the lysis buffer solubilized the protein.

3.2.2.6 Crystallization trials with GST.TPR1-2 protein

The protein was concentrated to 10 mg/ml and filtrated through a centrifuge filter device (cutoff 0.45 μ m) prior to crystallization trials. The sitting drop method was mainly used to screen the conditions of all available commercial kits. Moreover, a screening was carried out based on the successful cases of 'GST-carrier-driven' crystallization of small peptides and domains (Zhan et al., 2001). In most cases amorphous or heavy precipitant or denatured protein were observed in the drops.

Nonionic detergents like NP40 are known to be in general less denaturing for proteins than other types of detergents. Nevertheless, it could be argued that NP40 disrupted the GST.TPR1-2 structure and affected its 'crystallizability'. Furthermore, the significant degradation of the protein can also be blamed for increasing the heterogeneity of the sample, thus inhibiting the crystallization of the protein. The inter-domain flexibility introduced through the GST segment in the fusion protein could be responsible for the unsuccessful crystallization trials as well.

3.2.2.7 Expression of His.TPR1-6t protein

The failure to crystallize the shorter constructs and their problematic behavior concerning the solubility or the stability of the proteins led to the design of a longer construct, spanning the entire TPR domain and the isoform-specific sequence of the 'tail' region (residues 230-577). The addition of the KLC C-terminus region aimed to improve the solubility and/or stability of the protein. Furthermore, the KLC 'tail' sequence spans an isoform-specific signature (⁵⁵⁹VSMSVEWNG⁵⁶⁷ for KLC-C). It has been demonstrated that these isoform-specific sequences can direct kinesin to a specific cargoes (Khodjakov et al., 1997; Gyoeva et al., 2000).

Expression tests and solubility studies were carried out as the His.TPR1-6t protein proved to be insoluble (Fig. 27). Despite the intense efforts no improvement was observed.

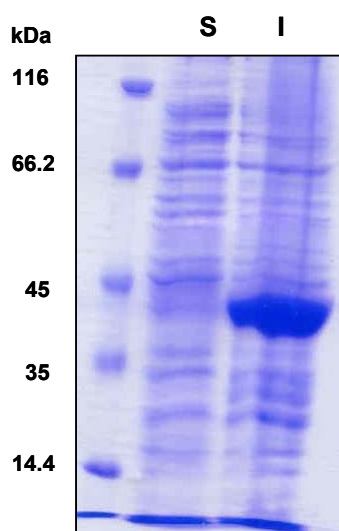


Fig. 27: Solubility study of His.TPR1-6t protein: S: soluble fraction; I: insoluble. BL21 RIL cells were used for this expression test.

3.2.2.8 Expression of the GST.TPR1-6t protein in SF9 insect cells

To further address the solubility problem a construct that spans the 6 TPR motifs and the c-terminal region of KLC-C was subcloned into the pDEST20 Gateway™ vector that is designed for baculovirus expression in SF9 insect cells. Expressing a protein in an eukaryotic expression system, such as the baculovirus expression system in insect cells, has the advantage of providing all post-translational modifications that an eukaryotic protein normally undergoes. In addition, chaperones that naturally exist in the cytoplasm of the insect cells can possibly help the newly synthesized proteins to fold properly.

The bacmid.GST.TPR1-6t construct was generated (section 2.2.9) and used to transfect *Sf9* insect cells. The *Sf9* culture is described in methods (section 2.3.5.1). The protein expression and isolation was carried out as described in methods (section 2.3.5.2).

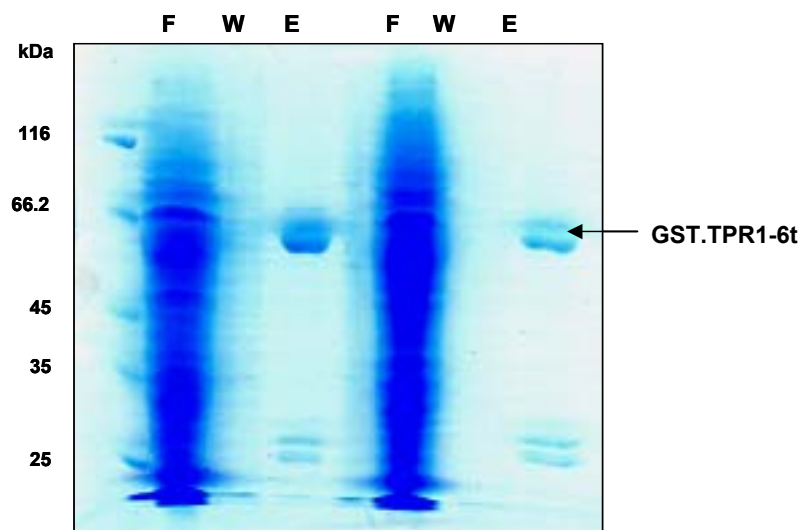


Fig. 28: Expression of the GST.TPR1-6t protein in SF9 insect cells: 10% SDS-PAGE gel of the purification of the GST.TPR1-6t protein expressed in *SF9* cells GST Sepharose spin columns were used. F: flowthrough; W: wash; E: eluate. Two 15 ml *SF9* cell cultures with a density of 1.8×10^6 cells/ml were lysed and the eluates loaded on the gel.

3.2.2.9 Removal of the GST-tag from the GST.TPR1-6t protein

GST.TPR1-6t has a TEV protease cleavage recognition site cloned immediately after the affinity tag, so that the tag can be removed in order to crystallize the protein by its own.

The efficiency of the cleavage was very low. Although in most cases a ratio of 1/50 of TEV protease to substrate is sufficient, in this case it proved inadequate. Cleavage was performed with purified protein or during incubation of the protein with the GST-sepharose, either at 4°C overnight or at 30°C. The low cleavage efficiency indicates that the TEV recognition site was not accessible for the protease. The addition of 0.5 M urea, in order to slightly disrupt the secondary structure of the protein and allow TEV to cleave the GST-tag, was not successful either. The amount of TEV used was increased up to 1:1 ratio, without improving the cleavage efficiency.

It is possible, that the α -helices of the TPR domain adopt a conformation in the three dimensional space, that 'protects' the cleavage sequence, preventing the protease from cleaving.

3.2.2.10 Expression of the GST.TPR1-6t protein in *E.coli*

The soluble GST-tagged fusion protein that was expressed in SF9 cells was recloned into an *E.coli* GatewayTM expression vector, generating the plasmid pDEST15.TPR1-6t that spans the entire TPR domain plus the 'tail' region of KLC-C. Expression tests in BL21 AI cells showed that the protein was partly soluble (Fig. 29).

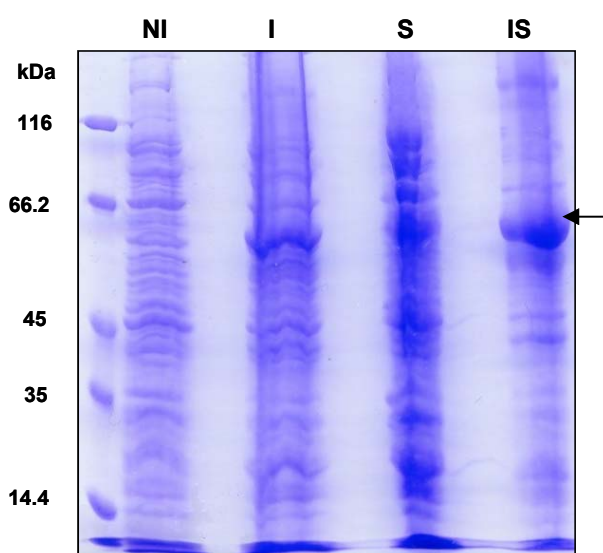


Fig 29: Expression and solubility test for the GST.TPR1-6t protein: BL21 AI cells were used for expression. NI: Non-induced cells; I: induced cells; S: soluble fraction of proteins; IS: insoluble fraction of proteins. The GST.TPR1-6t protein is indicated by an arrow.

The protein was purified according to a GST-affinity purification protocol and the purified sample was incubated with TEV protease to remove the tag. The efficiency of TEV cleavage was very low. It appeared that the TEV recognition site was not accessible.

3.2.2.11 Initial proteolytic analysis of the GST.TPR1-6 construct

A limited proteolysis analysis was performed for the GST.TPR1-6 protein (section 2.3.14) using trypsin protease. The result of the limited proteolysis was assessed in a 10% SDS-PAGE gel (Fig. 30). Trypsin efficiently cleaved GST.TPR1-6 (61 kD) decreasing its amount with the time of digestion. Apparently, GST was cleaved easily and accumulated (band at the range of 26 kD). The remaining TPR segment of the fusion protein should have a molecular mass of 35 kD. In fact a 35 kD band appeared and as the trypsin treatment proceeded it got further degraded. After 60 min of reaction, the fusion protein was almost entirely cleaved. One protein band (~32 kDa) appears to be stable, named 'TPR fragment' (Fig.30). Further efforts must be carried out to map this peptide.

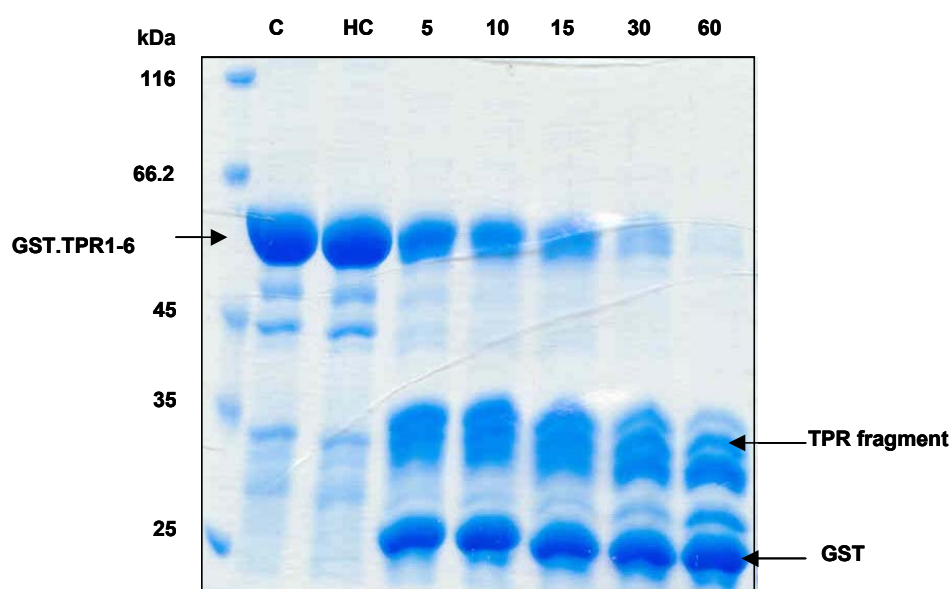


Fig. 30: Limited proteolysis analysis of the GST.TPR1-6 protein. For each reaction 400 µg of protein sample were incubated with 40 µg trypsin. C: untreated control; HC: heat control for 60 minutes; 5,10,15, 40, 60: time points of the trypsin treatment.

4 Discussion

4.1 Structural investigation of a conserved arginine in the switch-1 region of kinesin-1

Kinesin-1 is a plus-end-directed microtubule-based motor that transports its cargoes towards the synapse of neurons in a processive manner. The mechanism by which kinesin converts the energy from the ATP hydrolysis to motion has been approached by various biochemical and structural studies (review: Cross, 2004). In this context, the generation of the Nk355^{R207A}, Nk355^{R207K}, Rk354^{R204A} and Rk354^{R204K} mutant constructs aimed to contribute structural information about the conformational changes in the active site of the motor.

Studies with *Drosophila* kinesin, where Arg²¹⁰ has been substituted with an alanine (R210A), resulted in a motor that can bind ATP effectively, but is defective for ATP hydrolysis. Moreover, the mutant motor displayed reduced affinity to microtubules and a loss in cooperativity between the motor domains in the dimer (Farrell et al., 2002). Further investigation with a lysine substitution mutant (R210K) resulted in a motor with a defect in ATP hydrolysis, but restored microtubule affinity and motor domain cooperativity (Klumpp et al., 2003). This arginine participates in a critical salt bridge within the active site and is thus conserved in all conventional kinesins.

4.1.1 Cloning, expression and purification of point mutants

Both the alanine and lysine mutations were introduced into *R. norvegicus* and *N. crassa* monomeric constructs by site directed mutagenesis. The proteins were expressed and purified following a protocol of three steps (section 2.3.6.5). For the Nk355^{R207A} and Nk355^{R207K} proteins, two cation exchange columns (a phosphocellulose and a MonoS column) and a final gel filtration column were employed. For the Rk354^{R204A} and Rk354^{R204K} proteins the purification strategy consisted of a cation exchange column (Phosphocellulose

column), an anion exchange column (MonoQ) and a final gel filtration step. The purified proteins were highly concentrated in order to be used in crystallization trials.

4.1.2 Crystallization and preliminary X-ray analysis of the Nk355^{R207A} and Rk354^{R204A} constructs

The vapour diffusion sitting and hanging drop crystallization methods were mainly applied. Besides screening the crystallization conditions that have been used to crystallize the wild type proteins, a broad range of conditions was screened with commercial crystallization kits. All four proteins yielded small needle-like crystals and optimization trials were carried out. The Nk355^{R207A} protein crystals were optimized to plate-like crystals. The Rk354^{R204K} as well as the Rk354^{R204A} protein crystals were optimized to bigger needle-like crystals.

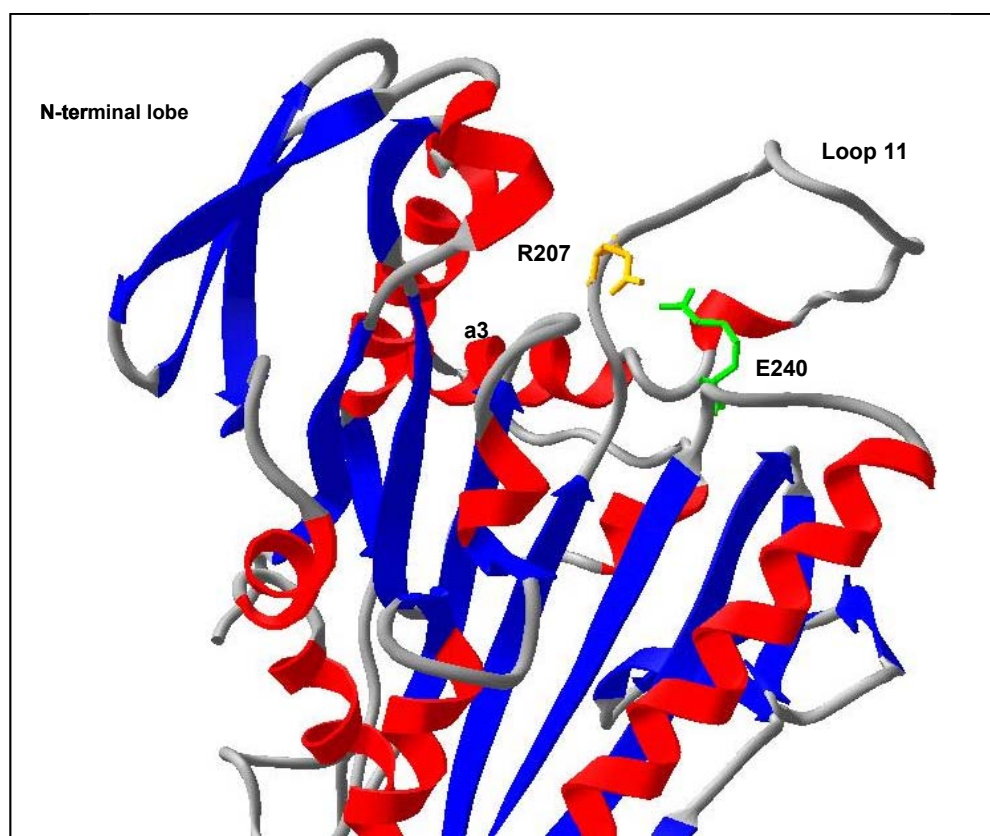


Fig. 31: Model of the salt bridge between R207 and E240 in *N. crassa*: detail of the structure of the motor domain of kinesin-1 (Song et al., 2001, PDB code: 1GOJ) depicting the residues R207, E240, the N-terminal lobe, the loop 11, the helix α_3 .

The Nk355^{R207A} and Rk354^{R207A} protein crystals were tested for diffraction at the synchrotron radiation beamline of the X13 consortium (EMBL, University of

Hamburg) and complete data sets were collected for both. Molecular replacement (MR) was performed and generated unique solutions, using the structures of the wild type proteins as search models. The arrangement of the molecules in the crystal of the Nk355^{R207A} protein can be seen in Fig. 32. Based on the MR solution, an initial electron density map of the molecule was generated (Fig. 20, section 3.1.6). As expected, there was not much electron density where the side chain of the arginine would be in the wild type, though at this stage of analysis, it would be too early to discuss small differences between the wild type and the mutated protein in the region where the arginine has been mutated to alanine. After further refinement a better defined electron density map should allow detection of any structural changes.

The crystals of the Nk355^{R207A} protein belong to a different space group than the wild type (P2₁ in contrast to P2₁2₁2₁), meaning there are differences in the packing of the molecules. Interestingly, despite of this fact (compare Fig. 32 with Fig. 33), molecule1 (yellow) and molecule 2 (green) in both crystals have the same conformation in the wild type and mutant, while molecule 3 (blue) and molecule 4 (red) have different orientations. This fact could indicate that the conformation of molecules 1 and 2 may be an energetically favorable interaction of molecules during formation of both types of crystals. Moreover, differences can be observed especially on surface elements as the loop 10 and loop 11 or the L2 finger (section 3.1.6). In order to investigate what structural changes are responsible for the deficiencies of the mutant protein within the switch-1 region a final refinement process will be necessary.

The mutated Arg²⁰⁷ belongs to the switch-1 motif that is conserved in all kinesins (Fig. 5). It participates in a salt bridge with a glutamate residue of the switch-2 region. This salt bridge positions a water molecule inside the active site of the motor, so the ATP hydrolysis can occur (Fig.34). An alanine in this position fails to carry out this function and the water molecule is not positioned properly, resulting in an ATP hydrolysis defect (Farrell et al., 2002; Klumpp et al., 2003).

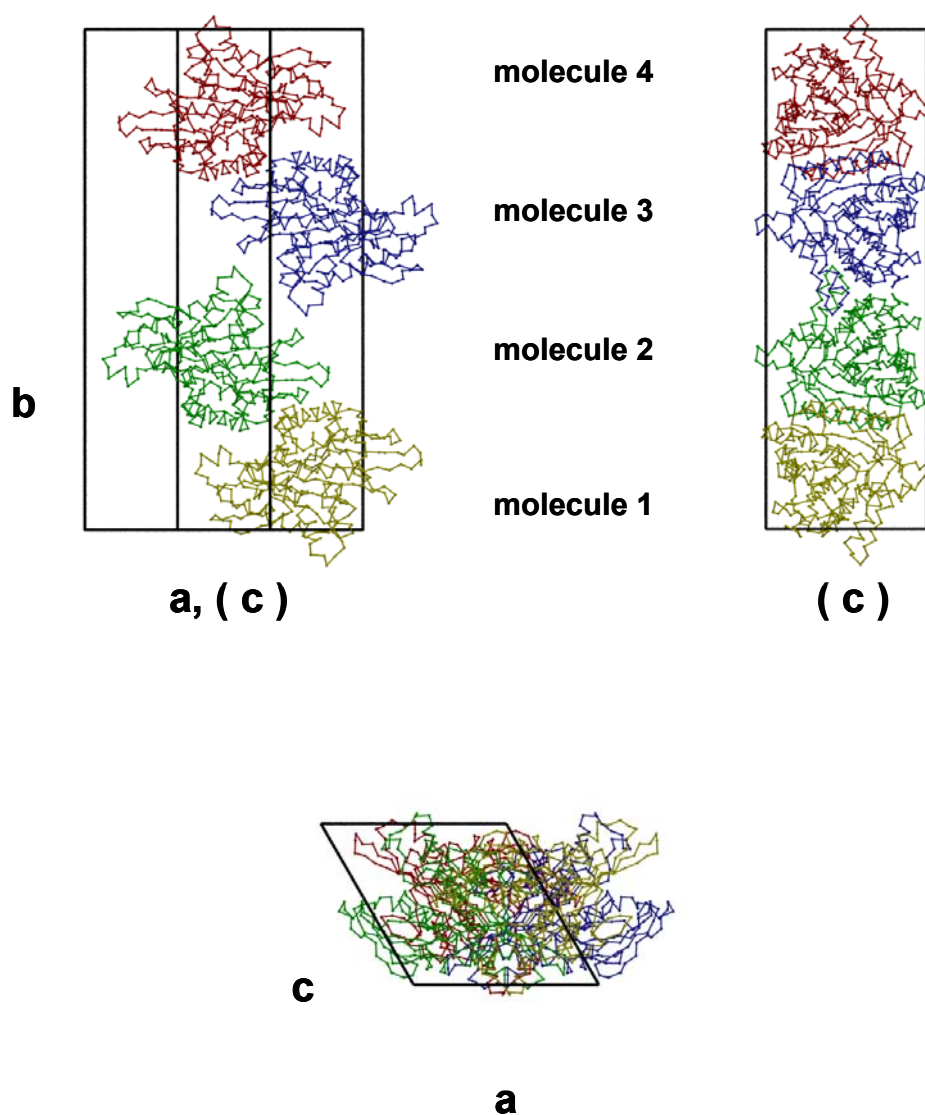


Fig. 32: Packing of protein molecules in the crystals of the mutant Nk355^{R207A}, space group P2₁; two molecules per asymmetric unit, two asymmetric units per unit cell, $a=51.454$ Å, $b=139.469$ Å, $c=51.754$ Å. (Cell constants in parentheses indicate that the corresponding cell edges are shown in projection). Figure was produced by Dr. A. Marx.

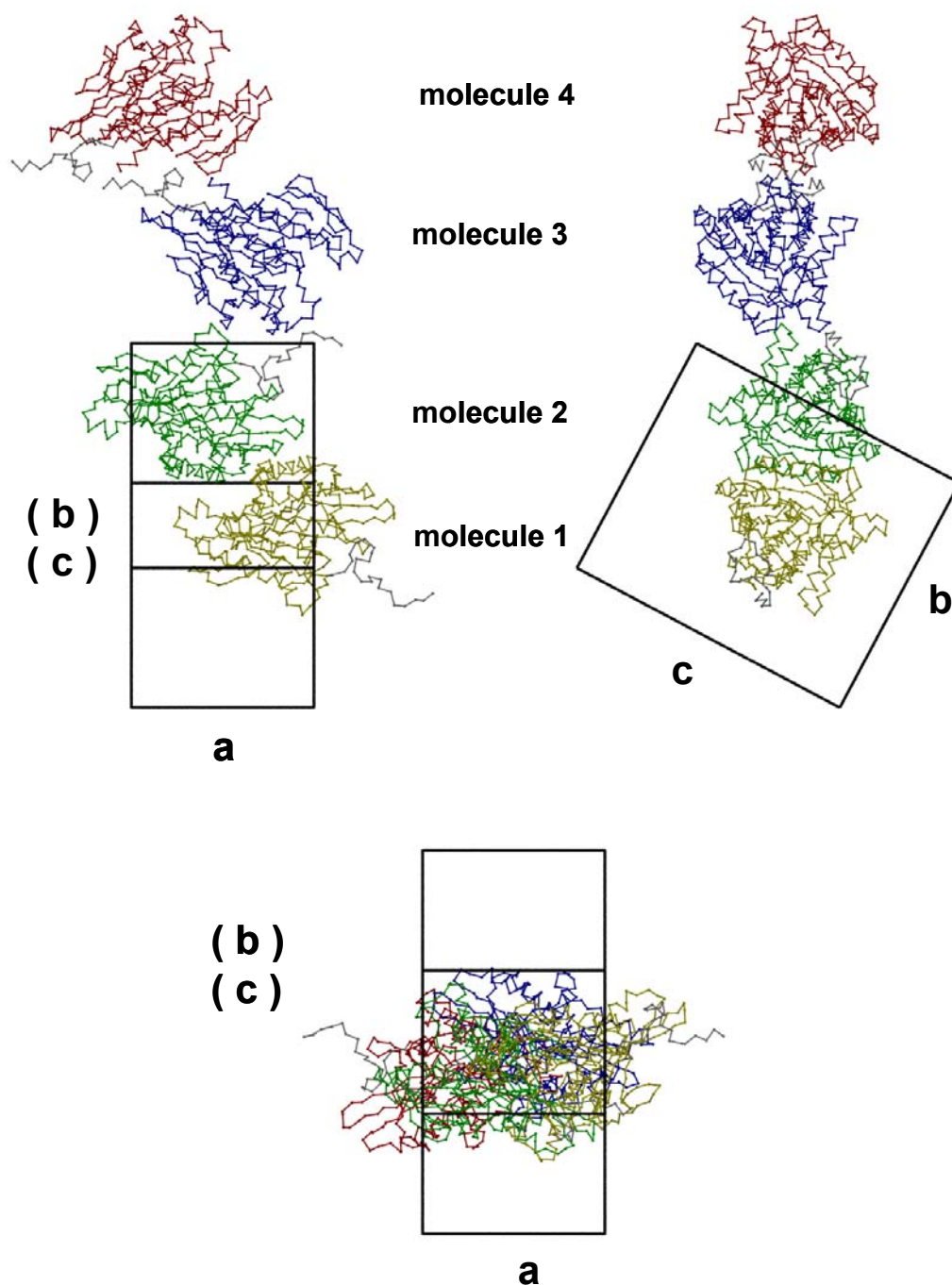


Fig. 33: Packing of protein molecules in the crystals of the wild type Nk355 (Song et al., 2001; PDB code: 1GOJ). Space group: P212121; one molecule per asymmetric unit, four asymmetric units per unit cell $a = 52.0 \text{ \AA}$, $b = 72.7 \text{ \AA}$, $c = 84.9 \text{ \AA}$. (Cell constants in parentheses indicate that the corresponding cell edges are shown in projection). Figure was produced by Dr. A. Marx.

The importance of this salt bridge for ATP hydrolysis is supported by experimental data in kinesins and myosins. The four elements (N1 to N4) that form the nucleotide-binding site in kinesin (Kull et al., 1996) are highly conserved in kinesins (Rice et al., 1999), myosins (Hua et al., 1997) and G-proteins. The salt bridge between switch-1 (NXXSSRSH) and switch-2 (DLAGSE) regions is also conserved (Yun et al., 2001; Song et al., 2001; Kozielski et al., 1997; Sack et al., 1997; Kull et al., 1996). Mutation of the switch-2 glutamate causes an ATP hydrolysis defect in myosin II and kinesins (Rice et al., 1999; Onishi et al., 1998; Suzuki et al., 1998; Furch et al., 1999; Sasaki et al., 1998). Furthermore, a double mutant in myosin that features an inverted salt bridge displays efficient ATP hydrolysis (Furch et al., 1999). Structural information from a crystal of the salt bridge mutation (R598A) in KAR3 (C-type kinesin-14 family) showed that the mutation destabilized the conformation around switch-1 (Yun et al., 2001).

It has been hypothesized (Klumpp et al., 2003) based on structural modeling of the Arg²⁰⁴ in the rat monomeric structure (Sack et al., 1997), that the Arg²⁰⁴-Glu²³⁷ salt bridge participates in a network of hydrogen bonds (Fig 34) that hold together the three essential and flexible regions for ATP hydrolysis: switch-1, switch-2 and helix α 4. The substitution of Arg²⁰⁴ with an alanine (R204A) disrupts these interactions. Lysine (R204K) on the other hand can donate three hydrogen bonds that cannot substitute the arginine's five hydrogen bonds; therefore it does not restore the motor function completely.

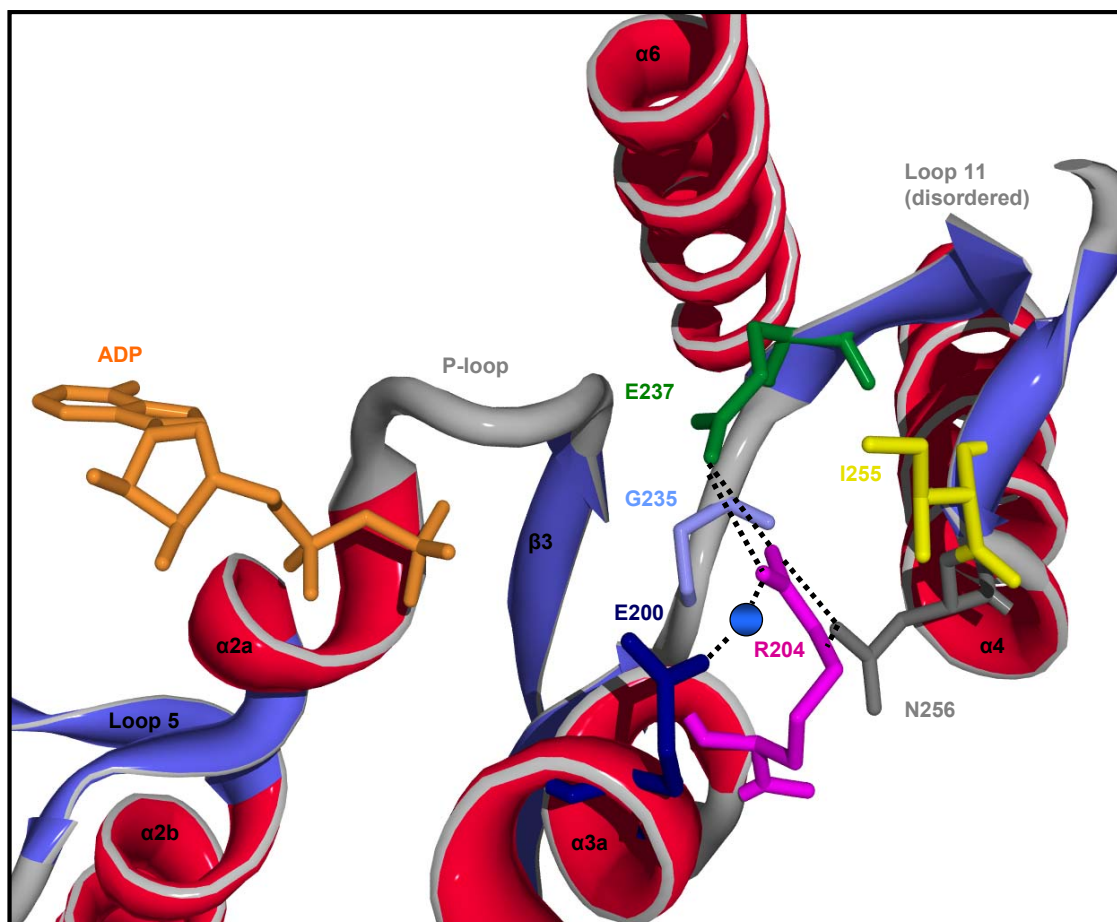


Fig. 34: Structural modeling of the Arg²⁰⁴ in the rat kinesin monomer structure (Sack et al., 1997, PDB code: 2KIN). ADP is shown in orange. Glu²³⁷ (green), Gly²³⁵ (light blue), Asn²⁵⁶ (dark gray) and H₂O 60 (blue) can form hydrogen bonds with Arg²⁰⁴ (magenta), illustrated by the black dashed lines. Ile²⁵⁵ (yellow) can interact with Arg²⁰⁴ via a van der Waals interaction. Arg²⁰⁴ and Glu²⁰⁰ (dark purple) stabilize the position of the water molecule. The figure was produced by the programs PDB viewer (Guex and Peitsch, 1997) and POV-Ray (<http://www.povray.org/>).

Although every catalytically essential structural region such as the P-loop, switch-1, switch-2 and the α 4-L12- α 5 microtubule-binding site are highly conserved in the entire kinesin superfamily, *N. crassa* kinesin-1 displays a series of unique features. That was the reason why it was selected to generate the two mutant constructs Nk355^{R207A} and Nk355^{R207K}. The fungal kinesin-1 structure is one of the few cases where loop 11 is ordered (Song et al., 2001; PDB code: 1GOJ). It has been suggested that loop 11 participates in microtubule binding (Sosa et al., 1997) and only then it obtains a rigid conformation that promotes the communication between the nucleotide and microtubule binding sites (Vale, 1996; Gulick et al., 1998). In addition, it has

been proposed (Kirchner et al., 1999) that the loop 11 may be responsible for the high velocity of 2.0-2.5 μm per second of *N. crassa* kinesin *in vitro* (mammalian kinesins exhibit a velocity of 0.6-0.8 μm per second). Furthermore, in *N. crassa* kinesin-1 three inter-switch salt bridges are present (E240-R207, K257-E204, D235-R194) (Song et al., 2001). The K257 (switch-2) - E204 (switch-1) salt bridge can only be observed in *N. crassa* where loop 11 is ordered.

Refinement of the Nk355^{R207A} model could test the hypothesis proposed in Klumpp et al., (2003) and possibly reveal other structural changes, such as residue movements in the switch-1 area or movements of other elements distal to this region that could be responsible for the functional deficiencies of the mutant.

Interestingly, the crystals of the Rk354R^{204A} construct belong to the same space group (P2₁) as the crystals of the Nk355^{R207A} protein. According to the MR solution the unit cell contains four molecules (2 asymmetric units). When the analysis of the measured Rk354R^{204A} crystal is completed, it will be interesting to examine whether the interactions of the molecules in the crystal are similar to the ones observed for the Nk355^{R207A} measured crystal. In addition, the comparison of the structural changes in both mutant constructs could reveal interesting information about the overall function of kinesin

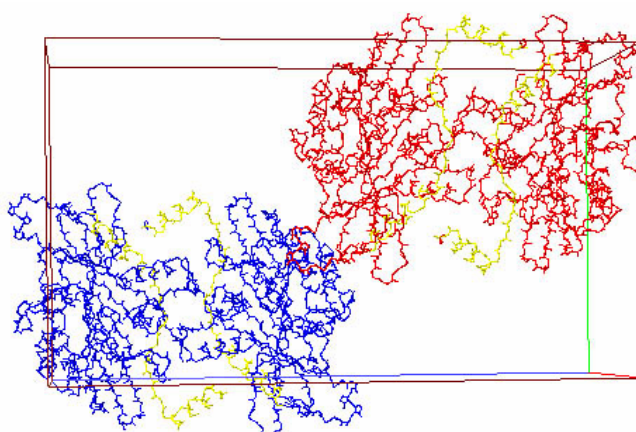


Fig. 35: The packing of protein molecules in the crystal of Rk354^{R204A}; Space group P2₁; two molecules per asymmetric unit, two asymmetric units per unit cell $a=57.400$ Å, $b=72.604$ Å, $c=128.249$ Å, $\alpha=90^\circ$, $\beta=86.899^\circ$, $\gamma=90^\circ$. Figure was produced by Dr. J. Mueller.

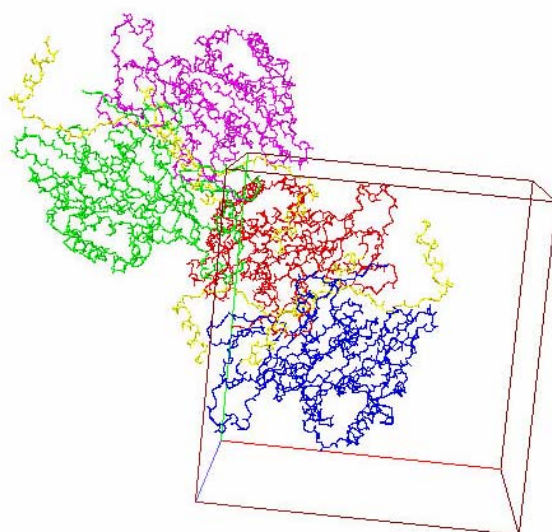


Fig. 36: The packing of protein molecules in the crystal of Rk354 wild type protein (Sack et al., 1997; PDB code: 2KIN); Space group P2₁2₁2₁; four molecules per asymmetric unit, one asymmetric unit per unit cell $a=71.556$ Å, $b=73.674$ Å, $c=74.128$ Å, $\alpha=90^\circ$, $\beta=90^\circ$, $\gamma=90^\circ$. Figure was produced by Dr. J. Mueller.

4.2 Investigation of a rat kinesin-1 loop11 deletion mutant

Within the sequence (or structure) of the kinesin-1 motor domain, loop 11 directly follows after the switch-1 region (Figure 5) and with its central position between switch-1 and switch-2 regions it must play an important role in the conformational changes of the active site of the motor. Interestingly, it is disordered in all kinesin-1 structures, with the exception of the *N.crassa* kinesin-1. Mutations in the loop11 region reduce the speed and ATPase activity of the motor (Brendza et al., 1999; Xing et al., 2000). Furthermore, loop11 is implicated in the microtubule binding (Sosa et al., 2001).

A mutant construct where loop 11 was deleted was generated from the monomeric rat kinesin-1 construct. This was achieved by site directed mutagenesis, where a set of primers were used to delete the loop 11 and at the same time to substitute a valine with a glycine, in order to serve as a bridge between the disrupted switch-1 and switch-2 regions of the motor. The construct was expressed and the protein was purified in three steps: with a cation exchange phosphocellulose column, an anion exchange MonoQ column and finally a gel filtration step. The purified protein was highly concentrated and used in crystallization trials. It tended to precipitate and the crystallization trials yielded no crystals.

Disordered structural elements such as loops or long sidechains of residues contribute to the disorder of protein crystals, which can limit the resolution. Therefore, deleting loop11 aimed to produce a crystal of better quality than the monomeric rat kinesin construct Rk354 crystals, by decreasing the disorder within them.

Helix $\alpha 4$ that follows directly after loop11 in the rat kinesin-1 motor domain structure, (Fig 5) can change in length depending on the conformational state of the motor (Turner et al., 2001; Yun et al., 2001). Reversible melting and reformation of $\alpha 4$ can play an important role in energy storage and conversion. Since the length of loop11 is inversely related to the length of $\alpha 4$, deleting

loop11 could force $\alpha 4$ to adopt different conformation that may be of functional interest.

Conformational changes in surface loops can result in different packing of molecules in the crystal lattice, generating a completely different type of crystal. For example, the motor domain of human Eg5 (kinesin-5 family) was crystallized in a complex with the small, antimitotic drug monastrol (Yan et al., 2004). Monastrol binds to loop 5 and stabilizes it, making loop 5 more rigid. This allows two molecules to form a dimer resulting in completely different crystal packing than observed in the structure without monastrol. Deletion of the surface loop 11 could trigger a conformational change that could in turn result in a different packing of molecules in the crystals of kinesin-1.

Crystallization of the RK354 Δ loop11 construct proved problematic. It is possible that the mutation of Val²³⁹ to a glycine in order to fill the gap and provide some flexibility in the structure after removal of loop 11, hindered the crystallizability of the construct. A loop 11 deletion construct with 2 or 3 glycine residues inserted in order to support the switch-1 and switch-2 regions, could be more successful in future crystallization trials.

4.3 Crystallization studies on the TPR region of the kinesin light chains

Motor-cargo recognition remains one of the least understood aspects of cytoskeletal motor-mediated transport. The TPR motifs of the KLC are known to interact with a variety of proteins and may prove to play a critical role in the attachment of kinesin to its cargoes. Structural investigations are essential for insight into the molecular basis of these potential cargo interactions. A number of TPR domains from a variety of proteins have been crystallized and reveal that though the general fold of the repeat is maintained unique features can also be observed. No structural information exists so far for the TPR motifs of KLC. To this end, expression and purification of various TPR constructs was carried out and crystallization trials performed.

4.3.1 Cloning, expression and purification of TPR constructs

The TPR domain spans six repeats. A number of constructs differing in the length of the TPR region were generated. A construct of the entire light chain was cloned as well. Primarily the efforts were focused on cloning the entire TPR region with different affinity tags (His or GST-tag). A longer construct was generated to include the tail sequences C-terminal to the TPR repeats again with His and GST-tags. These were cloned into vectors for *E. coli* and Baculovirus expression. Shorter constructs spanning two TPR motifs were also generated for crystallization and NMR studies.

The expression of the TPR constructs yielded in many cases insoluble proteins. The solubility problem was approached by recruiting different expression strains and varying the induction conditions (time of induction, temperature or IPTG/arabinose concentration). Further, trials with lysis buffers of different composition were carried out, by varying the pH, the salt concentration and the type of detergent when included. In cases where a combination of optimal induction conditions and use of lysis buffer resulted in soluble protein, purification was carried out and the proteins were used in crystallization trials.

The purification strategy for each construct included an affinity chromatography step with Ni-NTA or GST-Sepharose columns depending on the cloned affinity tag. Only a second step of gel filtration was normally employed as the affinity columns yielded in most cases highly pure proteins. Where necessary, an ion exchange step was additionally included.

4.3.2 Initial crystallization studies with GST.TPR1-6, GST.TPR1-2 and His.TPR1-6 proteins

The soluble proteins of GST.TPR1-6, GST.TPR1-2 and His.TPR1-6 constructs were used in crystallization trials. Numerous conditions were screened with the commercially available kits. In some cases GST tags have proven helpful in 'driving' the crystallization of fusion proteins (review: Zhan et al., 2001).

Therefore, such trials were carried out. However, the failure of the GST-tagged TPR constructs to crystallize could be attributed to the inter-domain flexibility that the GST segment introduces into the fusion protein. His-tagged constructs produced mainly insoluble proteins with the exception of His.TPR1-6. These results suggested that future crystallization trials should be focused on TPR constructs without tags that could interfere with the crystallization process. TEV-protease mediated removal of the GST- or His- tags from the purified recombinant TPR proteins proved problematic. New constructs re-designed around the GST and N-terminal TPR interface may circumvent these problems by increasing access of the TEV protease to its cleavage site: for example an insertion of 3 to 4 glycines as a spacer or incorporating more of the KLC sequence before the TPR motif in a longer construct. Should the removal of the tag not adversely affect the solubility of the KLC construct then crystallization trials could be more promising. Finally, partial proteolysis experiments could help to identify the borders of a new series of more compact constructs that will display better crystallizability (sections 2.3.14 and 3.2.2.11). As a protease cleaves flexible elements, the most compact part of a protein structure remains, thus, it is more likely to crystallize.

One important parameter that would be interesting to consider is the addition of a binding partner in the crystallization experiments. The TPR domain of KLC is known to participate in a series of interactions with other proteins (see in introduction section 1.3.1). Among them the interaction with JIP-1 is thought to be mediated by the carboxyl-terminus of the JIP-1 PTB domain (Verhey et al., 2001). A synthetic peptide of this carboxyl-terminus could be used in tests to enhance the crystallization of KLC TPR domain. Interestingly, the structure of the Jip PTB domain is also not known. Co-crystallization trials of this domain with the soluble TPR constructs described here may be a subject for future investigation.

Since the structure of the three-TPR motifs of PP5 was published (Das et al., 1998) a series of other TPR structures have been solved. Interestingly in some cases complexes have been crystallized between the TPR and a peptide or protein ligand. Examples include the structure of the TPR domain of the

Hsp70/Hsp90 organising protein (Hop) (Scheufler et al., 2000), cyclophilin 40 (Taylor et al., 2001), peroxin 5 (Gatto et al., 2000) and translocase of outer membrane (Tom20) (Abe et al., 2000).

TPR domains that have been crystallized display a versatility while maintaining the classical TPR-fold. Obtaining a crystal structure of the KLC TPR domain alone or in complex with one of its binding partners (e.g. Jip-1) would provide precious insights into how kinesin interacts with its cargo. Understanding how cargo is attached and transported by kinesin could in turn provide valuable insight into its cell biological role. In addition, it may aid the design of a new generation of molecular drugs, intended to attach to KLC and get targeted to the cellular compartments - such as the synapse - where they are needed.

5 Summary

Kinesin-1, the founding member of the kinesin superfamily, is a plus-end-directed microtubule motor that mediates the fast anterograde transport in neurons in a processive manner. Kinesin-1 is a heterotetramer of two heavy (KHCs) and two light chains (KLCs). Each heavy chain comprises three domains: the N-terminal motor domain, the central stalk domain and the C-terminal tail domain. The motor domain contains both the microtubule and the nucleotide (ATP) binding structural elements. Movement along microtubules is propelled by ATP hydrolysis. The kinesin light chain consists of an N-terminal heptad repeat region and a six-repeat TPR domain that is known to interact with a variety of proteins and may prove to play a critical role in the attachment of kinesin to its cargoes. C-terminal isoform-specific sequences of the light chain target kinesin to different cargoes. This thesis explored structural aspects of both the motor domain of the KHC from *Rattus norvegicus* and *Neurospora crassa* and the TPR domain of the KLC from *Rattus norvegicus*.

The entire KLC was cloned but its expression yielded insoluble protein. Further investigation was carried out by generating a series of constructs differing in the length of the TPR domain. In most cases the expression of these constructs yielded insoluble proteins. Strategies to increase the solubility were performed. These included changing the pH and components of the lysis buffer, recruitment of different bacterial expression strains and use of the baculovirus expression system. In cases where soluble proteins were obtained purification was then carried out. Crystallization trials were performed with purified proteins. Although the protein did not crystallize, the expression and purification experiments contribute valuable insight into the intrinsic properties of the specific KLC TPR domain.

Previous studies of the kinesin-1 motor domain in *Drosophila* revealed the importance of the arginine 210 of the switch-1 region to the function of the motor. This arginine is suggested to participate in the formation of a critical salt bridge that positions the water molecule within the active site. Additionally, it is

hypothesized to participate in a network of hydrogen bonds that hold together the three essential and flexible regions for ATP hydrolysis: switch-1, switch-2 and helix $\alpha 4$.

A series of four mutant constructs were generated by substituting this arginine to an alanine and lysine respectively in the motor domains from *Neurospora crassa* and *Rattus Norvegicus* (Nk355^{R207A}, Nk355^{R207K}, Rk354^{R204A} and Rk354^{R204K}). Moreover, a mutant construct was generated where the surface loop 11 (L11) was deleted. Loop 11 is important for microtubule binding. The proteins were expressed, purified and used in crystallization trials. In the case of the Nk355^{R207A} and Rk354^{R204A} proteins suitable crystals have been obtained and data sets were collected at a resolution of 3.05 Å. Molecular replacement produced unique solutions, using the structures of the wild type proteins as search models. Interestingly, the crystals of both mutants belong to the same space group $P2_1$, in contrast to the crystals of the wild type proteins that belong to the space group $P2_12_12_1$. Furthermore, in the case of the Nk355^{R207A} crystals, the orientation of two of the molecules relative to each other was found to be the same in crystals of both the wild type and the mutant proteins.

The aim of this study was to contribute structural information about different domains of the motor protein kinesin-1, using the X-ray crystallography technique. The crystallization of the motor domain mutants could provide interesting insight into the conformational changes in the active site of the motor that could increase our understanding of how the motor uses the energy from ATP hydrolysis to generate motion. Moreover, structural understanding of the TPR domain of the KLC could reveal how kinesin interacts with its cargo. In light of its association with proteins such as the Amyloid Precursor Protein or the JNK-Interacting Proteins, it would be interesting to determine the structural basis of these interactions.

6 References

- Abe, Y., Shodai, T., Muto, T., Mihara, K., Torii, H., Nishikawa, S., Endo, T. and Kohda, D. (2000) Structural basis of presequence recognition by the mitochondrial protein import receptor Tom20. *Cell*, **100**, 551-560.
- Beushausen, S., Kladakis, A. and Jaffe, H. (1993) Kinesin light chains: identification and characterization of a family of proteins from the optic lobe of the squid *Loligo pealii*. *DNA Cell Biol*, **12**, 901-909.
- Blatch, G.L. and Lassle, M. (1999) The tetratricopeptide repeat: a structural motif mediating protein-protein interactions. *Bioessays*, **21**, 932-939.
- Bowman, A.B., Kamal, A., Ritchings, B.W., Philp, A.V., McGrail, M., Gindhart, J.G. and Goldstein, L.S. (2000) Kinesin-dependent axonal transport is mediated by the sunday driver (SYD) protein. *Cell*, **103**, 583-594.
- Brendza, K.M., Rose, D.J., Gilbert, S.P. and Saxton, W.M. (1999) Lethal kinesin mutations reveal amino acids important for ATPase activation and structural coupling. *J Biol Chem*, **274**, 31506-31514.
- Brunger, A.T., Adams, P.D., Clore, G.M., DeLano, W.L., Gros, P., Grosse-Kunstleve, R.W., Jiang, J.S., Kuszewski, J., Nilges, M., Pannu, N.S., Read, R.J., Rice, L.M., Simonson, T. and Warren, G.L. (1998) Crystallography & NMR system: A new software suite for macromolecular structure determination. *Acta Crystallogr D Biol Crystallogr*, **54**, 905-921.
- Cai, Y., Singh, B.B., Aslanukov, A., Zhao, H. and Ferreira, P.A. (2001) The docking of kinesins, KIF5B and KIF5C, to Ran-binding protein 2 (RanBP2) is mediated via a novel RanBP2 domain. *J Biol Chem*, **276**, 41594-41602.
- Collaborative Computer Project Number 4. (1994) The CCP4 Suite: Programs for Protein Crystallography. *Acta Cryst. D*, **50**, 760-763.
- Cross, R. and Scholey, J. (1999) Kinesin: the tail unfolds. *Nat Cell Biol*, **1**, E119-121.
- Cross, R.A. (1995) On the hand-over-hand footsteps of kinesin heads. *J Muscle Res Cell Motil*, **16**, 91-94.
- Cross, R.A. (2001) Molecular motors: Kinesin's string variable. *Curr Biol*, **11**, R147-149.
- Cross, R.A. (2004) The kinetic mechanism of kinesin. *Trends Biochem Sci*, **29**, 301-309.

- Cyr, J.L., Pfister, K.K., Bloom, G.S., Slaughter, C.A. and Brady, S.T. (1991) Molecular genetics of kinesin light chains: generation of isoforms by alternative splicing. *Proc Natl Acad Sci U S A*, **88**, 10114-10118.
- D'Andrea, L.D. and Regan, L. (2003) TPR proteins: the versatile helix. *Trends Biochem Sci*, **28**, 655-662.
- Das, A.K., Cohen, P.W. and Barford, D. (1998) The structure of the tetratricopeptide repeats of protein phosphatase 5: implications for TPR-mediated protein-protein interactions. *Embo J*, **17**, 1192-1199.
- Derman, A.I., Prinz, W.A., Belin, D. and Beckwith, J. (1993) Mutations that allow disulfide bond formation in the cytoplasm of Escherichia coli. *Science*, **262**, 1744-1747.
- Diefenbach, R.J., Diefenbach, E., Douglas, M.W. and Cunningham, A.L. (2002a) The heavy chain of conventional kinesin interacts with the SNARE proteins SNAP25 and SNAP23. *Biochemistry*, **41**, 14906-14915.
- Diefenbach, R.J., Diefenbach, E., Douglas, M.W. and Cunningham, A.L. (2004) The ribosome receptor, p180, interacts with kinesin heavy chain, KIF5B. *Biochem Biophys Res Commun*, **319**, 987-992.
- Diefenbach, R.J., Mackay, J.P., Armati, P.J. and Cunningham, A.L. (1998) The C-terminal region of the stalk domain of ubiquitous human kinesin heavy chain contains the binding site for kinesin light chain. *Biochemistry*, **37**, 16663-16670.
- Diefenbach, R.J., Miranda-Saksena, M., Diefenbach, E., Holland, D.J., Boadle, R.A., Armati, P.J. and Cunningham, A.L. (2002b) Herpes simplex virus tegument protein US11 interacts with conventional kinesin heavy chain. *J Virol*, **76**, 3282-3291.
- Donahue, J.P., Patel, H., Anderson, W.F. and Hawiger, J. (1994) Three-dimensional structure of the platelet integrin recognition segment of the fibrinogen gamma chain obtained by carrier protein-driven crystallization. *Proc Natl Acad Sci U S A*, **91**, 12178-12182.
- Dower, W.J., Miller, J.F. and Ragsdale, C.W. (1988) High efficiency transformation of E. coli by high voltage electroporation. *Nucleic Acids Res*, **16**, 6127-6145.
- Endow, S.A. (1999) Determinants of molecular motor directionality. *Nat Cell Biol*, **1**, E163-167.
- Endow, S.A., Kang, S.J., Satterwhite, L.L., Rose, M.D., Skeen, V.P. and Salmon, E.D. (1994) Yeast Kar3 is a minus-end microtubule motor protein that destabilizes microtubules preferentially at the minus ends. *Embo J*, **13**, 2708-2713.

- Farrell, C.M., Mackey, A.T., Klumpp, L.M. and Gilbert, S.P. (2002) The role of ATP hydrolysis for kinesin processivity. *J Biol Chem*, **277**, 17079-17087.
- Ferreira, A., Niclas, J., Vale, R.D., Banker, G. and Kosik, K.S. (1992) Suppression of kinesin expression in cultured hippocampal neurons using antisense oligonucleotides. *J Cell Biol*, **117**, 595-606.
- Furch, M., Fujita-Becker, S., Geeves, M.A., Holmes, K.C. and Manstein, D.J. (1999) Role of the salt-bridge between switch-1 and switch-2 of Dictyostelium myosin. *Journal of Molecular Biology*, **290**, 797-809.
- Garcia-Saez, I., Yen, T., Wade, R.H. and Kozielski, F. (2004) Crystal structure of the motor domain of the human kinetochore protein CENP-E. *J Mol Biol*, **340**, 1107-1116.
- Gatto, G.J., Jr., Geisbrecht, B.V., Gould, S.J. and Berg, J.M. (2000) Peroxisomal targeting signal-1 recognition by the TPR domains of human PEX5. *Nat Struct Biol*, **7**, 1091-1095.
- Geeves, M.A. (1991) The dynamics of actin and myosin association and the crossbridge model of muscle contraction. *Biochem J*, **274** (Pt 1), 1-14.
- Gill, S.C. and von Hippel, P.H. (1989) Calculation of protein extinction coefficients from amino acid sequence data. *Anal Biochem*, **182**, 319-326.
- Gindhart, J.G., Jr., Desai, C.J., Beushausen, S., Zinn, K. and Goldstein, L.S. (1998) Kinesin light chains are essential for axonal transport in Drosophila. *J Cell Biol*, **141**, 443-454.
- Goldstein, L.S. and Yang, Z. (2000) Microtubule-based transport systems in neurons: the roles of kinesins and dyneins. *Annu Rev Neurosci*, **23**, 39-71.
- Guex, N. and Peitsch, M.C. (1997) SWISS-MODEL and the Swiss-PdbViewer: an environment for comparative protein modeling. *Electrophoresis*, **18**, 2714-2723.
- Guillaud, L., Setou, M. and Hirokawa, N. (2003) KIF17 dynamics and regulation of NR2B trafficking in hippocampal neurons. *J Neurosci*, **23**, 131-140.
- Gulick, A.M., Song, H., Endow, S.A. and Rayment, I. (1998) X-ray crystal structure of the yeast Kar3 motor domain complexed with Mg.ADP to 2.3 Å resolution. *Biochemistry*, **37**, 1769-1776.
- Gunawardena, S. and Goldstein, L.S. (2001) Disruption of axonal transport and neuronal viability by amyloid precursor protein mutations in Drosophila. *Neuron*, **32**, 389-401.

- Gunawardena, S. and Goldstein, L.S. (2004) Cargo-carrying motor vehicles on the neuronal highway: transport pathways and neurodegenerative disease. *J Neurobiol*, **58**, 258-271.
- Gyoeva, F.K., Bybikova, E.M. and Minin, A.A. (2000) An isoform of kinesin light chain specific for the Golgi complex. *J Cell Sci*, **113**, 2047-2054.
- Hackney, D.D., Levitt, J.D. and Suhan, J. (1992) Kinesin undergoes a 9 S to 6 S conformational transition. *J Biol Chem*, **267**, 8696-8701.
- Hanahan, D. (1983) Studies on transformation of *Escherichia coli* with plasmids. *J Mol Biol*, **166**, 557-580.
- Hirano, T., Kinoshita, N., Morikawa, K. and Yanagida, M. (1990) Snap helix with knob and hole: essential repeats in *S. pombe* nuclear protein nuc2+. *Cell*, **60**, 319-328.
- Hirokawa, N. (1998) Kinesin and dynein superfamily proteins and the mechanism of organelle transport. *Science*, **279**, 519-526.
- Hirokawa, N., Noda, Y. and Okada, Y. (1998) Kinesin and dynein superfamily proteins in organelle transport and cell division. *Curr Opin Cell Biol*, **10**, 60-73.
- Hoenger, A., Sack, S., Thormahlen, M., Marx, A., Muller, J., Gross, H. and Mandelkow, E. (1998) Image reconstructions of microtubules decorated with monomeric and dimeric kinesins: comparison with x-ray structure and implications for motility. *J Cell Biol*, **141**, 419-430.
- Hoenger, A., Thormahlen, M., Diaz-Avalos, R., Doerhoefer, M., Goldie, K.N., Muller, J. and Mandelkow, E. (2000) A new look at the microtubule binding patterns of dimeric kinesins. *J Mol Biol*, **297**, 1087-1103.
- Howard, J. (1996) The movement of kinesin along microtubules. *Annu Rev Physiol*, **58**, 703-729.
- Hua, W., Young, E.C., Fleming, M.L. and Gelles, J. (1997) Coupling of kinesin steps to ATP hydrolysis. *Nature*, **388**, 390-393.
- Hunter, A.W. and Wordeman, L. (2000) How motor proteins influence microtubule polymerization dynamics. *J Cell Sci*, **113 Pt 24**, 4379-4389.
- Hurd, D.D. and Saxton, W.M. (1996) Kinesin mutations cause motor neuron disease phenotypes by disrupting fast axonal transport in *Drosophila*. *Genetics*, **144**, 1075-1085.
- Ichimura, T., Wakamiya-Tsuruta, A., Itagaki, C., Taoka, M., Hayano, T., Natsume, T. and Isobe, T. (2002) Phosphorylation-dependent interaction of kinesin light chain 2 and the 14-3-3 protein. *Biochemistry*, **41**, 5566-5572.

- Inoue, S. and Salmon, E.D. (1995) Force generation by microtubule assembly/disassembly in mitosis and related movements. *Mol Biol Cell*, **6**, 1619-1640.
- Kamal, A., Almenar-Queralt, A., LeBlanc, J.F., Roberts, E.A. and Goldstein, L.S. (2001) Kinesin-mediated axonal transport of a membrane compartment containing beta-secretase and presenilin-1 requires APP. *Nature*, **414**, 643-648.
- Kamal, A. and Goldstein, L.S. (2000) Connecting vesicle transport to the cytoskeleton. *Curr Opin Cell Biol*, **12**, 503-508.
- Kamal, A., Stokin, G.B., Yang, Z., Xia, C.H. and Goldstein, L.S. (2000) Axonal transport of amyloid precursor protein is mediated by direct binding to the kinesin light chain subunit of kinesin-I. *Neuron*, **28**, 449-459.
- Khodjakov, A., Lizunova, E.M., Minin, A.A., Koonce, M.P. and Gyoeva, F.K. (1998) A specific light chain of kinesin associates with mitochondria in cultured cells. *Mol Biol Cell*, **9**, 333-343.
- Kikkawa, M., Okada, Y. and Hirokawa, N. (2000) 15 A resolution model of the monomeric kinesin motor, KIF1A. *Cell*, **100**, 241-252.
- Kikkawa, M., Sablin, E.P., Okada, Y., Yajima, H., Fletterick, R.J. and Hirokawa, N. (2001) Switch-based mechanism of kinesin motors. *Nature*, **411**, 439-445.
- Kirchner, J., Woehlke, G. and Schliwa, M. (1999) Universal and unique features of kinesin motors: insights from a comparison of fungal and animal conventional kinesins. *Biol Chem*, **380**, 915-921.
- Klumpp, L.M., Mackey, A.T., Farrell, C.M., Rosenberg, J.M. and Gilbert, S.P. (2003) A kinesin switch I arginine to lysine mutation rescues microtubule function. *J Biol Chem*, **278**, 39059-39067.
- Kozielski, F., De Bonis, S., Burmeister, W.P., Cohen-Addad, C. and Wade, R.H. (1999) The crystal structure of the minus-end-directed microtubule motor protein ncd reveals variable dimer conformations. *Structure Fold Des*, **7**, 1407-1416.
- Kozielski, F., Sack, S., Marx, A., Thormahlen, M., Schonbrunn, E., Biou, V., Thompson, A., Mandelkow, E.M. and Mandelkow, E. (1997a) The crystal structure of dimeric kinesin and implications for microtubule-dependent motility. *Cell*, **91**, 985-994.
- Kozielski, F., Schonbrunn, E., Sack, S., Muller, J., Brady, S.T. and Mandelkow, E. (1997b) Crystallization and preliminary X-ray analysis of the single-headed and double-headed motor protein kinesin. *J Struct Biol*, **119**, 28-34.

- Kull, F.J., Sablin, E.P., Lau, R., Fletterick, R.J. and Vale, R.D. (1996a) Crystal structure of the kinesin motor domain reveals a structural similarity to myosin. *Nature*, **380**, 550-555.
- Kull, F.J., Sablin, E.P., Lau, R., Fletterick, R.J. and Vale, R.D. (1996b) Crystal structure of the kinesin motor domain reveals a structural similarity to myosin. *Nature*, **380**, 550-555.
- Lawrence, C.J., Dawe, R.K., Christie, K.R., Cleveland, D.W., Dawson, S.C., Endow, S.A., Goldstein, L.S., Goodson, H.V., Hirokawa, N., Howard, J., Malmberg, R.L., McIntosh, J.R., Miki, H., Mitchison, T.J., Okada, Y., Reddy, A.S., Saxton, W.M., Schliwa, M., Scholey, J.M., Vale, R.D., Walczak, C.E. and Wordeman, L. (2004) A standardized kinesin nomenclature. *J Cell Biol*, **167**, 19-22.
- Lazarov, O., Morfini, G., Lee, E.B., Farah, M., Szodorai, A., DeBoer, S.R., Koliatsos, V., Kins, S., Lee, V., Wong, P.C., Price, D.L., Brady, S.T and Sisodia, S.S. (2005) Axonal transport, Amyloid Precursor Protein, Kinesin-1 and the processing Apparatus: Revisited. *The Journal of Neuroscience*, **25(9)**: 2386-2395.
- Lee, N., Francklyn, C. and Hamilton, E.P. (1987) Arabinose-induced binding of AraC protein to aral2 activates the araBAD operon promoter. *Proc Natl Acad Sci U S A*, **84**, 8814-8818.
- Leibler, S. and Huse, D.A. (1993) Porters versus rowers: a unified stochastic model of motor proteins. *J. Cell Biology*, **121**, 1357-1368.
- Mandelkow, E. and Johnson, K.A. (1998) The structural and mechanochemical cycle of kinesin. *Trends Biochem Sci*, **23**, 429-433.
- Maney, T., Hunter, A.W., Wagenbach, M. and Wordeman, L. (1998) Mitotic centromere-associated kinesin is important for anaphase chromosome segregation. *J Cell Biol*, **142**, 787-801.
- Matthews, B.W. (1968) Solvent content of protein crystals. *Journal of Molecular Biology*, **33**, 491-497.
- Morfini, G., Szebenyi, G., Elluru, R., Ratner, N. and Brady, S.T. (2002) Glycogen synthase kinase 3 phosphorylates kinesin light chains and negatively regulates kinesin-based motility. *Embo J*, **21**, 281-293.
- Morfini, G., Szebenyi, G., Brown, H., Pant, H., Pigino, G., DeBoer, S., Beffert, U. and Brady, S.T. (2004) A novel CDK5-dependent pathway for regulating GSK3 activity and kinesin-driven motility in neurons. *Embo J*, **23**, 2235-2245.
- Nagata, K., Puls, A., Futter, C., Aspenstrom, P., Schaefer, E., Nakata, T., Hirokawa, N. and Hall, A. (1998) The MAP kinase kinase kinase MLK2

- co-localizes with activated JNK along microtubules and associates with kinesin superfamily motor KIF3. *Embo J*, **17**, 149-158.
- Nitta, R., Kikkawa, M., Okada, Y. and Hirokawa, N. (2004) KIF1A alternately uses two loops to bind microtubules. *Science*, **305**, 678-683.
- Ogawa, T., Nitta, R., Okada, Y. and Hirokawa, N. (2004) A common mechanism for microtubule destabilizers-M type kinesins stabilize curling of the protofilament using the class-specific neck and loops. *Cell*, **116**, 591-602.
- Ong, L.L., Lim, A.P., Er, C.P., Kuznetsov, S.A. and Yu, H. (2000) Kinectin-kinesin binding domains and their effects on organelle motility [In Process Citation]. *J Biol Chem*, **275**, 32854-32860.
- Onishi, H., Kojima, S., Katoh, K., Fujiwara, K. and Martinez, H.M.M.M.F. (1998) Functional transitions in myosin - formation of a critical salt-bridge and transmission of effect to the sensitive tryptophan. *Proc. Natl. Acad. Sci. USA*, **95**:6653-6658.
- Otwinowski, Y., and Minor, W. (1997) *Processing of X-ray Diffraction Data Collected in Oscillation Mode*. Academic Press.
- Patel, N., Thierry-Mieg, D. and Mancillas, J.R. (1993) Cloning by insertional mutagenesis of a cDNA encoding *Caenorhabditis elegans* kinesin heavy chain. *Proc Natl Acad Sci U S A*, **90**, 9181-9185.
- Rahman, A., Friedman, D.S. and Goldstein, L.S. (1998) Two kinesin light chain genes in mice. Identification and characterization of the encoded proteins [published erratum appears in J Biol Chem 1998 Sep 11;273(37):24280]. *J Biol Chem*, **273**, 15395-15403.
- Ratner, N., Bloom, G.S. and Brady, S.T. (1998) A role for cyclin-dependent kinase(s) in the modulation of fast anterograde axonal transport: effects defined by olomoucine and the APC tumor suppressor protein. *J Neurosci*, **18**, 7717-7726.
- Reid, E., Kloos, M., Ashley-Koch, A., Hughes, L., Bevan, S., Svenson, I.K., Graham, F.L., Gaskell, P.C., Dearlove, A., Pericak-Vance, M.A., Rubinsztein, D.C. and Marchuk, D.A. (2002) A kinesin heavy chain (KIF5A) mutation in hereditary spastic paraplegia (SPG10). *Am J Hum Genet*, **71**, 1189-1194.
- Rice, S., Lin, A.W., Safer, D., Hart, C.L., Naber, N., Carragher, B.O., Cain, S.M., Pechatnikova, E., Wilson-Kubalek, E.M., Whittaker, M., Pate, E., Cooke, R., Taylor, E.W., Milligan, R.A. and Vale, R.D. (1999) A structural change in the kinesin motor protein that drives motility. *Nature*, **402**, 778-784.

- Rietdorf, J., Ploubidou, A., Reckmann, I., Holmstrom, A., Frischknecht, F., Zettl, M., Zimmermann, T. and Way, M. (2001) Kinesin-dependent movement on microtubules precedes actin-based motility of vaccinia virus. *Nat Cell Biol*, **3**, 992-1000.
- Sablin, E.P., Case, R.B., Dai, S.C., Hart, C.L., Ruby, A., Vale, R.D. and Fletterick, R.J. (1998) Direction determination in the minus-end-directed kinesin motor ncd. *Nature*, **395**, 813-816.
- Sablin, E.P. and Fletterick, R.J. (1995) Crystallization and preliminary structural studies of the ncd motor domain. *Proteins*, **21**, 68-69.
- Sack, S., Muller, J., Marx, A., Thormahlen, M., Mandelkow, E.M., Brady, S.T. and Mandelkow, E. (1997) X-ray structure of motor and neck domains from rat brain kinesin. *Biochemistry*, **36**, 16155-16165.
- Sanger, F., Nicklen, S. and Coulson, A.R. (1977) DNA sequencing with chain-terminating inhibitors. *Proc Natl Acad Sci U S A*, **74**, 5463-5467.
- Sasaki, N. and Sutoh, K. (1998) Structure-mutation analysis of the ATPase site of Dictyostelium discoideum myosin II. *Adv Biophys*, **35**, 1-24.
- Scheufler, C., Brinker, A., Bourenkov, G., Pegoraro, S., Moroder, L., Bartunik, H., Hartl, F.U. and Moarefi, I. (2000) Structure of TPR domain-peptide complexes: critical elements in the assembly of the Hsp70-Hsp90 multichaperone machine. *Cell*, **101**, 199-210.
- Schnitzer, M.J. and Block, S.M. (1997) Kinesin hydrolyses one ATP per 8-nm step. *Nature*, **388**, 386-390.
- Seiler, S., Kirchner, J., Horn, C., Kallipolitou, A., Woehlke, G. and Schliwa, M. (2000) Cargo binding and regulatory sites in the tail of fungal conventional kinesin. *Nat Cell Biol*, **2**, 333-338.
- Setou, M., Nakagawa, T., Seog, D.H. and Hirokawa, N. (2000) Kinesin superfamily motor protein KIF17 and mLin-10 in NMDA receptor-containing vesicle transport. *Science*, **288**, 1796-1802.
- Setou, M., Seog, D.H., Tanaka, Y., Kanai, Y., Takei, Y., Kawagishi, M. and Hirokawa, N. (2002) Glutamate-receptor-interacting protein GRIP1 directly steers kinesin to dendrites. *Nature*, **417**, 83-87.
- Sharp, D.J., Rogers, G.C. and Scholey, J.M. (2000) Roles of motor proteins in building microtubule-based structures: a basic principle of cellular design. *Biochim Biophys Acta*, **1496**, 128-141.
- Shipley, K., Hekmat-Nejad, M., Turner, J., Moores, C., Anderson, R., Milligan, R., Sakowicz, R. and Fletterick, R. (2004) Structure of a kinesin microtubule depolymerization machine. *Embo J*.

- Sikorski, R.S., Boguski, M.S., Goebel, M. and Hieter, P. (1990) A repeating amino acid motif in CDC23 defines a family of proteins and a new relationship among genes required for mitosis and RNA synthesis. *Cell*, **60**, 307-317.
- Sindelar, C.V., Budny, M.J., Rice, S., Naber, N., Fletterick, R. and Cooke, R. (2002) Two conformations in the human kinesin power stroke defined by X-ray crystallography and EPR spectroscopy. *Nat Struct Biol*, **9**, 844-848.
- Skoufias, D.A., Cole, D.G., Wedaman, K.P. and Scholey, J.M. (1994) The carboxyl-terminal domain of kinesin heavy chain is important for membrane binding. *J Biol Chem*, **269**, 1477-1485.
- Song, Y.H., Marx, A., Muller, J., Woehlke, G., Schliwa, M., Krebs, A., Hoenger, A. and Mandelkow, E. (2001) Structure of a fast kinesin: implications for ATPase mechanism and interactions with microtubules. *Embo J*, **20**, 6213-6225.
- Sosa, H., Dias, D.P., Hoenger, A., Whittaker, M., Wilson-Kubalek, E., Sablin, E., Fletterick, R.J., Vale, R.D. and Milligan, R.A. (1997) A model for the microtubule-Ncd motor protein complex obtained by cryo- electron microscopy and image analysis. *Cell*, **90**, 217-224.
- Sosa, H., Peterman, E.J., Moerner, W.E. and Goldstein, L.S. (2001) ADP-induced rocking of the kinesin motor domain revealed by single-molecule fluorescence polarization microscopy. *Nat Struct Biol*, **8**, 540-544.
- Steen, R., Dahlberg, A.E., Lade, B.N., Studier, F.W. and Dunn, J.J. (1986) T7 RNA polymerase directed expression of the Escherichia coli rrnB operon. *Embo J*, **5**, 1099-1103.
- Stenoien, D.L. and Brady, S.T. (1997) Immunochemical analysis of kinesin light chain function. *Mol Biol Cell*, **8**, 675-689.
- Storoni, L.C., McCoy, A.J. and Read, R.J. (2004) Likelihood-enhanced fast rotation functions. *Acta Crystallogr D Biol Crystallogr*, **60**, 432-438.
- Studier, F.W., Rosenberg, A.H., Dunn, J.J. and Dubendorff, J.W. (1990) Use of T7 RNA polymerase to direct expression of cloned genes. *Methods Enzymol*, **185**, 60-89.
- Suzuki, Y., Tanokura, M. and Shimizu, T. (1998) Evidence for existence of multiple conformations of kinesin and ncd motor domains in solution revealed by ³¹P-NMR of the tightly bound ADP. *Eur J Biochem*, **257**, 466-471.
- Svoboda, K., Schmidt, C.F., Schnapp, B.J. and Block, S.M. (1993) Direct observation of kinesin stepping by optical trapping interferometry [see comments]. *Nature*, **365**, 721-727.

- Tanaka, Y., Kanai, Y., Okada, Y., Nonaka, S., Takeda, S., Harada, A. and Hirokawa, N. (1998) Targeted disruption of mouse conventional kinesin heavy chain, *kif5B*, results in abnormal perinuclear clustering of mitochondria. *Cell*, **93**, 1147-1158.
- Taylor, P., Dornan, J., Carrello, A., Minchin, R.F., Ratajczak, T. and Walkinshaw, M.D. (2001a) Two structures of cyclophilin 40: folding and fidelity in the TPR domains. *Structure (Camb)*, **9**, 431-438.
- Taylor, S.S., Hussein, D., Wang, Y., Elderkin, S. and Morrow, C.J. (2001b) Kinetochore localisation and phosphorylation of the mitotic checkpoint components Bub1 and BubR1 are differentially regulated by spindle events in human cells. *J Cell Sci*, **114**, 4385-4395.
- Tekotte, H. and Davis, I. (2002) Intracellular mRNA localization: motors move messages. *Trends Genet*, **18**, 636-642.
- Terada, S., Kinjo, M. and Hirokawa, N. (2000) Oligomeric tubulin in large transporting complex is transported via kinesin in squid giant axons [In Process Citation]. *Cell*, **103**, 141-155.
- Towbin, H., Staehelin, T. and Gordon, J. (1979) Electrophoretic transfer of proteins from polyacrylamide gels to nitrocellulose sheets: procedure and some applications. *Proc Natl Acad Sci U S A*, **76**, 4350-4354.
- Tsai, M.Y., Morfini, G., Szebenyi, G. and Brady, S.T. (2000) Release of kinesin from vesicles by hsc70 and regulation of fast axonal transport. *Mol Biol Cell*, **11**, 2161-2173.
- Turner, J., Anderson, R., Guo, J., Beraud, C., Fletterick, R. and Sakowicz, R. (2001a) Crystal structure of the mitotic spindle kinesin Eg5 reveals a novel conformation of the neck-linker. *J Biol Chem*, **276**, 27.
- Turner, J., Anderson, R., Guo, J., Beraud, C., Fletterick, R. and Sakowicz, R. (2001b) Crystal structure of the mitotic spindle kinesin Eg5 reveals a novel conformation of the neck-linker. *J Biol Chem*, **276**, 25496-25502.
- Vale, R.D. (1996) Switches, latches, and amplifiers: common themes of G proteins and molecular motors. *J Cell Biol*, **135**, 291-302.
- Vale, R.D. (2003) The molecular motor toolbox for intracellular transport. *Cell*, **112**, 467-480.
- Vale, R.D. and Fletterick, R.J. (1997) The design plan of kinesin motors. *Ann. Rev. Cell Dev. Biol.*, **13**, 745-777.
- Vale, R.D., Funatsu, T., Pierce, D.W., Romberg, L., Harada, Y. and Yanagida, T. (1996) Direct observation of single kinesin molecules moving along microtubules. *Nature*, **380**, 451-453.

- Vale, R.D., Reese, T.S. and Sheetz, M.P. (1985) Identification of a novel force-generating protein, kinesin, involved in microtubule-based motility. *Cell*, **42**, 39-50.
- Verhey, K.J., Lizotte, D.L., Abramson, T., Barenboim, L., Schnapp, B.J. and Rapoport, T.A. (1998) Light chain-dependent regulation of Kinesin's interaction with microtubules. *J Cell Biol*, **143**, 1053-1066.
- Verhey, K.J., Meyer, D., Deehan, R., Blenis, J., Schnapp, B.J., Rapoport, T.A. and Margolis, B. (2001) Cargo of kinesin identified as JIP scaffolding proteins and associated signaling molecules. *J Cell Biol*, **152**, 959-970.
- Vinogradova, M.V., Reddy, V.S., Reddy, A.S., Sablin, E.P. and Fletterick, R.J. (2004) Crystal structure of kinesin regulated by Ca(2+)-calmodulin. *J Biol Chem*, **279**, 23504-23509.
- Walczak, C.E. and Mitchison, T.J. (1996) Kinesin-related proteins at mitotic spindle poles: function and regulation. *Cell*, **85**, 943-946.
- Woehlke, G., Ruby, A.K., Hart, C.L., Ly, B., Hom-Booher, N. and Vale, R.D. (1997) Microtubule interaction site of the kinesin motor. *Cell*, **90**, 207-216.
- Xia, C., Rahman, A., Yang, Z. and Goldstein, L.S. (1998) Chromosomal localization reveals three kinesin heavy chain genes in mouse. *Genomics*, **52**, 209-213.
- Xia, C.H., Roberts, E.A., Her, L.S., Liu, X., Williams, D.S., Cleveland, D.W. and Goldstein, L.S. (2003) Abnormal neurofilament transport caused by targeted disruption of neuronal kinesin heavy chain KIF5A. *J Cell Biol*, **161**, 55-66.
- Xing, H., Zhang, S., Weinheimer, C., Kovacs, A. and Muslin, A.J. (2000) 14-3-3 proteins block apoptosis and differentially regulate MAPK cascades. *Embo J*, **19**, 349-358.
- Yan, Y., Sardana, V., Xu, B., Homnick, C., Halczenko, W., Buser, C.A., Schaber, M., Hartman, G.D., Huber, H.E. and Kuo, L.C. (2004) Inhibition of a mitotic motor protein: where, how, and conformational consequences. *J Mol Biol*, **335**, 547-554.
- Yildiz, A. and Selvin, P.R. (2005) Kinesin: walking, crawling or sliding along? *Trends Cell Biol*, **15**, 112-120.
- Yu, H., Toyoshima, I., Steuer, E.R. and Sheetz, M.P. (1992) Kinesin and cytoplasmic dynein binding to brain microsomes. *J Biol Chem*, **267**, 20457-20464.

- Yun, M., Zhang, X., Park, C.G., Park, H.W. and Endow, S.A. (2001) A structural pathway for activation of the kinesin motor ATPase. *EMBO J*, **20**, 2611-2618.
- Zhan, Y., Song, X. and Zhou, G.W. (2001) Structural analysis of regulatory protein domains using GST-fusion proteins. *Gene*, **281**, 1-9.
- Zhang, Y., Qiu, W.J., Liu, D.X., Neo, S.Y., He, X. and Lin, S.C. (2001) Differential molecular assemblies underlie the dual function of Axin in modulating the WNT and JNK pathways. *J Biol Chem*, **276**, 32152-32159.

7 Appendix

7.1 List of Abbreviations

Å	Angstrom (0.1 nm)
ADP	Adenosine- 5'- diphosphate
AIEX	Anion exchange chromatography
Amp	Ampicillin
APP	Amyloid precursor protein
A _x	UV Absorbance at x nm
ATP	Adenosine triphosphate
CHAPS	3-(3-Cholamidopropyl)dimethylamino-1-propanesulphonate
CIEX	Cation exchange chromatography
Chl	Chloramphenicol
DESY	Deutsches Elektronen-Synchrotron
DNTP	Deoxynucleotides triphosphate
DORIS	Double Storage Ring (Doppelring-Speicher)
DTT	Dithiothreitol
EDTA	Ethylendiaminetetraacetate
EGTA	Ethylenglycol-bis-(2-aminoethylether)-N, N, N', N'-tetra acetic acid
GST	Glutathione-S-transferase
HEPES	N-2-Hydroxyethyl-piperazine-N-2-ethanesulfonic acid
His ₆ -tag	(Polyhistidine) ₆ tag
IEX	Ion exchange chromatography
IMAC	Immobilized metal chelating chromatography
IPTG	Isopropyl-D-β-galactopyranoside
JIPs	c-jun NH2-terminal kinase (JNK)-interacting proteins
Kan	Kanamycin
K _d	Dissociation constant
KDa	Kilodalton(s)
KHC	Kinesin heavy chain
k _{hyd}	ATP hydrolysis constant
K _{cat}	catalytic activity
KLC	Kinesin light chain
k _{off}	off rate constant
k _{on}	on rate constant
Krpm	1000x revolutions per minute
LB	Luria-Bertani
MR	Molecular replacement
Nk355	<i>Neurospora crassa</i> motor domain construct (residues 1-355)
NMR	Nuclear magnetic resonance spectroscopy
OD _x	Optical density at x nm
PAGE	Polyacrylamide gel electrophoresis
PDB	Protein Data Bank
PEG	Polyethylenglycol
pI	isoelectric point
PIPES	Piperazine-N,N'- bis- (2-ethanesulfonic) acid

PMSF	Phenyl methyl sulfonyl fluoride
PTB	Phosphotyrosine binding domain
Rk354	<i>Rattus norvegicus</i> motor domain construct (residues 1-354)
TE	Tris-EDTA
T _m	Melting temperature
TPR	Tetratricopeptide repeat
Tris	Tris- (Hydroxymethyl)-aminomethane
Triton X-100	Polyoxyethylen-(9-10)-p-t-octylphenol
Tween 20	Polyoxyethylen-sorbitanmonolaurate
(v/v)	Volume per volume
(w/v)	Weight per volume

7.2 List of Figures

Figure 1: Phylogenetic tree of the kinesin superfamily

Figure 2: Domain structure of rat kinesin-1

Figure 3: Motor domain structures of *N. crassa* and *R. norvegicus* kinesin-1

Figure 4: The nucleotide-binding site of rat kinesin motor domain

Figure 5: Alignment of primary sequences of kinesin-1 motor domains from various species

Figure 6: Alignment of KLCs

Figure 7: The TPR motif

Figure 8: A TPR - ligand interaction paradigm

Figure 9: Overview of the Gateway™ technology

Figure 10: Setup of crystallization trials with the vapour diffusion method

Figure 11: A batch crystallization experiment set up

Figure 12: The chromatograms of the sequencing analysis for the motor domain mutants

Figure 13: Purification of the Nk355^{R207A} mutant

Figure 14: Purified NK355^{R207K} mutant

Figure 15: Purification of the Rk354^{R204A} mutant

Figure 16: Purified Rk354^{R204K} mutant

Figure 17: Pictures of crystals

Figure 18: Sample diffraction pattern of the measured Nk355^{R207A} crystal

Figure 19: Packing of the protein molecules in the crystals of Nk355^{R207A} mutant according to the PHASER solution

Figure 20: Composite omit maps for Nk355^{R207A} mutant calculated with the MR solution of Phaser

Figure 21: Depiction of RK354 Δ loop11 construct

Figure 22: Purification of RK354 Δ loop11

Figure 23: Purification of GST.TPR1-6 protein

Figure 24: Gel filtration eluate fractions of His.TPR1-6 construct

Figure 25: Solubility study with the His.TPR1-2 and His.TPR3-4 constructs

Figure 26: Expression of GST.TPR1-2 protein

Figure 27: Solubility study of His.TPR1-6t protein

Figure 28: Expression of the GST.TPR1-6t protein in SF9 insect cells

Figure 29: Expression and solubility test for the GST.TPR1-6t protein

Figure 30: Limited proteolysis analysis of the GST.TPR1-6 protein

Figure 31: Depiction of the salt bridge between R207 and E240 in *N. crassa*

Figure 32: Packing of protein molecules in the crystals of the mutant Nk355^{R207A}

Figure 33: Packing of protein molecules in the crystals of the wild type Nk355

Figure 34: Structural modeling of the Arg²⁰⁴ in the rat kinesin monomer structure

Figure 35: The packing of protein molecules in the crystal of Rk354^{R204A}

Figure 36: The packing of protein molecules in the crystal of Rk354 wild type protein

7.3 List of Tables

Table 1: Cell strains and feature list

Table 2: A summary of the vectors used in this study

Table 3: Summary of reactions and nomenclature in Gateway™

Table 4: Solutions for preparing SDS-PAGE gels

Table 5: Crystallization conditions for successfully crystallized kinesin motor domains

Table 6: Data collection details for the measured Nk355^{R207A} crystal

Table 7: Data collection details for the measured Rk354^{R204A} crystal

Table 8: Summary of constructs of rat KLC-C

7.4 Oligonucleotides

Oligonucleotides for mutagenesis

Nk355^{R207A}:

Nk207f: 5'-GAACCAGGAGTCGTCGGCTTCGCATTCCATCTTCGTCATC-3'

Nk207r: 5'-GATGACGAAGATGGAATGCGAAGCCGACGACTCCTGGTTC-3'

Nk355^{R207K}

Nk207Kf: 5'-GAACCAGGAGTCGTCGAAATCGCATTCCATCTTCGTCATC-3'

Nk207Kr: 5'-GATGACGAAGATGGAATGCGATTTCGACGACTCCTGGTTC-3'

Rk354^{R204A}

Rk204Af: 5'-AACGAACACAGCTCCGCGAGTCACAGTATCTTCCTG-3'

Rk204Ar: 5'-CAGGAAGATACTGTGACTCGCGGAGCTGTGTTTCGTT-3'

Rk354^{R204K}

Rk204Kf: 5'-AACGAACACAGCTCCAAGAGTCACAGTATCTTCCTG-3'

Rk204Kr: 5'-CAGGAAGATACTGTGACTCTTGGAGCTGTGTTTCGTT-3'

RK354Δloop11

RkΔL11f:

5'-

ATTTGGTTGATTTGGCTGGATCCGAAAAGGGCAATATCAACAAGTCTTTG-
3'

RkΔL11r:

5'-

CAAAGACTTGTTGATATTGCCCTTTTCGGATCCAGCCAAATCAACCAAAT-
3'

Primers for sequencing:

NkinS1: 5'-CTTTGATCGGCTCG-3'

NkinS2: 5'-CGCCTCAGACTACG-3'

NkinS3: 5'-CGCTGGAGGGGTCA-3'

Rk1f: 5'-CGGAGGTCATGGATG-3'

Rk1r: 5'-CCAAATACAGCTTCCCGCTG-3'

PT7_7f: 5'-GGGAGACCACAACGGTTTC-3'

PT7_7r: 5'-CGATGATAAGCTTGGGCTG-3'

Oligonucleotides for generation of KLC constructs**Oligonucleotides for mutagenesis of pHA.GST.TPR**

Histprnde: 5'-GATGATGAAAACAAGCCAATATGGATGCACGCGGAG-3'

Histprnde_comp: 5'-CTCCGCGTGCATCCATATTGGCTTGTTTTTCATCATC-3'

pET16b.Nhis.TPR:

Smhisklc1: 5'-GCCATATGGCGGCCGCGCCGCCCAG-3'

Smhisklc2: 5'-GCGGATCCTTATTCCTCCAGTGTCTCCGCAGCTTC-3'

pNG2.Chis TPR:

SpyHis1:

CGGGATCCCTAATGATGATGATGATGATGTTCTCCAGTGTCTCCGCAGC
TTCAAAC-3' 5'-

SpyHis2: 5'-GCCATATGGCGGCCGCGCCGCCCAG-3'

Oligonucleotides for sequencing:

Chis31: 5'-TGGCTGCGACCCTCAAC-3'

Chis32: 5'-CGGGTCCGAGCTTCGTC-3'

Chis5: 5'-CTGGCTATCCGTGAGAA-3'

Chis4: 5'-CCTTCTCCCTGATCTCC-3'

Chis3: 5'-TCATCATCCACAGATCC-3'
Chis2: 5'-TGGCCTTGCTGTGCCAG-3'
Chis1: 5'-GGTGTACAGGGATCAGA-3'
Nhis1: 5'-CCCAGCAGGGCGGCTAC-3'
Nhis2: 5'-TGTTGAGGGTCGCAGCC-3'
Nhis3: 5'-GCCGAGCCGCTGTGCAA-3'
Nhis4: 5'-GGGAGTTTGGATCTGTGG-3'
Spyseq1: 5'-CAGACAGATGAGTCAAC-3'
Spyseq2: 5'-CTTTTGGACAACCACCC-3'
Spyseq3: 5'-GAGCGTGCAGAGATTTC-3'
Spyseq4: 5'-CTTGCCAGCCCTGCAAA-3'
Spyseq5: 5'-GCCACGTTTGGTGGTGG-3'
Spyseq6: 5'-CGGATAGCCAGGGCATC-3'
Spyseq7: 5'-GTGAGAAAACCCTGGGC-3'
Spyseq8: 5'-GGAAGCCAGGTTATTCT-3'

Gateway™ oligonucleotides:

AttB1f: 5'-GGGGACAAGTTTGTACAAAAAAGCAGGCT-3'
AttB1r: 5'-GGGGACCACTTTGTACAAGAAAGCTGGGT-3'

pDEST15.TPR1-6t , pDEST20.TPR1-6t and pDEST17.TPR1-6t:

GF1:
5'-
AAAAAGCAGGCTTCGAAAACCTGTATTTTCAGGGCCTGCGCACGCTCCAC
AACCTG-3'

GR4:
5'-AGAAAGCTGGGTCTTATTTAACCAGCCCGAGCTTCATCTTTC-3'

pDEST15.TPR1-2 and pDEST17.TPR1-2:

GF1:
5'-
AAAAAGCAGGCTTCGAAAACCTGTATTTTCAGGGCCTGCGCACGCTCCAC
AACCTG-3'

GR1:
5'-AGAAAGCTGGGTCTTAGGTTTTCTCACGGATAGCCAGGGC-3'

pDEST17.TPR3-4:

GF1:
5'-
AAAAAGCAGGCTTCGAAAACCTGTATTTTCAGGGCCTGCGCACGCTCCAC
AACCTG-3'

GR2:

5'-AGAAAGCTGGGTCTTACTTCGTCTGGTAGATCTCCAGGGCC-3'

Oligonucleotides for sequencing:

T7tp: 5'- GCTAGTTATTGCTCAGCGG-3'

attLf: 5'-TCGCGTTAACGCTAGCATGGATCTC-3'

attLr: 5'-GTAACATCAGAGATTTTGAGACAG-3'

M13f: 5'-GTTTTCCCAGTCACGAC-3'

M13r: 5'-CAGGAAACAGCTATGAC-3'

7.5 Purification buffers**Nk355^{R207A} and Nk355^{R207K} proteins:**

Lysis buffer: 50mM Pipes pH=6.9, 1mM MgCl₂, 1 mM EGTA, 1mM DTT, 50mM NaCl.

PC buffer A: 50mM Pipes pH=6.9, 1mM MgCl₂, 1 mM EGTA, 1mM DTT, 50mM NaCl.

PC buffer B: 50mM Pipes pH=6.9, 1mM MgCl₂, 1 mM EGTA, 1mM DTT, 500mM NaCl.

MonoS buffer A: 50mM Pipes pH=6.9, 1mM MgCl₂, 1 mM EGTA, 1mM DTT, 50mM NaCl.

MonoS buffer B: 50mM Pipes pH=6.9, 1mM MgCl₂, 1 mM EGTA, 1mM DTT, 1M NaCl.

Gel filtration buffer: 20mM Tris-HCL pH=8.0, 5mM MgCl₂, 1 mM EGTA, 1mM DTT, 100mM NaCl, 0.5mM ATP

Rk354^{R204A} and Rk354^{R204K} proteins

Lysis buffer: 50mM Pipes pH=6.9, 1mM MgCl₂, 1 mM EGTA, 1mM DTT, 50mM NaCl.

PC buffer A: 50mM Pipes pH=6.9, 1mM MgCl₂, 1 mM EGTA, 1mM DTT, 50mM NaCl.

PC buffer B: 50mM Pipes pH=6.9, 1mM MgCl₂, 1 mM EGTA, 1mM DTT, 500mM NaCl.

MonoQ buffer A: 50mM Pipes pH=6.9, 1mM MgCl₂, 1 mM EGTA, 1mM DTT, 50mM NaCl.

MonoQ buffer B: 1M Pipes pH=6.9, 1mM MgCl₂, 1 mM EGTA, 1mM DTT, 1M NaCl.

Gel filtration buffer: 20mM Pipes pH=6.9, 1mM DTT, 1mM EGTA, 5mM MgCl₂, 100mM NaCl

RK354Δloop11 protein

Lysis buffer: 50mM Pipes pH=6.5, 1mM MgCl₂, 1 mM EGTA, 1mM DTT, 50mM NaCl.

PC buffer A: 50mM Pipes pH=6.5, 1mM MgCl₂, 1 mM EGTA, 1mM DTT, 50mM NaCl.

PC buffer B: 50mM Pipes pH=6.5, 1mM MgCl₂, 1 mM EGTA, 1mM DTT, 500mM NaCl.

MonoQ buffer A: 50mM Pipes pH=6.5, 1mM MgCl₂, 1 mM EGTA, 1mM DTT, 50mM NaCl.

MonoQ buffer B: 1M Pipes pH=6.5, 1mM MgCl₂, 1 mM EGTA, 1mM DTT, 1M NaCl.

Gel filtration buffer: 20mM Pipes pH=6.5, 1mM DTT, 1mM EGTA, 5mM MgCl₂, 100mM NaCl

His.KLC-C:

Lysis buffer: 50mM Pipes pH=6.9, 1mM MgCl₂, 1 mM EGTA, 1mM DTT, 50mM NaCl.

Ni²⁺-NTA buffer A: 50mM Pipes pH=6.9, 1mM MgCl₂, 1 mM EGTA, 1mM DTT, 50mM NaCl, 25mM Imidazole

Ni²⁺-NTA buffer B: 50mM Pipes pH=6.9, 1mM MgCl₂, 1 mM EGTA, 1mM DTT, 50mM NaCl, 500mM Imidazole

GST.TPR1-6:

Lysis buffer: 50mM Pipes pH=6.9, 1mM MgCl₂, 1 mM EGTA, 1mM DTT, 50mM NaCl.

GST binding buffer: 50mM Pipes pH=6.9, 1mM MgCl₂, 1 mM EGTA, 1mM DTT, 50mM NaCl.

GST elution buffer: 50mM Tris-HCl pH=8, 10mM reduced glutathione, 100mM NaCl, 1mM DTT

Gel filtration buffer: 50mM Tris-HCl pH=8, 200mM NaCl, 1mM DTT

Protease reaction buffer: 50mM Pipes pH=7.0, 300mM NaCl, 5mM β -mercaptoethanol, 2.5mM CaCl_2

His.TPR1-6:

Lysis buffer: 100mM Tris-HCl pH=8.0, 1mM MgCl_2 , 1 mM EGTA, 5mM DTT, 300mM NaCl.

Ni^{2+} -NTA buffer A: 100mM Tris-HCl pH=8.0, 5mM β -mercaptoethanol, 300mM NaCl, 25mM Imidazole

Ni^{2+} -NTA buffer B: 100mM Tris-HCl pH=8.0, 5mM β -mercaptoethanol, 300mM NaCl, 500mM Imidazole

Gel filtration buffer: 30mM Tris-HCl pH=8.0, 300mM NaCl, 5mM DTT

GST.TPR1-6t:

Lysis buffer: 50mM Tris-HCl pH=8.0, 5mM DTT, 150mM NaCl.

GST binding buffer: 50mM Tris-HCl pH=8.0, 1 mM EDTA, 2mM DTT, 150mM NaCl.

GST elution buffer: 50mM Tris-HCl pH=8.0, 1 mM EDTA, 2mM DTT, 150mM NaCl, 10mM reduced glutathione

His.TPR1-6t:

Solubility studies were carried out as described in methods.

GST.TPR1-2:

Lysis buffer: 50mM Tris-HCl pH=9.0, 5mM DTT, 200mM NaCl, 5mM β -mercaptoethanol, 0.2% NP40

GST binding buffer: 100mM Tris-HCl pH=9.0, 5mM DTT, 200mM NaCl, 0.2% NP40

GST elution buffer: 50mM Tris-HCl pH=9.0, 5mM DTT, 200mM NaCl, 10mM reduced glutathione, 0.2% NP40

MonoQ buffer A: 50mM Tris-HCl pH=9.0, 5mM DTT, 50mM NaCl, 0.05% NP40

MonoQ buffer BA: 50mM Tris-HCl pH=9.0, 5mM DTT, 500mM NaCl, 0.05% NP40

Gel filtration buffer: 50mM Tris-HCl pH=9.0, 5mM DTT, 50mM NaCl, 0.05% NP40

His.TPR1-2 and His.TPR3-4:

Solubility studies were carried out as described in methods.

In all buffers protease inhibitors were added in the following concentrations:
1mM PMSF, 1mM Benzamidine, 1µg/ml Pepstatin, 1µg/ml Leupeptine

7.6 Acknowledgements

I owe special thanks to Dr Alexander Marx and Dr Jens Mueller for their invaluable help during the data collection and analysis, collaboration in the production of some of the figures for this thesis and their expert advice throughout this thesis.

I want to thank Dr. Claire Goldsbury for her many insightful suggestions, help and critical reading of this thesis, as well as her continuous support all these years.

I want to thank Dr. Stefan Wiemann for his expert advice concerning the GatewayTM cloning techniques.

I am grateful to Prof. Dr. Eckhard Mandelkow and Dr. Eva Mandelkow for their support and for giving me the opportunity to do my doctoral research in their laboratory.

I was born in Athens in 1976. Having studied biology in the University of Athens and graduated in 2000, I worked as a tutor of Biology and Physics in a private test preparation center. In September 2001 I started my Ph.D. thesis in the Max-Planck Research Unit for Structural Molecular Biology. Aim of my doctorate work was to contribute structural information about different domains of the motor protein kinesin-1, using the X-ray crystallography technique.

Dr. Will Stanley
EMBL-Hamburg
Notkestrasse 85
22607 Hamburg
Tel: (040)89902188

17 August 2005

To whom it may concern,

This letter is to certify that as a native English speaker I have read the Ph.D. thesis entitled ' Structural Studies on Kinesin-1 Motor Domain and Light Chain from *Rattus norvegicus* and *Neurospora crassa*'. This thesis is to be submitted to the University of Hamburg by Spyridon Mylonas.

Sincerely Yours,

Will Stanley